AN ABSTRACT OF THE THESIS OF

Scott T. Allen for the degree of Master of Science in Water Resources Engineering presented on June 12, 2012

Title: Trickle-down Ecohydrology: Complexity of Rainfall Interception and Net Precipitation under Forest Canopies

Abstract approved:

_____ _____

Barbara J. Bond Jeffrey J. McDonnell

Rainfall interception is a primary control over the moisture input to a forested ecosystem through the partitioning of precipitation into throughfall, stemflow, and an evaporated component (i.e. the interception loss). Rainfall interception is a spatially and temporally varying process at multiple scales, but heterogeneity in interception processes are poorly understood and poorly described in the literature. We need to know how net precipitation varies in ecosystems because natural systems are driven by non-linear ecohydrological processes where mean values cannot capture localized effects or the cumulative consequences associated with an extremely heterogeneous input. In this thesis, we present two studies that investigate the heterogeneity of interception loss and throughfall in a forested catchment in the western Cascades range of Oregon. In one study, we examined the spatio-temporal patterns among point measurements of throughfall depth and isotopic composition to determine the cause of isotopic differences between throughfall and rainfall. Our results indicated that the residual moisture retained on the canopy from previous events plays a major role in

determining the isotopic composition of the next event's throughfall. Differences between the isotopic composition of throughfall samples could indicate further partitioning of throughfall into various flow-paths from the canopy. The second project examined the question of how vegetation variability and terrain complexity drive interception loss heterogeneity at the whole-catchment scale. We applied a simple interception model to a watershed gridded at a 50 m resolution to investigate the relative importance of topographic and vegetative controls over the spatial variability of interception loss. We found that storm characteristics are crucial regarding the impact of spatial heterogeneities in vegetation and evaporation rates. In the Pacific Northwest climate, interception loss is not highly variable for the majority of the year because the annual precipitation is dominated by large storms with low interception losses. However, the net precipitation input to a watershed becomes extremely heterogeneous in the summer due to high interception loss variability. Summer interception loss could be an important control over the spatial variability of the availability of moisture, coinciding with when vegetation is most water-limited.

Trickle-down Ecohydrology: Complexity of Rainfall Interception and Net Precipitation under Forest Canopies

by
Scott T. Allen

A THESIS

submitted to

Oregon State University

in partial fulfillment of
the requirements for the
degree of

Master of Science

Presented June 12, 2012
Commencement June 2013

Master of Science thesis of Scott T. Allen presented on
June 12, 2012.

APPROVED:

_____

Co-Major Professor, representing Water Resources Engineering

_____

Co-Major Professor, representing Water Resources Engineering

_____

Director of the Water Resources Graduate Program

_____

Dean of the Graduate School

I understand that my thesis will become part of the permanent collection of Oregon State University libraries. My signature below authorizes release of my thesis to any reader upon request.

_____

Scott T. Allen, Author

ACKNOWLEDGEMENTS

First, I would like to thank my advisory committee. Thank you Barb and Jeff for taking a risk on accepting a student with no background in hydrology or ecophysiology with an application for admission that must have read "I have no idea what I want to do." Barb, I appreciate your impassioned introduction to the field of ecohydrology, and your persistent support and willingness to let me explore my ideas. I have enjoyed our conversations, from which I not only take away advice on how to succeed in academia, but also in life as a whole. Jeff, your enthusiasm and ability to guide / facilitate the development of ideas and thought is both motivating and inspiring. Renée, you have been a role model and your contributions have come at crucial times when I was otherwise lost. Thank you all for your patience and generosity.

Most of all, I thank my family. Not only for their continued support, but for their influence and guidance over my lifetime that has shaped the values I have today.

My friends and colleagues in the McDonnell lab, FES, and the WRGP have been crucial for help with analyses, developing ideas, field-work and just general support (and much needed distractions from work).

Financial support for this project was provided through the H.J. Andrews Experimental Forest, the Water Resources Graduate Program, and Dr. Barbara Bond's research funds. My work was also only possible through the efforts of the H.J. Andrews's staff and researchers for their data collection, data management, and on-site management.

CONTRIBUTION OF AUTHORS

Chapter 2: J.R. Brooks, J.J. McDonnell, and B.J. Bond provided guidance in analysis, writing and editing.

Chapter 3: B.J. Bond guided the initial ideas and provided assistance in editing. J.J. McDonnell assisted in guiding the writing of the introduction and discussion section.

TABLE OF CONTENTS

Page

1 INTRODUCTION 2

1.1 OVERVIEW 3

1.2 DESCRIPTION OF CHAPTERS 7

1.3 REFERENCES 13

2 THE ROLE OF PRE-EVENT CANOPY WATER STORAGE ON THE ISOTOPIC COMPOSITION OF THROUGHFALL AND STEMFLOW 17

2.1 INTRODUCTION 18

2.2 METHODS 21

2.3 RESULTS 27

2.4 DISCUSSION 35

2.5 CONCLUSIONS 47

2.6 ACKNOWLEDGEMENTS 48

2.7 REFERENCES 48

3 SPATIAL PATTERNS OF CANOPY INTERCEPTION LOSS IN A HEADWATER CATCHMENT: CONTROLS AND INTERACTIONS 68

3.1 INTRODUCTION 69

3.2 METHODS 74

3.3 RESULTS 93

3.4 DISCUSSION 100

3.5 CONCLUSIONS 113

3.6 ACKNOWLEDGEMENTS 114

3.7 REFERENCES 114

4 CONCLUSIONS 146

4.1 CHAPTER 2 147

4.2 CHAPTER 3 150

4.3 BROADER IMPLICATIONS 153

4.4 REFERENCES 158

LIST OF FIGURES

Figure Page

2.1 Conceptual diagram of water fractionation processes plotted in dual isotope space.. 53

2.2 Box-plots for throughfall (TF) depth fraction (TF/P_g), and relative $\triangle(TF-P_g)$ $\delta^{18}O$ and d-excess for 11 events in the fall and 7 events in the spring sampling periods..... 55

2.3 Dual isotope plots for select events in the fall collection periods. 56

2.4 Previous event differences versus $TF-P_g$ differences 57

2.5 Time-stability plots. 64

2.6 Time-stability plot for 'V' storms.. 65

2.7 Plot layout for the two plots of the spring collection period. 58

2.8 Experimental variograms for SAP (top) and NAP (bottom) of the spring collection period..... 59

2.9 Depth and isotopic composition versus distance from stem 61

2.10 Spatial variability versus distance from stem for the North Aspect Plot and South Aspect Plot from the spring collection period..... 62

2.11 Data collected by Dewalle and Swistock (1994) reanalyzed for investigating residual moisture carryover.. 66

2.12 Probability density histograms for depth and $\delta^{18}O$ deviation from the seasonal mean values. 67

3.1 Model diagram for input data-sets and interception modeling. 126

3.2 Map of WS1 in relation to H.J. Andrews Experimental Forest 127

3.3 Modeled versus measured solar radiation at Primet meteorological station, H.J. Andrews Experimental Forest. 128

3.4 Solar radiation diel patterns over a winter and spring period showing radiation patterns during clear and cloudy conditions..... 129

3.5 Wind speed at 30m, 33m and 37m.. 130

3.6 Total interception loss of the 2006-2008 water years. 132

3.7 Canopy cover distribution (A; unitless) and canopy storage capacity distribution (B; mm) on WS1. 134

LIST OF FIGURES (Continued)

Figure Page

3.8 Time-weighted average of global solar radiation (k_g) during rain events of the 2006-2008 water years.. 135

3.9 Individual event range of spatial variation in interception loss.. 137

3.10 Controls over the IL spatial distribution.. 139

3.11 Time-stability plots. 140

3.12 Precipitation distribution.. 142

3.13 Total interception loss for the 2006-2008 water years with spatially variable precipitation..... 143

3.14 Net precipitation (P_n) with spatially variable gross precipitation (P_g) and interception loss. 144

LIST OF TABLES

Table Page

2.1 Depth, intensity and isotope values of TF and P_g for events during the fall and spring collection periods.. 54

2.2 Spherical variogram model fitting parameters for the spring collection period.. .. 60

3.1 Monthly-mean weather measured at H.J. Andrews over the two years study period. 131

3.2 Interception loss descriptive statistics and meteorological data. 133

3.3 Calculations of annual interception loss using alternate inputs. 136

3.4 Temporal controls over amount of IL and IL variability. 138

3.5 Individual variables' effects on IL variability. 141

3.6 Individual variables' effects on the P_n distribution. 145

Trickle-down Ecohydrology: Complexity of Rainfall Interception and Net Precipitation under Forest Canopies

1 INTRODUCTION

1.1 OVERVIEW

Interception of precipitation is a critical area of study in forest hydrology because interception dramatically alters the amount, spatial distribution, and timing of the precipitation input to the forest floor. Plant canopies intercept and temporarily store a large amount of moisture, typically less than 2 mm, or 0.15 to 0.5 mm per unit leaf area index (Carlyle-Moses and Gash, 2011), but as much as 5 mm has been observed (Pypker *et al.*, 2006). Interception loss (evaporation of intercepted moisture that is retained on canopy surfaces and in the bark matrix) results in a large fraction of the annual water budget being lost due to the evaporation occurring during and between precipitation events. The water that is not evaporated (net precipitation) travels to the forest floor, partitioned between stemflow, flowing along branch and stem surfaces and down the bole of the tree, and throughfall, which splashes off of leaves or trickles down from persistent drip points off branches and leaves (Herwitz, 1987).

In most forested regions, annual interception loss varies between 10 – 50 % of annual precipitation (Carlyle-Moses and Gash, 2011), depending on the vegetation type, evaporation rates, and the precipitation regime. This amount is maximized when small, frequent rainstorms are coupled with high storage capacity forests or high evaporation rates. This is most evident in the coastal mountain ranges of Puerto Rico where annual interception loss exceeds 50% due to small, daily, low-intensity storms (Schellekens, 2000). Perhaps surprisingly, even in the damp climate of northwestern Europe, interception losses can be over 40% (Rutter et al., 1975) due to the frequent

low-intensity rain events. In the Pacific Northwest, interception loss is 10 – 20 % of the annual precipitation, at the lower end of the spectrum despite the high storage capacity of dense coniferous canopies (Rothacher, 1963; Link *et al.*, 2004; Pypker *et al.*, 2005). The interception loss is low because the bulk of annual precipitation occurs during large winter storms, where the canopy storage capacity is far exceeded and evaporation rates are very low (Rothacher, 1963). However, due to meteorological conditions associated with the Pacific Northwest's Mediterranean climate, the warm dry summers have much higher values of interception loss (Rothacher, 1963).

Probably the most prolific area of interception loss research has been the development and parameterization of approaches for predicting interception loss (Rutter *et al.*, 1971; Gash, 1979; Calder, 1986; Valente *et al.*, 1997). These approaches allow for a short period of field measurements to be used in parameterizing a model that can predict interception loss using just meteorological inputs. However, because these modeling approaches are designed for the stand scale (Muzylo *et al.*, 2009), and often applied as a spatially uniform value for the whole-watershed scale (Schellekens, 2000; Fleischbein *et al.*, 2005; Zhang *et al.*, 2006), spatial heterogeneity in interception loss and throughfall depth at smaller scales are often ignored.

Interception processes are highly variable, driven by different processes at different scales. At the tree, plot or stand spatial scale, variations in throughfall depth are due to the physical redistribution of moisture (Levia *et al*., 2011), while the effects of interception loss at this scale are unknown due to measurement challenges.

Between stands, variations in vegetation and microclimate could drive differences in interception loss, resulting in variations in net precipitation across a landscape or watershed. It is necessary to consider the heterogeneity of interception because it is a primary control over the water input to an ecosystem and therefore a control over ecological, hydrological, and biogeochemical processes. Ecological and hydrological systems are regulated by complex, threshold-dependent processes, where the spatial-mean of net precipitation may not be sufficient for characterizing the cumulative effect of net precipitation at every individual point.

1.1.1 Intra-stand heterogeneity

The highly heterogeneous distribution of throughfall underneath single trees or groups of trees is caused by the redistribution of moisture within the canopy (Keim *et al.,* 2005; Bouten *et al.,* 1992; Staelens *et al.,* 2006) and partitioning between various drainage pathways from the canopy (Herwitz, 1987; Moss and Green, 1987; Dunkerley, 2009). Depending on whether a throughfall collector is under a drip point or not, it could receive no throughfall or it could receive > 300 % of the depth of gross precipitation (Keim *et al.,* 2005). This small-scale spatial variability creates considerable difficulties for constraining estimates on the actual amount of interception lost (Holwerda *et al*., 2006).

In addition to being a sampling obstacle, this heterogeneity caused by vegetation's physical structure manipulating the precipitation input could drive ecohydrological processes. The enormously heterogeneous input of net precipitation

to the soil can potentially affect soil moisture distributions (Navar and Bryan, 1990; Bouten *et al.,* 1992; Raat *et al.,* 2002), vegetation survival during drought conditions (Navar and Bryan, 1990), and local subsurface flow rates (Hopp and McDonnell, 2011).

1.1.2 Inter-stand heterogeneity

Spatial heterogeneity has made it difficult to quantify the stand-average interception loss because of the number and spatial extant of samples required. Thus it is also difficult to compare differences between stands. Interception loss, as well as related parameters (i.e. the fraction intercepted and the canopy storage capacity), are extremely variable between stands or plots, even if they are similar by other characteristics of stand structure, most notably leaf area index (Carlyle Moses and Gash 2011). One example is described in Pypker *et al.* (2005): Pypker *et al.* (2005) reported a 25 year-old stand of Douglas-fir to have a storage of 1.26 mm, while Klaasen *et al.* (1998) found a stand of roughly the same age and leaf-area-index (LAI) to have a storage of 2.4 mm. This heterogeneity between seemingly similar stands hinders the feasibility of predicting interception loss where parameters are not directly measured.

We could overcome this site-to-site heterogeneity if there were more well-documented relationships for scaling interception characteristics from commonly measured parameters (e.g. LAI: Keim *et al.,* 2006 ; Normalized Difference Vegetation Index: Jong and Jetten, 2007). Although these relationships are frequently assumed to

be valid (Wigmosta *et al*., 1994; Tague and Band, 2004), there have been very few studies validating them at the inter-stand scale, attributable to the difficulty in obtaining well-constrained field measurements of plot / stand-interception loss. The lack of inter-stand comparisons of interception characteristics severely limits the potential to understand the over-arching controls over these inter-stand differences. As a result, there is little information available on how interception loss varies across a watershed with energy and vegetation variability.

1.2 DESCRIPTION OF CHAPTERS

1.2.1 The role of pre-event canopy water storage on the isotopic composition of throughfall and stemflow

1.2.1.1 Background

In Chapter 2, we tackle the question of what drives the variability of throughfall isotopic composition at the plot-scale. Stable isotopes are extremely useful tracers and indicators of hydrological and ecological processes (Gat, 1996; Marshall *et al.*, 2007). All sources of water are naturally "tagged" with a distinct isotopic composition, determined by the relative abundance of the heavy isotopes (^{2}H, ^{17}O, and ^{18}O) and light isotopes (^{1}H and ^{16}O) of water. These isotopes are stable, meaning that the atom itself does not change and therefore the abundance of each does not change, allowing them to be used as a conservative tracer of flows through ecosystems. Isotopes can be used for tracing water movement through / exchanges to

and from: plants (Flanagan and Ehleringer, 1991; Brooks *et al.*, 2002), soil (Brooks *et al.*, 2009), aquifers (Gat 1974), head-water streams (McDonnell *et al.*, 1991), rivers (Brooks *et al.*, 2012), lakes (Gibson *et al.*, 1996), and the atmosphere (Salati *et al.*, 1979).

Although stables isotopes do not change at the atomic level, the exchange of water molecules between different sources and sinks of water can result in a change of their relative abundance of each isotope via fractionation. Fractionation is a change in isotope ratio as a function of physical and chemical properties associated with the flux into or out of a source/sink. Put simply, heavier isotopes move more slowly, diffuse more slowly, and therefore tend to stay in lower-energy pools (i.e. an evaporating liquid's relative abundance of heavy isotopes in the residual water will increase). Heavier isotopes also have stronger bond strengths, and therefore light isotopes are preferentially used by biological and chemical processes. Fractionation processes create considerable complexity in using stable isotopes as a tracer. However, fractionation provides the physical basis for being able to use isotopes as a meaningful tracer. Because isotopes are a conservative tracer, the isotopic composition of any "parcel" of water is an integration of all of the fractionation and mixing processes it has experienced in its transit through the hydrological cycle.

If fractionation did not occur, there would be no cause for spatial or temporal variations in the isotopic composition of water in the natural environment. These spatio-temporal variations create the basis for differentiating between the sources and processes contributing to a water-body. For example, the isotopic composition varies

between and throughout rain events which allows us to segregate water by age and calculate event-water contribution to streamflow (McDonnell *et al.*, 1991; Uhlenbrook *et al.*, 2002) as well as the transit time distribution (McGuire and McDonnell, 2006). Spatial variation occurs due to the rainout effect: the progressive increase in the relative abundance of light isotopes in a air mass as heavy isotopes preferentially condense and fall as rain (Dansgaard, 1964). Clouds become increasingly depleted of heavy-isotopes as a storm progresses, resulting in isotopically-lighter precipitation at inland and high-elevation locations (Dansgaard, 1964). Temperature and relative humidity are major controls over fractionation as well (Gat, 1996; Kendall and Caldwell, 1998). Temperature determines the fractionation factor for equilibrium conditions (Gat, 1996). Relative humidity determines the relative influence influence of kinetic fractionation versus equilibrium fractionation on fractionation process.

The interception process is a convoluted integration of many isotopic processes: mixing, isotopic exchange, evaporation, and temporal / spatial redistribution. Therefore it is not a surprise that the isotopic composition of net precipitation is highly variable, and different from open precipitation (Dewalle and Swistock, 1994; Brodersen *et al.*, 2000). Our lack of understanding of interception-isotope processes, particularly with respect to the spatial heterogeneity of throughfall isotopic composition, is indicative of how little we know about how water moves within the canopy. Further investigation of the controls over throughfall isotopic composition could provide for a better prediction of throughfall-rain isotope

differences as well as a better understanding of the mechanisms of interception loss and throughfall redistribution.

1.2.1.2 Abstract

Stable isotopes are a valuable tool for research in hydrological processes and are a potential means for better tracing of the redistribution, storage and evaporation associated with rainfall interception. However, this is not currently possible due to a poor understanding of interception-caused isotopic heterogeneity. Isotopic differences between throughfall and rainfall have often been attributed to three mechanisms: evaporation, isotopic exchange, and the temporal redistribution due to selective canopy storage. Selective canopy storage, often identified as the main driver in throughfall-rainfall differences, is an isotopic shift that results from the canopy's varying transmittance of water throughout the event, while the isotopic composition of rain also varies, resulting in a net isotopic difference between rain and throughfall. Evaporative enrichment and isotopic exchange with ambient vapor may also affect throughfall-rainfall differences. We emphasize the potential importance of a fourth mechanism: rainfall mixing with water retained on the canopy and bark from prior rain events, which could be especially important in the dense, moist forests of the Pacific Northwest. We conducted a study to evaluate the relative importance of these four mechanisms and to characterize the spatial variability of throughfall depth and isotopic composition under a Douglas-fir canopy in the Cascade Range of Oregon. Throughfall was often isotopically different from rainfall, but even more pronounced

was the spatial variability of throughfall. The isotopic heterogeneity of net precipitation appeared to be controlled by the varying influence of residual precipitation from previous events. Therefore, isotopic heterogeneity could indicate local storage characteristics, and the partitioning of flow-paths within the canopy.

1.2.2 Spatial Patterns of Interception Loss in Complex Terrain

1.2.2.1 Background

In Chapter 3, we approached the question of how complex terrain drives interception loss variability at a watershed scale, and whether this variability is ecohydrologically significant. This question initially arose due to observations of major differences in throughfall amounts between one of our plots on a north-aspect slope and one on a south-aspect slope, despite their similar vegetation (see Section 2.2). To our knowledge, no previous studies have investigated topography's effects on interception loss, but topography potentially influences all of the characteristics that determine the amount of interception loss: vegetation characteristics, precipitation depth and intensity, and evaporation rates. Therefore, we hypothesize that interception loss could be highly heterogeneous with the spatial distribution driven by topography. We developed a simple 50 m resolution watershed-scale model of distributed solar radiation with spatially explicit vegetation values to estimate interception loss at each grid-cell and investigate the causes of interception loss heterogeneity in complex terrain.

1.2.2.2 Abstract

Spatial heterogeneity exists in the natural environment at all scales. Spatial heterogeneity in throughfall and interception loss is typically addressed either by averaging, or it is left unaddressed. Thus, the potentially dramatic effects of interception loss heterogeneity on ecohydrological processes have been largely ignored. Interception loss (the evaporation of moisture intercepted by plant canopies) typically comprises 10 – 50 % of the annual water budget, depending on local vegetation and climate. The spatial variability of the net precipitation is critical because it implies that interception is a direct control over precipitation input, which is essential to both ecologic and hydrologic processes. In this study, we applied a novel, spatially-explicit approach to modeling interception loss at 50 m resolution across a 1 km^2 watershed in the western Cascades Range of Oregon. The approach accounted for heterogeneity in vegetation, and topography-induced solar radiation and precipitation variability. Using the model, we conducted virtual experiments to elucidate the primary controls over the interception loss heterogeneity, addressing the question, "Why does interception loss vary and does its variability matter?" We found that annual interception loss averaged 10.7 % of gross precipitation, varying spatially from 3.5 % to 14.6 %, mostly reflecting the spatial pattern of the vegetation. However, the spatial variability of interception loss during large storms was fairly small, and did not have a substantial effect on the resulting net precipitation compared to heterogeneity in net precipitation caused by gross precipitation variability. However, interception loss was much higher and more variable for summer rain

events, which could result in spatial variability of a critical moisture input to plants during water-limited conditions.

1.3 REFERENCES

Bouten W, Haimovaara TJ, Tiktak A. 1992. Spatial patterns of throughfall and soil water dynamics in a Douglas fir stand. *Water Resources Research* **28**: 3227-3233.

Brodersen C, Pohl S, Lindenlaub M, Leibundgut C, Wilpert Kv. 2000. Influence of vegetation structure on isotope content of throughfall and soil water. *Hydrological Processes* **14**: 1439-1448.

Brooks JR, Meinzer FC, Coulombe R, Gregg J. 2002. Hydraulic redistribution of soil water during summer drought in two contrasting Pacific Northwest coniferous forests. *Tree Physiology* **22** (15-16): 1107-1117.

Brooks JR, Barnard HR, Coulombe R, McDonnell JJ. 2010. Ecohydrologic separation of water between trees and streams in a Mediterranean climate. *Nature: Geoscience* **3**: 100-104.

Brooks JR, Wigington Jr PJ, Phillips DL, Comeleo R, Coulombe R. 2012. Willamette River Basin surface water isoscape ($\delta^{18}O$ and $\delta^{2}H$): temporal changes of source water within the river. *Ecosphere* **3**(5): Article 39.

Calder IR. 1986. A Stochastic model of Rainfall Interception. *Journal of Hydrology* **89** (1-2): 65-71.

Dansgaard W. 1964. Stable isotopes in precipitation. Tellus **16**: 436-438.

Jong SMd, Jetten VG. 2007. Estimating spatial patterns of rainfall interception from remotely sensed vegetation indices and spectral mixture analysis, *International Journal of Geographical Information Science* **21**(5): 529-545.

Dewalle DR, Swistock BR. 1994. Differences in Oxygen-18 content of throughfall and rainfall in hardwood and coniferous forests. *Hydrological Processes* **8**: 75-82.

Dunkerley DL. 2009. Evaporation of impact water droplets in interception processes: Historical precedence of the hypothesis and a brief literature overview. *Journal of Hydrology* **376**: 599-604.

Flanagan LB, Ehleringer JR. 1991. Stable isotope composition of stem and leaf water: applications to the study of plant water use. *Functional Ecology* **5**: 270-277.

Fleischbein K, Wilcke W, Goller R, Boy J, Valarezo C, Zech W, and Knoblich K. 2005. Rainfall interception in a lower montane forest in Ecuador: effects of canopy properties. *Hydrological Processes* **19**: 1355-1371.

Gash JHC. 1979. An analytical model of rainfall interception by forests. Quarterly *Journal of the Royal Meteorological Society* **105**: 43-55.

Gat JR. 1974. Desert isotope hydrology: water source of the Sinai Desert. *Geochimica et Cosmochimica Acta* **38** (7): 1117-1131.

Gat JR. 1996. Oxygen and hydrogen isotopes in the hydrologic cycle. *Annual review of Earth and Planetary Sciences* **24**: 225-262.

Gibson JJ, Edwards TWD, Prowse TD. 1996. Development and validation of an isotopic method for estimating lake evaporation. *Hydrological Processes* **10**(10): 1369-1382.

Herwitz SR. 1987. Raindrop impact and water flow on the vegetative surfaces of trees and the effects on stemflow and throughfall generation. *Earth Surface Processes and Landforms* **12**: 425-432.

Holwerda F, Scatena FN, Bruijnzeel LA. 2006. Throughfall in a Puerto Rican lower montane rain forest: A comparison of sampling strategies. *Journal of Hydrology* **327** (3-4): 592-602.

Hopp L, McDonnell JJ. 2011. Examining the role of throughfall patterns on subsurface stormflow generation. *Journal of Hydrology* **409**: 460-471.

Keim RF, Skaugset AE, Weiler M. 2005. Temporal persistence of spatial patterns in throughfall. *Journal of Hydrology* **314**: 263-274.

Keim RF, Skaugset AE, Weiler M. 2006. Storage of water on vegetation under simulated rainfall of varying intensity. *Advances in Water Resources* **29**: 974-986.

Kendall C, Caldwell EA. 1998. Fundamentals of Isotope Geochemistry. In *Isotope Tracers in Catchment Hydrology*. Kendall C, McDonnell JJ (eds)., Elsevier Science B.V., Amsterdam. 51-86.

Klaassen W, Bosveld F, Water ED. 1998. Water storage and evaporation as constituents of rainfall interception. *Journal of Hydrology* **212-213**: 36-50.

Levia DF, Keim RF, Carlyle-Moses DE, Forest EE. 2011. Throughfall and stemflow in wooded ecosystems. In *Forest Hydrology and Biogeochemistry: Synthesis of Past Research and Future Directions.* Levia DF, Carlyle-Moses DE, Tanaka T (eds). Springer-Verlag: Heidelberg, Germany.

Link TE, Unsworth MH, Marks D. 2004. The dynamics of rainfall interception by a seasonal temperate rainforest. *Agricultural and Forest Meteorology* **124:** 171-191.

Marshall JD, Brooks JR, Lajtha K. 2007. Sources of variation in the stable isotopic composition of plants. In *Stable Isotopes in Ecology and Environmental Science* (eds). Michener R, Lajtha K. Blackwell Publishing: Malden, MA, USA. 22-60.

McDonnell JJ, Stewart MK, Owens IF. 1991. Effects of catchment-scale subsurface watershed mixing on stream isotopic response. *Water Resources Research* **27**(12): 3065-3073.

McGuire KJ, McDonnell JJ. 2006. A review and evaluation of catchment transit time modeling. *Journal of Hydrology* **330**(3-4): 543-563.

Moss AJ, Green TW. 1987. Erosive effects of the large water drops (gravity drops) that fall from plants. *Australian Journal of Soil Research* **25** (1): 9-20.

Navar J, Bryan R. 1990. Interception loss and rainfall redistribution by three semi-arid growing shrubs in northeastern Mexico. *Journal of Hydrology* **115**: 51-63.

Pypker TG, Bond BJ, Link TE, Marks D, and Unsworth MH. 2005. The importance of canopy structure in controlling the interception loss of rainfall: Examples from a young and an old-growth Douglas-fir forest. *Agricultural and Forest Meteorology* **130** (1-2): 113-129.

Pypker TG, Unsworth MH, Bond BJ. 2006. The role of epiphytes in rainfall interception by forests in the Pacific Northwest. II. Field measurements at the branch and canopy scale. *Canadian Journal of Forest Research* **36**: 819-832.

Raat KJ, Draaijers GPJ, Schaap MG, Tietema A, Verstraten JM. 2002. Spatial variability of throughfall water and chemistry and forest floor water content in a Douglas fir forest stand. *Hydrology and Earth System Sciences* **6**: 363-374.

Rothacher J. 1963. Net Precipitation under a Douglas-fir forest. *Forest Science* **9**(4): 423-429.

Rutter AJ, Kenshaw KA, Robins PC, Morton AJ. 1971. A predictive model of rainfall interception in forests. I. Derivation of the demo from observation in a plantation of Corsican pine. *Agricultural and Forest Meteorology* **9**: 367-384.

Salati E, Dall'Olio A, Matsui E, Gat JR. 1979. Recycling of water in the Amazon basin: An isotopic study. *Water Resources Research* **15** (5): 1250-1258.

Schellekens J. 2000. The interception and runoff generating processes in the Bisley Catchment, Luquillo Experimental Forest, Puerto Rico. *Physics and Chemistry of the Earth, Part B: Hydrology, Oceans and Atmosphere* **25** (7-8): 659-664.

Staelens J, Schrijver AD, Verheyen K, Verhoest NEC. 2006. Spatial variability and temporal stability of throughfall water under a dominant beech (*Fagus sylvatica L.*) tree in relationship to canopy cover. *Journal of Hydrology* **330**: 651-662.

Tague CL, Band LE. 2004. RHESSys: Regional hydro-ecologic simulation system-An object-oriented approach to spatially distributed modeling of carbon, water, and nutrient cycling. *Earth Interactions* **8**: 1-42.

Uhlenbrook S, Frey M, Leibundgut C, Maloszewski P. 2002. Hydrograph separations in a mesoscale mountainous basin at event and seasonal timescales. *Water Resources Research* **38** (6). DOI: 10.1029/2001WR000398.

Valente F, David JS, Gash JHC. 1997. Modeling interception loss for two sparse eucalypt and pine forests in central Portugal using reformulated Rutter and Gash analytical models. *Journal of Hydrology* **190**: 141-162.

Wigmosta MS, Vail LW, Lettenmaier DP. 1994. A distributed hydrology-vegetation model for complex terrain. *Water Resources Research* **30**(6): 1665-1679.

Zhang G, Zeng GM, Jiang YM, Huang GH, Li JB, Yao JM, Tan W, Xiang R, Zhang XL. 2006. Modeling and measurement of two-layer-canopy interception loss in a subtropical evergreen forest of central-south China. *Hydrology and Earth System Sciences* **10** (1): 65-77.

2 THE ROLE OF PRE-EVENT CANOPY WATER STORAGE ON THE ISOTOPIC COMPOSITION OF THROUGHFALL AND STEMFLOW

Allen, S. T.

Brooks, J. R.

Bond, B. J.

McDonnell, J. J.

Journal: *Hydrological Processes*

John Wiley and Sons, Ltd. Massachusetts, USA

In Preparation

2.1 INTRODUCTION

Forest canopies are capable of intercepting large quantities of falling gross-precipitation (P_g), dramatically altering the spatial and temporal inputs of precipitation to forested landscapes (Levia *et al*., 2011). The repeated drying and refilling of the canopy storage can result in a large fraction (10 – 50 %) of the annual precipitation being lost to evaporation (Carlyle-Moses and Gash, 2011). The remaining water that is not evaporated flows down stems as stemflow (SF), and drips or splashes off of branches and leaf surfaces (Herwitz, 1987) as throughfall (TF), resulting in a patchy distribution of water inputs to the forest floor (Bouten *et al.*, 1992; Keim *et al.*, 2005; Staelens *et al.*, 2006) that can have consequences for the hydrology (Gerrits *et al*., 2010; Hopp and McDonnell, 2011) and the ecology of forests (Navar and Bryan, 1990; Raat *et al*., 2002).

Quantifying throughfall and stemflow dynamics is a measurement challenge (e.g. Holwerda *et al*., 2006). Most field studies have employed hydrometric techniques (Levia *et al*., 2011). However, there are potentially other approaches. Naturally occurring, stable isotope tracers of water (^{18}O and ^{2}H) have been highly instructive in other areas of ecohydrology (e.g. Brooks *et al*., 2010). One common application of stable isotopes is quantifying evaporation from bodies of water or entire watersheds (Gibson *et al*., 1996; Kubota and Tsuboyama, 2004). While it may seem reasonable to expect that isotopes could be used to quantify evaporation of intercepted water, previous studies have found this to be unfeasible because the isotopic indicators of evaporation are obscured by isotopic exchange and mixing processes (Dewalle and

Swistock, 1994). As a consequence of the evaporation, mixing, and spatio-temporal redistribution caused by the canopy, the isotopic composition of TF and SF can be highly different from rainfall (Saxena, 1986 ; Dewalle and Swistock, 1994; Brodersen *et al.*, 2000; Kubota and Tsuboyama, 2003).

Previous TF isotope studies have focused on three factors that could drive the differences between TF and P_g, which will undoubtedly cascade through the entire hydrologic system, affecting soil water, groundwater, and streamwater (Gibson *et al.*, 2000; Kubota and Tsuboyama, 2003). These three factors are: evaporation from the canopy during or between storms (Saxena, 1986; Dewalle and Swistock, 1994); the so-called selective canopy storage effect, where water is differentially retained or transmitted by the canopy throughout storms (Dewalle and Swistock, 1994; Brodersen *et al*., 2000; Ikawa *et al.*, 2011); and isotopic exchange with ambient vapor in the canopy air-space (Saxena, 1986; Kendall, 1993; Ikawa *et al.*, 2011). Evaporation is unlikely to have a large effect unless the intercepted moisture evaporates between events and washes down during the subsequent event (Gat and Tzur, 1967); otherwise, isotopic exchange may control fractionation during the high humidity conditions associated with interception loss (Kendall, 1993). However, most studies have attributed the bulk of TF-P_g differences to selective storage, which may cause TF to be isotopically heavier than P_g through a process in which the last segment of a storm, which is generally most depleted, remains retained on the canopy after the storm ends, not contributing to the TF (Dewalle and Swistock, 1992).

In humid forested catchments, particularly in energy limited systems such as the Pacific Northwest of the USA, we also need to consider that a substantial amount of water may be retained within the canopy between events (Pypker *et al*., 2011). The role of pre-event canopy water storage on the isotopic composition of throughfall and stemflow has not been sufficiently considered. Here we examine the effect of pre-event canopy water on TF-P_g isotopic differences and TF isotopic heterogeneity for several storms through the Fall wet-up cycle at the H.J. Andrews Experimental Forest in Oregon, USA. Our conception going into this work is that since the rainfall isotopic composition changes from event to event (Brooks *et al*., 2010), so too could the canopy water retained in the leaves, needles, branches and bark from the previous event. We hypothesize this residual water contributes greatly to the isotopic composition of TF. To illustrate such an effect, we consider a canopy saturated with the last 3 mm of a rain event with $\delta^{18}O$ of -25 ‰, which is immediately followed by a storm of 30 mm depth that has a mean $\delta^{18}O$ of -3 ‰; fractionation excluded, this could result in a $\delta^{18}O$ of throughfall being -2 ‰ less than rainfall, just from mixing. We further hypothesize that enrichment of the residual water could enhance the differences caused by pre-event canopy water if the following storm is isotopically lighter than the previous event, or diminish the effect if the following storm is isotopically heavier.

The objective of this study is to (1) investigate the controls over and causes of isotopic heterogeneity and (2) characterize the spatial relationships and patterns of the isotopic composition of throughfall. We use the background variability of

meteorological conditions as a natural experiment to test the hypothesis that pre-event canopy water has a measurable effect on observed $\triangle\delta^{18}O$ and d-excess values. We combine results from two sampling periods. We use a dual isotope approach for a sequence of eleven events collected during the Fall 2010 wet-up to assess pre-event canopy water's effect with dual-isotope variations of incremental P_g, bulk TF, and SF. We then use a Spring 2011 dataset to focus on the spatial patterns, using a high spatial resolution collector deployment but lower temporal resolution than the Fall period.

2.2 METHODS

2.2.1 Site description

This study was conducted in Watershed 1 (WS1) of the H.J. Andrew's Experimental Forest in the western Cascade Range of Oregon. The steeply-sloped, 960 m^2 basin was clear-cut harvested in the late 1960's and is now covered with a dense canopy dominated by Douglas-fir (*Pseudotsuga menziesii*), western hemlock (*Tsuga heterophylla*), red alder (*Alnus rubra*) and bigleaf maple (*Acer macrophyllum*). The climate is typical of the Pacific Northwest with annual precipitation of over 2000 mm with 80% falling between October and April. The climate, vegetation, management history, and geology of the H.J. Andrews and of WS1 have been extensively described in previous work (e.g. Jones and Grant, 1996; Moore *et al.*, 2004). All TF collection was at plots at roughly 500 m elevation.

2.2.2 Fall sample collection

The sampling plot used for the Fall 2010 measurements was located on a 75 m long section of a north-south transect crossing the riparian area in WS1. Rainfall was collected in a clearing 100 m away. The canopy cover in this plot was dominated by Douglas-fir. Canopy cover and storage capacity were not quantified for this plot, but were likely similar to the Spring collection sites (described in section 2.3).

TF and P_g were collected using commercially fabricated rain gages (EZ-read, Headwind Consumer Products) which have a plastic float for easy visibility; for our purposes, this float functions to reduce air exchange and evaporation from the water surface. The gages had a 9.5 cm diameter opening. Thirteen TF collectors and two P_g collectors were used. All TF gages were placed under Douglas-firs. Additionally SF was collected off of two trees in WS1 (both 40 cm diameter). The SF collectors were made from sliced Tygon tubing sealed with silicone caulk (e.g. Herwitz, 1986) routed into 20 l plastic containers. We did not calculate relative depth and contribution of SF because of our small sample size. SF collection and passively collected incremental samples (Kennedy *et al.,* 1979; McDonnell *et al.,* 1990) of P_g began during the third collection period.

Storms were sampled per-event, only after precipitation ceased so the entire wet-up to drip process could be accounted for. Logistical constraints forced some sampling periods to last several days and consist of multiple consecutive storm events. Intra-event dry periods never exceeded 2 days. This resulted in a total of 11 collection periods. Potential for evaporation from collectors is low over this period with a mean relative humidity of 99% over the Fall collection periods.

2.2.3 Spring sample collection

After observing considerable spatial variability in the Fall period, we increased spatial frequency of collection to better observe spatial patterns. Two plots were established, one north-aspect-plot (NAP) and one south-aspect-plot (SAP), on steep slopes to maximize energy differences. Both plots were laid out in a rectangular shape of 12 m x 5 m. SAP had a canopy cover of 92% and NAP has a cover of 95% estimated using Fusion software (United Stated Forest Service Remote Sensing Applications Center, Salt Lake City, UT) from a LiDAR flight in August, 2008. Canopy storage was estimated using an iterative dual-regression line method (Licata *et al.*, 2011) with a 9 m x 0.1 m trough leading to a tipping bucket; we estimated storage to be 2.6 mm in the SAP and 2.9 mm in the NAP.

For the Spring period, TF and rainfall were collected on a roughly weekly interval from April 2011-June 2011. However the sampling periods were often extended to avoid sampling during an event. Within the sampling periods, there was never more than 1 calendar-day without rain. There were a total of seven collection periods between April 2011 and July 2011 used for the analyses in this paper (Table 1). TF and P_g were collected in 2 l polyethylene bottle attached to 15.5 cm diameter funnels. The volume of each collector was measured and a 20 ml subsample was taken with a 20 ml glass vial for isotope analysis. Three collectors were used as P_g collectors, placed in a clearing 180 m from the two TF collection sites. Thirty-six collection points were randomly positioned in each plot. Eighteen TF collectors were

used at each plot and were randomly relocated among the thirty-six fixed locations for each sampling period.

2.2.4 Ancillary measurements

Meteorological data were measured at the H. J. Andrews benchmark meteorological station, "PrimeMet" (Henshaw *et al.*, 1998) located ~500 m from the study plots. This station was used for relative humidity measurements and calculating rainfall intensity as the average hourly P_g depth for every hour in which there was rain throughout the collection period. Positions of collectors and trees within each of NAP and SAP were surveyed manually.

2.2.5 Analyses

All isotope data are expressed in terms δ values in units of ‰ with δ calculated as,

$$\delta = \left(\frac{R_{sample}}{R_{V-SMOW}} - 1\right) \times 1000\ ‰$$

where V-SMOW is the Vienna Standard Mean Ocean Water (Kendall and Caldwell, 1998) and R is the ratio of $^{18}O/^{16}O$ or $^{2}H/^{1}H$. Water samples were analyzed for $\delta^{2}H$ and $\delta^{18}O$ on a LGR LWIA (Los Gatos Research, Mountain View, CA) by the Institute for Water and Watersheds Collaboratory (Corvallis, Oregon). The isotope analysis accuracy was 0.18 ± 0.07 ‰ and -1.02 ± 0.92 ‰ (mean ± standard error) for $\delta^{18}O$ and $\delta^{2}H$ respectively, calculated from the deviation of a third standard from an interpolated value estimated using the other two standards. All three standards were used in the

actual data calibration which would further improve accuracy beyond the reported precision. The precision was 0.07 ‰ and 0.28 ‰ for $\delta^{18}O$ and $\delta^{2}H$ respectively. Samples from the Spring 2011 dataset were analyzed on a Picarro L-1102 CRDS isotope analyzer (Picarro Inc., Santa Clara, CA). The accuracy of our analyses was -0.28 ± 0.09 ‰ and -0.68 ± 0.77 ‰ for $\delta^{18}O$ and $\delta^{2}H$ respectively, calculated using the same protocol as for the Fall dataset. The precision is 0.12 ‰ and 0.57 ‰ for $\delta^{18}O$ and $\delta^{2}H$ respectively.

The index d-excess was often used in the presentation of results, where d-excess = $\delta^{2}H - 8(\delta^{18}O)$. This index describes deviation from the meteoric water line (MWL) and can be used to indicate kinetic (i.e. non-equilibrium) fractionation effects of evaporation (Kendall, 1993) (Fig. 2.1). With lower humidity, faster evaporation rates reduce discrimination and decrease the slope of $\delta^{2}H$ versus $\delta^{18}O$, and thus greater deviations from the meteoric water line (Gat, 1996). In this paper, TF $\delta^{18}O$ and d-excess values are often reported as $\triangle$ values, indicating the TF $-P_g$ difference (i.e. $\triangle\ \delta^{18}O = TF\ \delta^{18}O - P_g\ \delta^{18}O$).

All statistical analyses were run on MATLAB (MathWorks Natick, MA) except for regression line fitting which was done on Sigmaplot 12.0 (SYSTAT Chicago IL), and mixing model calculations with IsoSource (Phillips and Gregg, 2003; EPA Western Ecology Division, Corvallis, OR). Isosource was used to quantify relative proportions of P_g increments contributing to TF. Only $\delta^{2}H$ data were used for the mixing model analysis because dual isotopes were unnecessary since the data mostly fell along a line.

2.2.5.1 Time-stability plots

Although the proportion of TF relative to P_g varied significantly from one sampling position to another, temporal stability of the spatial pattern was analyzed with time-stability plots (Keim *et al.,* 2005) by determining if the relative proportion tended to be consistent over time. This was done for depth, $\delta^{18}O$ and d-excess. All data points were normalized for each event by subtracting the event mean and dividing by the event standard deviation. The assumptions of normality and homoscedasticity were met for TF depth for NAP, SAP, tested using a Schapiro-Wilk Test and Levene's test respectively. A Tukey honestly significant difference multiple comparison test was conducted using the one way analysis of variance test (ANOVA) statistics of all collectors at each plot to calculate a 95% confidence interval around each collector's mean relative depth. Although Fall depth, $\delta^{18}O$ and d-excess, and Spring $\delta^{18}O$ and d-excess data were not normally distributed, we applied the Kruskall-Wallis test, a non-parametric analog to the ANOVA.

2.2.5.2 Variograms

Variograms were used to assess the spatial dependence between the collector locations for values of TF depth, $\delta^{18}O$, and d-excess. Experimental variograms (Matheron, 1963; Keim *et al.,* 2005) were created with the semivariance, γ, defined as

$$\gamma = 0.5 \cdot (z_x - z_{x+h})^2$$

Where z_x refers the value of the parameter of interest (Depth, d-excess or $\delta^{18}O$) at a single point and z_{x+h} refers to the value at another point separated by a lag

distance of h. The maximum lag distance in our analyses was fixed at one half of the highest observed lag distance within each plot. The semivariances were binned into 15 evenly spaced bins evenly dividing the distance from zero to the maximum lag distance. For the experimental variograms, the average semivariance for each bin was plotted against the mean lag distance. A spherical variogram model was fit to each of the variograms, defining the best fit values for the nugget (c_0) sill (c) and range (a) (Diggle and Riberio, 2007). The spherical variogram model used is defined as:

$$\gamma_{sph}(h) = \begin{cases} c_0 + c \cdot (1.5 \cdot \frac{h}{a} - 0.5 \left(\frac{h}{a}\right)^3) & \text{for } 0 \leq h \leq a \\ c_0 + c & \text{for } h > a \end{cases}$$

The range is the maximum distance at which there is observed correlation. The sill is the value where the semivariance stabilizes once the lag distance exceeds the range. The nugget is described by the y intersect representing the background "noise" or variability between points infinitely close.

2.3 RESULTS

2.3.1 Controls over throughfall isotopic composition

2.3.1.1 Overview

The interception loss (1-TF/P_g) during the Fall period (mean = 13 %) was lower than it was for the Spring period (mean = 31 %), which was expected because Fall events had greater continuous precipitation and higher humidity (Table 2.1). For

the Fall, △TF $\delta^{18}O$ was positive for eight out of eleven events (Table 2.1), equal to P_g for two events, and depleted for one event ($p < 0.05$). F10, the lowest depth event also had a $\triangle\delta^{18}O$ of -1.1 ‰, but d-excess was not also different from P_g. Event-mean TF d-excess was not consistently greater or less than that of P_g. For the Spring, $\delta^{18}O$ of TF was heavier than P_g for both plots for all collection periods (at $p < 0.01$) except for S2 ($p = 0.014$ for N-Aspect and $p = 0.07$ for S-Aspect). Overall, the greatest TF-P_g difference was event S5 with a 1.8 ‰ $\triangle\delta^{18}O$.

For both the Spring and Fall periods, the events with the lowest depths generally had the highest isotopic deviation from rainfall; however there was no statistically significant relationship between event size and the absolute value of $\triangle\delta^{18}O$. $\triangle\delta^{18}O$ was not strongly correlated with event size, interception loss, or precipitation intensity for the Fall or Spring. Surprisingly, △d-excess was inversely correlated with event depth ($r^2 = 0.38$, $p < 0.05$) and precipitation intensity ($r^2 = 0.67$, $p < 0.05$) for the Fall, which is the opposite of what would be expected if evaporation was controlling d-excess values.

TF depth variability was fairly consistent from event to event with the low end of the range being 20-40 % and the high end frequently exceeding 100 % of P_g (Fig. 2.2), especially for one collector (hereafter Collector1) in the Fall period that often had a TF depth fraction exceeding 200 %. Within single sampling periods, there was typically a range of TF $\delta^{18}O$ exceeding 1 ‰ but as high as 3.7 ‰ in F5 (Fig. 2.2). TF d-excess similarly was highly variable within certain events with simultaneous positive and negative values of △d-excess. The spatial range in d-excess exceeded 8

‰ in one event (F7). In addition to frequently receiving very high TF depths, Collector1 (marked with an X in Fig. 2.2), in the Fall dataset, also tended to have the largest deviation from P_g's isotopic composition, but not in a consistent direction. Another collector, Collector2 (Fig. 2.2), also had highly variable isotopic compositions and depths, which illustrated some degree of threshold effects. In most events where SF was measured (Fig. 2.2), the absolute value of SF $\triangle\delta^{18}O$ was greater than the 90 % CI of TF, but not consistently heavier or lighter than TF (Fig. 2.3).

2.3.1.2 Residual moisture effect on TF – P_g differences

If the throughfall isotopic composition was a mixture of the current event's precipitation and the residual canopy water from the previous event's precipitation, then events preceded by events with a higher $\delta^{18}O$ should have more positive $\triangle\delta^{18}O$ of TF and events that are preceded by events with a lower $\delta^{18}O$ should have lower $\triangle\delta^{18}O$ of TF. Events following a more enriched event had an average $\triangle\delta^{18}O$ of 0.63 ± 06 ‰ and events following a more depleted event had an average $\triangle\delta^{18}O$ of 0.30 ± 0.06 ‰ (mean ± pooled SE). Because humidity was always high, we can also use d-excess as an indicator of mixing. There also was a significant ($\alpha = 0.05$) difference in the $\triangle$d-excess of TF between events preceded by higher (0.79 ± 0.13 ‰) versus lower $\triangle$d-excess values (-1.00 ± 0.2 ‰). $\triangle$d-excess of both TF and SF for the Fall was strongly correlated with the difference between each event's d-excess and the previous event's d-excess ($r^2 = 0.55$ and $r^2 = 0.76$ respectively) (Fig. 2.4). There was a weaker negative correlation for $\triangle\delta^{18}O$. F1 and F10 were excluded because we did not have

data for the immediately preceding event. The correlation between $\triangle\delta^{18}O$ and $\triangle$d-excess versus the differences between events suggests the potential importance of carryover between events.

2.3.1.3 Residual moisture effect on TF heterogeneity

Dual isotope plots of the Fall events (Fig. 2.3) revealed strong evidence of residual moisture controlling heterogeneity in throughfall isotopic composition. The Fall dataset was used for these analyses because the sampling periods were shorter and thus samples did not integrate over multiple events.

We considered each plot (Fig. 2.3) as a mixing diagram, where both TF and SF measurements must have been a mixture of the contributing end-members, which included incremental P_g and the previous events residual moisture (assumed to be equal to the previous storm's last P_g increment). Most of the collectors' TF isotopic compositions were bracketed by many incremental rainfall samples, so the relative proportions could not be calculated. However, TF Collector1 and SF were frequently skewed from the middle of the mixture. With excluding the previous event's moisture: event F7's Collector1's TF had to have received 45-73 % of its volume from the first of six incremental samples, F11's third P_g increment contributes 68-83 % of the SF's isotopic composition and for F4, 67-88 % of the SF isotopic composition appears to have come from the ninth of eleven increments. These examples illustrated that it was difficult to explain the observed isotopic compositions of SF and Collector1 when the residual moisture's effect was excluded.

With the previous event added into the models as an additional end-member (i.e. residual moisture of the canopy reservoir), it reduced the previously heavily-weighted increments to a potential minimum contribution of zero percent; that is, no longer did a majority of the isotopic composition of SF or TF come from single increments. The weighting of those single increments reduced so dramatically because SF, and often Collector1, deviated from P_g in the same direction as the isotopic composition of the previous event (Fig. 2.3). The only event where SF did not deviate from P_g was F6, which followed a four day drying period, minimizing the residual storage. The effect of this drying period was also illustrated by the relatively lower depth of TF at Collector1, likely because storage deficit had to be refilled.

2.3.1.4 Evaporation

Only at the most coarse time-scale, between seasons, did isotopic differences appear to indicate differences in evaporation. Coinciding with the higher Spring interception loss, Spring TF $\triangle\delta^{18}O$ was greater (0.67 ± 0.02 ‰; mean ± pooled SE), than Fall $\triangle\delta^{18}O$ (0.32 ± 0.02 ‰; mean ± pooled SE) and the $\triangle$d-excess of the Spring period (-0.80±0.06 ‰; mean± pooled SE) was lower than the $\triangle$d-excess of the Fall period (-0.36 ± 0.13 ‰; mean ± pooled SE).

Within either season, isotopic enrichment was not related to the amount evaporated, which is consistent with other studies (Dewalle and Swistock, 1994; Brodersen *et al.*, 2000) that also reported not seeing an evaporation signal. Also, TF did not consistently plot below the MWL and we were also not able to distinguish any

evaporative differences between the NAP and SAP. Differences in the evaporation of the residual moisture could either cause increases or decreases in TF $\delta^{18}O$ depending on the direction of fractionation, the amount of residual moisture, and isotopic difference between the residual moisture and the next rain event.

2.3.1.5 Selective storage

Selective storage has been identified as the primary reason why TF's isotopic composition is more positive than P_g: precipitation at the end of a rainstorm is usually the most isotopically depleted and precipitation at the end of storm remains intercepted and does not contribute to TF (Pionke and Dewalle, 1992; Dewalle and Swistock, 1994). However this process cannot have caused all of the positive values of $\triangle\delta^{18}O$ that we observed because only two out of the seven events with incremental samples became more depleted throughout the event (F7, F9). For the other five events (F4, F5, F6, F8, and F11), where the last incremental sample was more enriched than the average P_g bulk sample (in the "V" pattern described by Kendall [1993]), selective storage alone would have resulted in TF being isotopically lighter than P_g. However, TF $\delta^{18}O$ was lighter than P_g values for only F8 of the V events, and heavier for F4, F5, F6 and F11, suggesting that selective storage did not cause the TF-P_g isotopic differences.

Further, the mixing model analysis, which indicated the need to include residual moisture as an end-member, also establishes that selective storage alone could not have feasibly resulted in observed isotopic compositions of TF and SF. SF and

Collector1 TF were not always skewed towards the beginning of the event, and they were not always isotopically heavier (Fig. 2.3).

2.3.2 Spatial relationships of throughfall isotopic composition and depth

There were no immediately discernible spatial patterns in the relative depth or isotopic composition (Fig. 2.5). However, TF depth and $\delta^{18}O$ (Fig. 2.6) followed a typical variogram form (Matheron, 1963) where semivariance increased with lag distance, indicating that proximity was related to similarity in isotopic composition and depth. However, d-excess observations did not fit a variogram model form. The nugget was near/at the origin in both plots for both $\delta^{18}O$ and depth. The variograms demonstrate a degree of spatial autocorrelation for $\delta^{18}O$ up to a range of 3 m (Table 2.2) for $\delta^{18}O$, which was larger than the expected correlation range .

The distance to the nearest tree for each collector was tested as an explanatory variable driving variation in TF depth and $\delta^{18}O$ and d-excess (Fig. 2.7). Only depth versus distance on the SAP had a statistically significant regression line ($p < 0.05$), which only explained 20 % of the variability in TF depth.

We also found that the spatial variability of d-excess decreased toward the stem of trees in the SAP (Fig. 2.8), quantified by plotting the standard deviation of time-averaged d-excess values of sets of six binned collectors against the distance to the nearest stem ($r^2 = 0.76$). Pooling the NAP and SAP results, we found that $\delta^{18}O$ variability also decreased significantly closer to the stem of trees ($r^2 = 0.37$; $p < 0.05$). Alternatively we observed TF depth values tended to be more variable towards the

stem but not at a 0.05 level of significance. If the selective storage effect was controlling this variability, more intercepted water in the canopy center should result in a greater selective storage effect, and therefore a bigger isotopic deviation from P_g. However, we observed spatial variability decreased closer to the stem of trees, which is the opposite of what we would expect selective storage to cause. Thus, selective storage does not appear to be a dominant control over TF isotope variability.

The spatial distribution of TF depth was generally persistent from event to event in both the Spring and Fall datasets, illustrated by the time-stability plots (Fig. 2.9). That is, high-depth locations remained high-depth, and low-depth locations remained low-depth. For both the Fall and Spring collection periods, patterns were not stable for either $\delta^{18}O$ or d-excess. The averaging of non-persistent normalized values caused the mean $\delta^{18}O$ and d-excess to be almost constant across all of the collectors for the Fall dataset, despite that collectors with a high $\delta^{18}O$ deviation for one event, tended to deviate more in both directions around the mean for other events (Fig. 2.9).

For the Fall, each collector's depth was, on average, different from 2.15 other collectors (KW test, $\chi^2 = 67.68$, df = 12, $p < 0.001$). For the Spring, depth at each collector was significantly different from an average of 9.8 other collectors on the SAP (ANOVA test, $F = 12.94$, df = 35, $p = < 0.001$) and 2.6 other collectors on NAP ($F = 5.45$, df = 35, $p < 0\ .001$). The TF $\delta^{18}O$ and d-excess data were similarly tested, and we found that no collectors were significantly different from each other for Fall or Spring.

The residual moisture effect is evident in the Fall period's time-stability plot. Collectors that have large deviations from the mean, deviate in both directions of the mean indicating collector locations that have a bigger interaction with residual moisture. Alternatively, if we had observed the direction of deviation was temporally stable, this might have indicated evaporative fractionation controlling the distribution because we would expect relative evaporation rates to be a function of location and therefore be stable. However, they were not stable (Fig. 2.9).

If all of the events' P_g followed a persistent isotope temporal pattern (e.g. Rayleigh distillation or the "V" pattern), the time-stability plots would also indicate whether selective storage was a major control on the spatial variability. Collectors with greater localized storage capacity would consistently deviate more from P_g because more of the end of the storm would remain intercepted. We re-created the time-stability plots for the Fall dataset (Fig. 2.10) using just events where the last increment was more enriched than the total P_g, so we would expect collectors with normalized isotopic composition to be persistent among these events if selective storage was determining the isotopic composition. However we again observed that normalized depth was persistent, but $\delta^{18}O$ and d-excess were not.

2.4 DISCUSSION

The goal of this study was to understand the role of pre-event canopy water storage, selective storage, and evaporative fractionation on the isotopic composition of throughfall and stemflow. We found that residual canopy water indeed played an

important role in the isotopic differences between rainfall, throughfall, and stemflow. We did not observe any indicators of selective storage or evaporation affecting TF and SF isotopic compositions, but that does not negate their potential impact. However, it does suggest that selective storage is not the primary control over TF isotopic composition in this environment, and that it does not always result in the last increment of rain being withheld. Spatial patterns and relationships were generally not very strong; however, the lack of temporal stability in relative isotopic composition further supports the residual moisture hypothesis.

2.4.1. Residual moisture: a primary control over TF isotopic composition?

For every event where there was moisture on the stem or canopy at the start of the event, that moisture must affect the throughfall isotopic composition. Our results cannot confirm this for certain, but the general trends suggest that residual canopy moisture is important. After the second rain event of the Fall sampling period, the duration of rainless periods were generally less than a day, and relative humidity was always high. Even if the residual films on leaf surfaces dried out, bark and epiphytes can hold a substantial amount of water (Pypker *et al.*, 2011); additionally bark has a morphology that can minimize evaporation rate and maximize retention times (Pypker *et al.*, 2011). While this bark storage component could become evaporated in between events (Gat and Tzur, 1967), the storm to storm difference (on average 4.1 ‰ $\delta^{18}O$ and 5.5 ‰ d-excess) was probably more significant than fractionation under the high humidity conditions we observed.

In our analyses, we implicitly made the assumption that fractionation of the residual moisture was negligible. Under high humidity conditions, fractionation is driven by isotopic exchange (Gat, 1996), which would have little effect if the vapor in the canopy air-space is in equilibrium with the precipitation at the end of the previous event (Dansgaard, 1964). For that reason it also was safe to use d-excess as an indicator of mixing, rather than evaporation, since fractionation effects on d-excess would be minimal during high humidity conditions. Transpired water would likely not contribute to the ambient vapor isotopic composition because of the small vapor pressure gradient. However, we do not actually know how these factors might affect the inter-event fractionation of residual water. We do know that residual moisture was not the only factor affecting isotopic composition of TF and SF because otherwise we would have observed negative $\triangle\delta^{18}O$ of TF as often as positive.

Residual moisture carryover has the potential to cause spatial variability of TF through three mechanisms: variability in intra-event evaporation resulting in an isotopically homogeneous canopy reservoir; variability in canopy storage capacity and therefore amount of residual water; and variability in the degree of mixing with that residual water. Bark moisture could greatly enhance the potential residual moisture effect on stemflow and throughfall pathways that have greater travel and source water from a larger area of the canopy. Interactions with bark moisture may explain why the biggest isotopic deviation were observed in SF and the TF collector that demonstrated an extended period of filling storage deficits.

2.4.2 Implications and Applications

2.4.2.1 Insights to rainfall partitioning

The partitioning of throughfall into various isotopically distinct points of net precipitation under the canopy indicated a level of partitioning beyond just the "throughfall" and "stemflow" classifications.

The similarity between SF and Collector1 indicated that the TF flowing to Collector1 had a similar substantial interaction with the residual water. Higher depth flow-paths source water from further distances, and therefore have more storage deficit to fill (Herwitz, 1987). Once filled, the areas with a greater deficit would be saturated with a larger reservoir to mix with. After the Collector1 flow path was active by the third event, this collector consistently received TF depths far exceeding the 90 % confidence interval and was isotopically different from the mean of TF. Event F6 was an exception because it was preceded by an extended drying period.

Besides Collector1, the rest of the collectors seemed to receive TF that had much less interaction with residual moisture and a less apparent flow threshold. Alternatively, the isotopic composition of the high-depth areas suggests that water traveling to these points had a substantially different interaction with the canopy. There is a potential explanation for these differences: Moss and Green (1987) described TF as being composed of both "gravity" droplets, which are large droplets that collect and drip off the canopy, and "impact" droplets that result from intercepted rain splashing off of the canopy, which can result in thousands of splash droplets, some smaller than 5 µm radius (Dunin *et al.*, 1988; Murakami, 2006; Dunkerley, 2009).

The differences in the gravity droplets versus impact droplets could account for our observed isotopic heterogeneities. Ikawa *et al.* (2011) described the potential for rapid isotopic exchange of falling impact droplets, which would occur nearly instantaneously because small droplets can equilibrate with vapor within meters of falling (Friedman *et al.*, 1962), with minimal kinetic fractionation (Miyake *et al.*, 1968; Stewart, 1975). Alternatively if the drip-points for gravity droplets are sourcing moisture from a larger area, mixing with bark water along the way, these large droplets are going to be composed of more residual moisture and have less exchange while falling. A range of TF isotopic variations could result from various mixtures of gravity droplets and impact droplets received at different points under the canopy.

With TF partitioned into two components, one with substantial interaction with bark-moisture and one without, we must consider how mixing with bark (Levia and Herwitz, 2005), and running along branch surfaces (Puckett, 1991) may have ecological and biogeochemical significance. If functionally important, this isotopic heterogeneity between TF samples could indicate persistent biogeochemically-distinct hot spots (Zimmermann *et al.*, 2007). The coupling of the high-flow locations with also being chemically distinct may have unknown ecohydrological importance.

2.4.2.2 Limits of residual moisture effect and relevance in other environments

The limits of the residual moisture effect are determined by: (1) the amount of storage, (2) the temporal variability in rain's isotopic composition, and (3) the frequency of rain events. Therefore, the frequent rain and dense coniferous forests of

the Pacific Northwest may maximize the residual moisture effect. SF has a much higher potential effect from residual moisture because trunk storage can be nearly as high as canopy storage (Rutter *et al.,* 1975), but SF typically only makes up 5 – 10 % of the net precipitation (Rutter *et al.,* 1975; Pypker *et al.,* 2005). Thus there is a higher ratio of trunk-storage:SF than canopy-storage:TF. TF-P_g (and SF-P_g) isotopic variations could be enhanced by any attributes of the tree that increase storage and decrease evaporation rates such as epiphytes (Pypker *et al.,* 2006); epiphytic mosses and lichens were present on the tree above Collector1.

While no other studies have reported the residual moisture effect, Dewalle and Swistock's (1994) data do show some evidence of a residual moisture effect. Re-plotting their data for just consecutive events (time between sampling is less than three days), we found a trend in their data similar to what we saw in our data: a relationship between $\triangle\delta^{18}O$ and difference between successive events P_g (Fig. 2.11). This only gave us 5 data points for each species, but they Fall along a line with the slope (i.e. strength of effect from residual moisture carryover) apparently ranked by relative storage capacity: spruce with highest, pine, and deciduous with the least storage (Fig. 11). Less storage would result in less residual moisture. However, this study did not provide enough data to make any strong inferences regarding the residual moisture effect, and this was just an exploratory analysis.

2.4.2.3 Assessing local storage capacity

The residual moisture effect needs to be validated by measuring the isotopic composition of bark and canopy water as well as amount of storage immediately previous to rain events. This could be verified using a simple mixing model of P_g and canopy storage to see how well TF isotopic composition can be predicted.

If the residual moisture effect is verified as the primary control of TF-P_g isotopic differences, there is an opportunity for a new method of estimating local storage capacity. Measurements of mean TF, P_g, and pre-event canopy / bark isotopic composition, as well as P_g and TF depth could be used to quantify mean canopy storage capacity. Alternatively, if we did not know the pre-event canopy / bark isotopic composition, but we did have an estimate of the plot-mean storage through traditional methods (Rutter *et al.*, 1971), we could solve for mean pre-event canopy/bark water isotopic composition. Using the mean canopy isotopic composition, P_g depth, P_g isotopic composition, and each individual collector's depth and isotopic composition, we could solve this mixing model for each collector to get the localized canopy storage associated with each individual collector. This could provide a potentially quicker and less data intensive method of measuring local storage size of local storage (Link *et al.*, 2004; Carlyle-Moses *et al.*, 2004), compared to the other methods requiring sampling over numerous events (Link *et al.*, 2004).

2.4.2.4 Throughfall sampling

Our results allow new insight to sampling throughfall for isotopic composition in environments where residual moisture might affect TF isotopic composition. For

isotope techniques that are used on a single-event time-scale, it is necessary to sample TF at multiple points because single TF $\delta^{18}O$ measurements deviated from the mean by as much as 3 ‰. Based on measurements from Collector1 and Collector2, collectors that had a depth threshold effect also were accompanied with large isotopic deviations, which is consistent with the residual moisture hypothesis. Therefore, depth outliers should be regarded with caution.

Regarding accumulated throughfall over an entire season, heterogeneity can also be important. Individual TF collectors' weighted-mean depths and isotopic compositions were considerably different from the entire season's spatial-mean TF (Fig. 2.12), but much less so than it was for individual events. For isotope measurement, it may be beneficial to keep a collector in the same location consistently because collectors that had large positive deviations from the mean also had large negative deviations (i.e. averaging itself out as demonstrated by Fig. 2.9), although this will result in a poorer estimate of TF depth (Holwerda *et al.*, 2006). Even though Gibson *et al*. (2000) found that Tf-P_g differences are unimportant on the seasonal time-scale, our data shows that variations within TF can exceed the difference between TF and P_g.

Spatial variability decreased towards the stem of the tree, which would make closer to the stem a more ideal location for sampling. However, more data from other sites is necessary to validate this finding. Ultimately, the most important way to reduce error is to increase number of throughfall samples, regardless of the study's

spatial extant, as has been reported by numerous studies (e.g. Kendall, 1993; Genereux and Hooper, 1998).

2.4.3 On the effects of selective storage and evaporation

It is well known that both evaporation and some form of selective storage take place as part of the interception process because evaporation of intercepted water undoubtedly occurs (Carlyle-Moses and Gash, 2011) and it is well documented that interception results in precipitation time shifts (e.g. Keim and Skaugset, 2004). Additionally, if residual moisture was the only control over Tf-P_g differences, these differences would average out to zero over an extended period of measurement, which was not what we observed. However it is unclear how these processes affect the isotopic composition of TF.

2.4.3.1 Evaporation

By regressing event interception loss against event-mean TF $\delta^{18}O$ enrichment and not finding any significant relationship, other studies have concluded that evaporation was not a primary control over TF-P_g isotopic differences (DeWalle and Swistock, 1994; Brodersen *et al.*, 2000). Our results were similar. However, common isotopic indicators of evaporation (i.e. enrichment and deviation from the MWL) are not appropriate for distinguishing evaporation at 99 % relative humidity. During high humidity conditions, the vapor isotopic composition is going to control the near-equilibrium fractionation processes (Kendall, 1993). If the evaporation of impact-

droplets (Murakami, 2006) causes most of evaporation, then the evaporation process would result in minimal fractionation (Friedman et al., 1962).

It seems equally unlikely to expect differences in fractionation to cause TF isotopic heterogeneity, evidenced by the lack of temporal stability in relative isotopic composition for each collector. Very little is known about intra-canopy variations of the evaporation rate, although it undoubtedly varies due to differences in air movement through the canopy (Daudet *et al.,* 2007). But because exchange overwhelms the evaporative influence (Saxena, 1986), it is more important to determine how variability in exchange could affect TF isotopic composition, which has yet to be determined.

2.4.3.2 Selective storage

Although others identified selective storage as the primary control over TF isotopic composition (Gat, 1996), there is generally not strong evidence for selective storage. Often the justification for selective storage has been the lack of an alternative explanation for TF-P_g differences, which is not adequate. In studies where interception loss was not correlated with $\triangle\delta^{18}O$, the difference has been attributed to selective storage because there was no evident evaporative enrichment signal (Dewalle and Swistock, 1994; Brodersen *et al.,* 2000). However, neither Dewalle and Swistock (1994) or Brodersen *et al.* (2000) used incremental measurements of P_g or dual isotopes which are essential for disentangling the effects of evaporation and selective storage from other processes. Kendall (1993) also hypothesized that TF isotope

variations were due to selective storage but settled at just verifying that selective storage could have theoretically resulted in the magnitude of observed TF-P_g variations (using incremental measurements of P_g).

Although TF was isotopically heavier than P_g for the majority of events, in agreement with other studies (Saxena, 1986; Dewalle and Swistock, 1994; Brodersen *et al.*, 2000), we could not also attribute our results to selective storage because we know that P_g increments did not follow a continual depletion trend. It was also evident that selective storage could not account for the full range of spatial heterogeneity and did not have a persistent effect on individual collectors. However, this does not discount the possibility of selective storage having an effect on isotopic composition of TF; selective storage may just be stochastic in nature, confounding the effects of other processes, as opposed to a systematic exclusion of the last rainfall increment (Dewalle and Swistock, 1994).

Brodersen *et al.* (2000) attributed strong isotopic heterogeneity to selective storage to explain why they observed light TF (as low as -1.9‰ $\triangle\delta^{18}O$) in one location of the catchment and heavier (> 1 ‰ $\triangle\delta^{18}O$) in another location during the same event. For these differences to have been caused by selective storage, the temporal pattern of transmittance by the canopy must have varied drastically between the plots. With our data, we are unable to comment on selective storage as a stochastic process capable of causing such differences. Our results show a considerable amount of heterogeneity not accounted for by the residual moisture effect, so it is clear that other processes are causing isotopic variations in TF.

Conceptually, the occurrence of some form of selective storage seems undeniable: the differences in local storage capacity should cause differences in selective storage that affect the spatial variability of TF isotopic composition by varying the temporal input of P_g to TF. However, if the falling precipitation was always well mixed with the canopy reservoir, this would diminish selective storage effects. Further research on the degree of mixing in the canopy could help explain how selective storage functions.

2.4.4 Unanswered questions

2.4.4.1 Why did we not see stronger spatial patterns?

Spatial factors seemed relatively unimportant as drivers in pattern of TF isotope processes. This does not agree with the results of Brodersen *et al*. (2000), which showed different TF depths and isotopic compositions between inner and peripheral canopy space. We observed that TF depth slightly spatially dependent to a scale of meters, which was surprising because the processes we identified as causing variability were unlikely to be similar on that scale. The presence of one drip point (sourcing water from a larger area than the collector) should reduce the likelihood of other drip-points being nearby. It is also not surprising that TF isotopic composition was not temporally stable if the residual moisture effect was the primary control over TF heterogeneity. Whether the previous storm is high versus lower will have opposing effects on TF isotopic composition at each collector, averaging out to near zero over many events.

2.4.4.2 Why d-excess increased with intensity?

If evaporative enrichment was driving isotopic fractionation, we would have expected d-excess to decrease with decreasing precipitation intensity, but we observed the opposite. Splash droplet evaporation can potentially explain the unexpected relationship between d-excess and intensity. Dunin *et al.* (1988) hypothesized that drag from the atmosphere on falling raindrops will increase with rainfall intensity, which will pull down dry air from above the canopy and replace near-saturated air, increasing evaporation. This quick turnover could result in the kinetic fractionation signal shown by the d-excess values. Splash droplets would become in equilibrium with this fractionated vapor. To our knowledge, this ventilation process has not yet been investigated (Dunkerley, 2009).

2.5 CONCLUSIONS

Our study, in agreement with previous studies, has shown that TF's isotopic composition can be significantly different than P_g, and there are rarely simple linear relationships that explain these differences. However one consistent feature was the apparent effect of the residual moisture retained on the canopy. It is likely that a large component of residual moisture from previous rain events was retained within bark and on the canopy, which, in mixing with the new rainfall resulted in a striking heterogeneity of throughfall and stemflow isotopic compositions. We infer that this heterogeneity was caused by various degrees of mixing with the residual moisture reservoir, dependent on the path along which the intercepted water flowed. This

isotopic heterogeneity illuminates the variety and importance of the pathways intercepted water can travel to the forest floor.

2.6 Acknowledgements

Data and facilities and financial support were provided by the HJ Andrews Experimental Forest research program, funded by the National Science Foundation's Long-Term Ecological Research Program (DEB 08-23380), US Forest Service Pacific Northwest Research Station, and Oregon State University. We thank Paul Sims, Allison Danner, and Matthias Ritter for field assistance and Tina Garland and Caroline Patrick for assistance in lab analyses.

2.7 References

Bouten W, Haimovaara TJ, Tiktak A. 1992. Spatial patterns of throughfall and soil water dynamics in a Douglas fir stand. *Water Resources Research* **28**: 3227-3233.

Brodersen C, Pohl S, Lindenlaub M, Leibundgut C, Wilpert Kv. 2000. Influence of vegetation structure on isotope content of throughfall and soil water. *Hydrological Processes* **14**: 1439-1448.

Brooks JR, Barnard HR, Coulombe R, McDonnell JJ. 2010. Ecohydrologic separation of water between trees and streams in a Mediterranean climate. *Nature: Geoscience* **3**: 100-104.

Carlyle-Moses DE, Gash JHC. 2011. Rainfall interception loss by forest canopies. In *Forest hydrology and biogeochemistry: synthesis of past research and future directions*. Levia DF, Carlyle-Moses D, Tanaka T (eds). Ecological Studies. Vol. **216**. Springer: New York.

Craig H, Gordon LI. 1965. Deuterium and oxygen-18 variations in the ocean and the marine atmosphere. *Stable Isotopes in Oceanographic Studies and Paleotemperatures*. Ed. E. Tongiorgi. 9-130.

Carlyle-Moses DE, Laureano JSF, Price AG. 2004. Throughfall and throughfall spatial variability in Madrean oak forest communities of northeastern Mexico. *Journal of Hydrology* **297**: 124-135.

Dansgaard W. 1964. Stable isotopes in precipitation. *Tellus* **16**: 436-438.

Daudet FA, Roux XL, Sinoquet H, Adam B. 1999. Wind speed and leaf boundary layer conductance variation with tree crown consequences on leaf-to-atmosphere coupling and tree functions. *Agricultural and Forest Meteorology* **97**: 171-185.

Dewalle DR, Swistock BR. 1994. Differences in Oxygen-18 content of throughfall and rainfall in hardwood and coniferous forests. *Hydrological Processes* **8**: 75-82.

Diggle PJ, Ribeiro PJ. 2007. *Model-based Geostatistics*. Springer, New York, NY.

Dunin FX, O'Loughlin EM, Reyenga W. 1988. Interception loss from eucalypt forest: Lysimeter determination of hourly rates for long term evaluation. *Hydrological Processes* **2**(4): 315-329.

Dunkerley DL. 2009. Evaporation of impact water droplets in interception processes: Historical precedence of the hypothesis and a brief literature overview. *Journal of Hydrology* **376**: 599-604.

Friedman I. 1962. Water-vapor exchange between a water droplet and its environment. *Journal of Geophysical Research* **67**: 2761-2766.

Gat JR, Tzur Y. 1967. Modification of the isotopic composition of rainwater by processes which occur before groundwater recharge. *Proceeding of the Symposium on Isotopes in Hydrology*. International Atomic Energy Agency, Vienna. 14-18 November 1966; 49-60.

Gat JR. 1996. Oxygen and hydrogen isotopes in the hydrologic cycle. *Annual review of Earth and Planetary Sciences* **24**: 225-262.

Genereux DP, Hooper RP. 1998. Oxygen and Hydrogen isotopes in rainfall-runoff Studies. In *Isotope Tracers in Catchment Hydrology*. Kendall C, McDonnell JJ (eds). Elsevier Science B.V.: Amsterdam; 319-346

Gibson JJ, Price JS, Aravena R, Fitzgerald DF, Maloney D. 2000. Runoff generation in a hypermaritime bog-forest upland. *Hydrological Processes* **14**: 2711-2730.

Gibson JJ, Edwards TWD, Prowse TD. 1996. Development and validation of an isotopic method for estimating lake evaporation. *Hydrological Processes* **10**(10): 1369-1382.

Gerrits AMJ. 2010. The role of interception in the hydrological cycle. PhD thesis, Delft University of Technology, Delft.

Gerrits AMJ, Pfister L, Savenije HHG. 2010. Spatial and temporal variability of canopy and forest floor interception in a beech forest. *Hydrological Processes* **24**: 3011- 3025. DOI: 10.1002/hyp.7712

Herwitz SR. 1986. Infiltration-excess caused by stemflow in a cyclone-prone tropical rainforest. *Earth Surface Processes and Landforms* **11**(4): 401-412.

Herwitz SR. 1987. Raindrop impact and water flow on the vegetative surfaces of trees and the effects on stemflow and throughfall generation. *Earth Surface Processes and Landforms* **12**: 425-432.

Henshaw DL, Bierlmaier FA, Hammond HE. 1998. The H.J. Andrews climatological field measurement program. *In Data and information management in the ecological sciences: a resource guide*. Michener WK, Porter JH, Stafford SG, (eds). 117–122. LTER Network Office, University of Mexico.

Holwerda F, Scatena FN, Bruijnzeel LA. 2006. Throughfall in a Puerto Rican lower montane rain forest: A comparison of sampling strategies. *Journal of Hydrology* **327** (3-4): 592-602.

Hopp L, McDonnell JJ. 2011. Examining the role of throughfall patterns on subsurface stormflow generation. *Journal of Hydrology* **409**: 460-471.

Ikawa R, Yamamoto T, Shimada J, Shimizu T. 2011. Temporal variations of isotopic composition in gross rainfall, throughfall, and stemflow under a Japanese cedar forest during a typhoon event. *Hydrological Research Letters* **5**: 32-36.

Kennedy VC, Zellweger GW, Avanzino RJ. 1979. Variation of rain chemistry during storms at two sites in northern California, *Water Resources Research,* **15**(3): 687–702.

Keim RF, Skaugset AE. 2004. A linear system model of dynamic throughfall rates beneath forest canopies. *Water Resources Research* **40**: W05208, doi:10.1029/2003WR002875.

Keim RF, Skaugset AE, Weiler M. 2005. Temporal persistence of spatial patterns in throughfall. *Journal of Hydrology* **314**: 263-274.

Kendall C, Caldwell EA. 1998. Fundamentals of isotope geochemistry. In *Isotope Tracers in Catchment Hydrology*. Kendall C, McDonnell JJ (eds). Elsevier Science: Amsterdam; 51-86.

Kendall C. 1993. Impact of isotopic heterogeneity in shallow systems on stormflow generation. PhD dissertation. University of Maryland: College Park MD.

Kubota T, Tsuboyama Y. 2003. Intra and inter-storm oxygen-18 and deuterium variations of rain, throughfall, and stemflow, and two-component hydrograph separation in a small forested catchment in Japan. *Journal of Forest Research* **8**: 179-190.

Kubota T, Tsuboyama Y. 2004. Estimation of evaporation rate from the forest floor using oxygen-18 and deuterium compositions of throughfall and stream water during a non-storm runoff period. *Journal of Forest Research* **9**: 51-59.

Levia DF, Keim RF, Carlyle-Moses DE, Forest EE. 2011. Throughfall and stemflow in wooded ecosystems. In *Forest Hydrology and Biogeochemistry: Synthesis of Past Research and Future Directions.* Levia DF, Carlyle-Moses DE, Tanaka T (eds). Springer-Verlag: Heidelberg, Germany.

Levia DF, Herwitz SR. 2005. Interspecific variation of bark water storage capacity of three deciduous tree species in relation to stemflow yield and solute flux to forest soils. *Catena* **64** (1): 117-137.

Licata JA, Pypker TG, Weigandt M, Unsworth MH, Gyenge JE, Fernandez ME, Schlichter TM, Bond BJ. 2011. Decreased rainfall interception balances increased transpiration in exotic ponderosa pine plantations compared with native cypress stands in Patagonia, Argentina. *Ecohydrology* **4**: 83-93.

Link TE, Unsworth MH, Marks D. 2004. The dynamics of rainfall interception by a seasonal temperate rainforest. *Agricultural and Forest Meteorology* **124**: 171-191.

Matheron G. 1963. Principles of Geostatistics. *Economic Geology* **58** (8): 1246-1266.

McDonnell JJ, Bonell M, Stewart MK, Pearce AJ. 1990. Deuterium variations in storm rainfall: Implications for stream hydrograph separation. *Water Resources Research* **26**: 455-458.

Miyake Y, Matsubaya O, Nishihara C. 1968. An isotopic study on meteoric precipitation. *Papers in Meteorology and Geophysics* **19**: 243-266.

Moss AJ, Green TW. 1987. Erosive effects of the large water drops (gravity drops) that fall from plants. *Australian Journal of Soil Research* **25** (1): 9-20.

Murakami S. 2006. A proposal for a new forest canopy interception mechanism: Splash droplet evaporation. *Journal of Hydrology* **319**: 72-82.

Pionke HB, Dewalle DR. 1992. Intra-and inter-storm $\delta^{18}O$ trends for selected rainstorms in Pennsylvania. *Journal of Hydrology* **138** (1): 131-143.

Phillips DL, Gregg JW. 2003. Source partitioning using stable isotopes: coping with too many sources. *Oecologia* **136**, pp. 261-269.

Puckett LJ. 1991. Spatial variability and collector requirements for sampling throughfall volume and chemistry under a mixed-hardwood canopy. *Canadian Journal of Forest Research* **21**: 1581-1588.

Pypker TG, Levia DF, Staelens J, Van Stan JR. 2011. Canopy structure in relation to hydrological and biogeochemical fluxes. In *Forest Hydrology and Biogeochemistry: Synthesis of Past Research and Future Directions*. Levia DF, Carlyle-Moses DE, Tanaka T (eds). Springer-Verlag: Heidelberg, Germany.

Pypker TG, Unsworth MH, Bond BJ. 2006. The role of epiphytes in rainfall interception by forests in the Pacific Northwest. II. Field measurements at the branch and canopy scale. *Canadian Journal of Forest Research* **36**: 819-832.

Raat KJ, Draaijers GPJ, Schaap MG, Tietema A, Verstraten JM. 2002. Spatial variability of throughfall water and chemistry and forest floor water content in a Douglas fir forest stand. *Hydrology and Earth System Sciences* **6**: 363-374.

Saxena RK. 1986. Estimation of canopy reservoir capacity and Oxygen-18 fractionation in throughfall in a pine forest. *Nordic Hydrology* **17**: 251-260.

Stewart MK. 1975. Stable isotope fractionation due to evaporation and isotopic exchange of falling water drops: applications to atmospheric sciences and evaporation of lakes. *Journal of Geophysical Research* **80**: 1133-1146.

Staelens J, Schrijver AD, Verheyen K, Verhoest NEC. 2006. Spatial variability and temporal stability of throughfall water under a dominant beech (*Fagus sylvatica L.)* tree in relationship to canopy cover. *Journal of Hydrology* **330**: 651-662.

Zimmerman A, Wilcke W, Elsenbeer H. 2007. Spatial and temporal patterns of throughfall quantity and quality in a tropical montane forest in Ecuador. *Journal of Hydrology* **343** (1-2): 80-96.

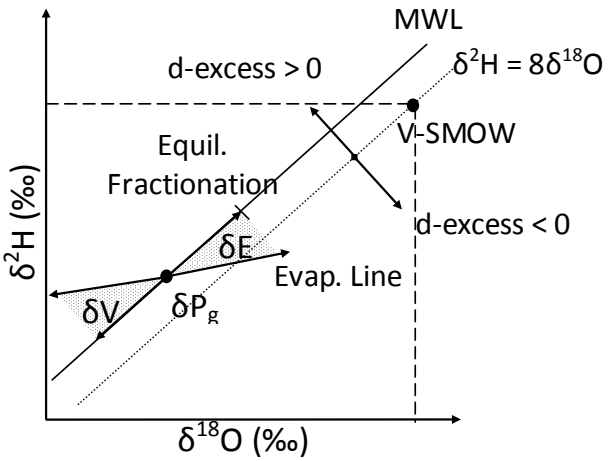

Figure 2.1 Conceptual diagram of water fractionation processes plotted in dual isotope space. δP_g is the precipitation, falling along the Meteoric Water Line (MWL) with a d-excess of 10. δE is the isotopic composition of an evaporated source, and δV indicates the vapor coming from this source. Adapted from Gat (1996).

Table 2.1 Depth, intensity and isotope values of TF and P_g for events during the fall and spring collection periods. Data are reported as mean ± standard deviation. △ indicates the difference of throughfall minus gross precipitation.

		Fall Rain				Fall TF			Fall TF-P_g differences		
	Events	Depth (mm)	Intensity (mm/hr)	$\delta^{18}O$ (‰)	d-excess (‰)	Depth (mm)	$\delta^{18}O$ (‰)	d-excess (‰)	Loss (%)	$\triangle\delta^{18}O$ (‰)	△d-excess (‰)
F1	10-9 to 10-10	39.6	1.7	-6.7	11.7	30 ± 6	-6.7 ± 0.3	11.0 ± 0.4	24	0.0	-0.7
F2	10-22 to 10-23	14.2	0.8	-9.7	10.3	10 ± 3	-8.5 ± 0.4	11.1 ± 0.6	28	1.3	0.8
F3	10-23 to 10-24	62.2	2.9	-14.2	13.0	52 ± 9	-14 ± 0.4	11.2 ± 0.8	16	0.4	-1.8
F4	10-24 to 10-27	81.9	1.7	-8.8	21.7	68 ± 22	-8.4 ± 0.4	20.5 ± 1.0	17	0.4	-1.2
F5	10-27 to 11-2	42.6	0.8	-10.1	8.4	40 ± 27	-9.3 ± 0.9	10.0 ± 0.7	6	0.8	1.6
F6	11-2 to 11-8	52.1	1.5	-15.4	9.6	43 ± 9	-15 ± 0.4	8.4 ± 2.2	17	0.4	-1.2
F7	11-8 to 11-10	48.7	1.5	-10.9	16.7	46 ± 27	-10 ± 0.5	16.4 ± 2.5	5	0.5	-0.3
F8	10-10 to 10-16	31.8	0.6	-6.2	11.8	30 ± 8	-6.2 ± 0.2	11.8 ± 1.1	5	0.1	0.0
F9	11-16 to 11-19	44.7	2.0	-10.9	12.7	42 ± 21	-10 ± 0.3	12.8 ± 0.6	7	0.7	0.1
F10	12-6 to 12-8	10.8	1.1	-9.9	15.0	9 ± 3	-11 ± 0.4	15.4 ± 1.2	21	-1.1	0.4
F11	12-8 to 12-10	48.7	1.7	-7.5	18.7	44 ± 27	-7.2 ± 0.3	17.1 ± 1.5	9	0.3	-1.7

		Spring Rain				Spring South Aspect Plot TF			TF-P_g differences		
	Events	Depth (mm)	Intensity (mm/hr)	$\delta^{18}O$ (‰)	d-excess (‰)	Depth (mm)	$\delta^{18}O$ (‰)	d-excess (‰)	Loss (%)	$\triangle\delta^{18}O$ (‰)	△d-excess (‰)
S1	4-2 to 4-9	82.7	1.4	-9.7	11.0	58 ± 18	-9 ± 0.3	10 ± 1.2	30	0.7	-0.8
S2	4-10 to 4-16	90.6	1.1	-12.7	10.4	63 ± 17	-13 ± 0.3	11 ± 0.6	31	0.1	0.5
S3	4-20 to 4-26	64.7	0.9	-8.0	8.5	37 ± 11	-7.3 ± 0.2	8.5 ± 0.8	42	0.7	0.1
S4	5-2 to 5-12	35.0	0.7	-9.6	6.4	19 ± 6	-9.3 ± 0.2	5.2 ± 0.7	47	0.3	-1.2
S5	5-15 to 5-22	24.6	0.8	-8.1	11.4	14 ± 4	-6.1 ± 0.3	9.4 ± 1.0	45	2.0	-1.9
S6	5-22 to 5-27	69.4	1.3	-10.0	8.9	45 ± 14	-9.8 ± 0.2	8.4 ± 0.6	36	0.2	-0.5
S7	6-28 to 7-1	15.4	1.0	-8.0	4.5	9 ± 4	-7.2 ± 0.2	2.6 ± 0.8	38	0.8	-1.9

	Spring North Aspect Plot TF			TF-P_g differences		
	Depth (mm)	$\delta^{18}O$ (‰)	d-excess (‰)	Loss (%)	$\triangle\delta^{18}O$ (‰)	△d-excess (‰)
S1	68 ± 14	-8.9 ± 0.2	11 ± 0.9	18	0.8	-0.1
S2	72 ± 12	-13 ± 0.2	10 ± 0.5	20	0.1	0.1
S3	48 ± 9	-7.4 ± 0.2	8.9 ± 0.7	25	0.6	0.5
S4	21 ± 4	-9.3 ± 0.1	5.6 ± 0.7	39	0.3	-0.8
S5	15 ± 4	-6.5 ± 0.4	9 ± 1.4	40	1.6	-2.3
S6	49 ± 13	-9.8 ± 0.3	8.5 ± 1.1	29	0.2	-0.4
S7	11 ± 2	-7.2 ± 0.3	2.2 ± 1.0	28	0.7	-2.3

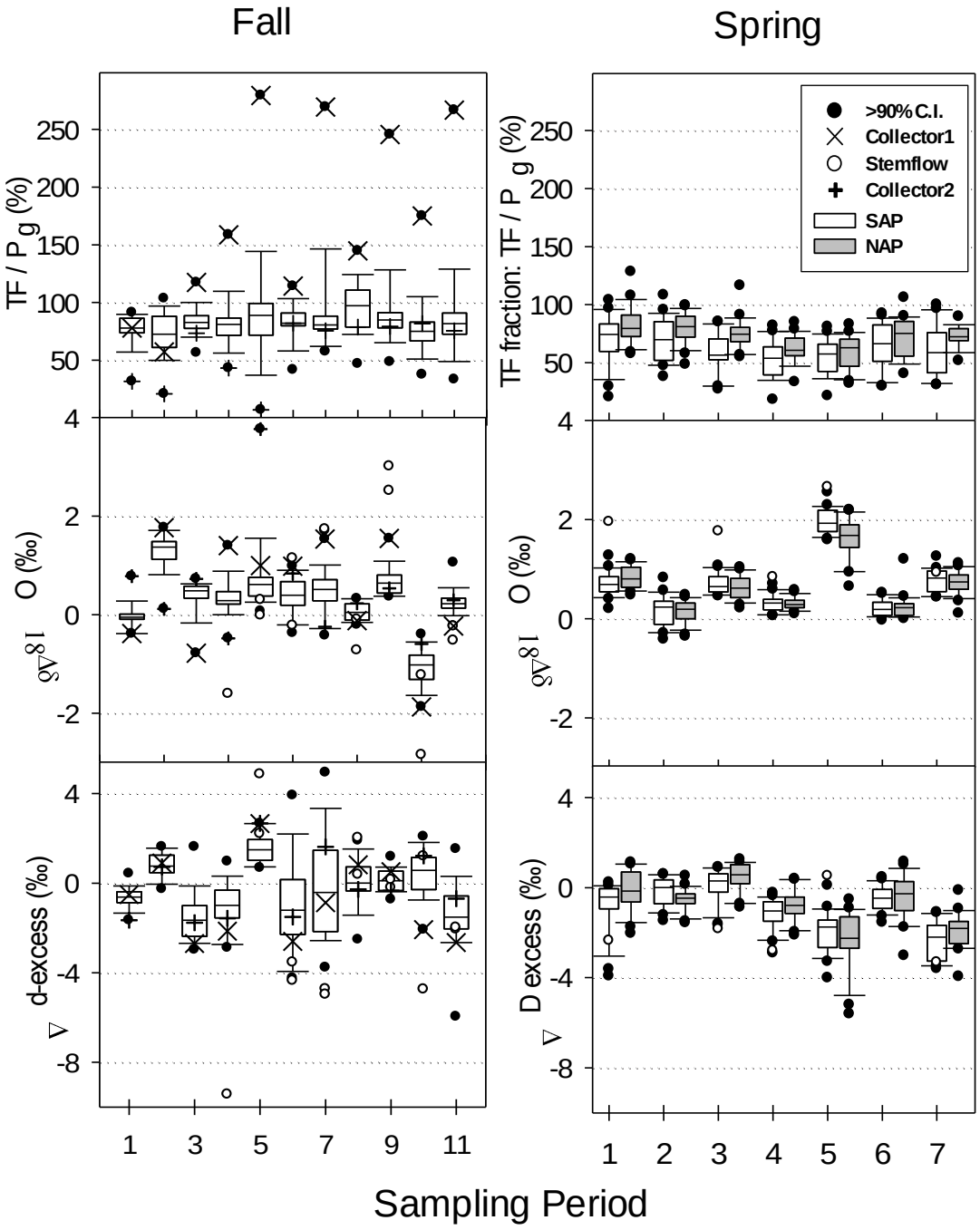

Figure 2.2 Box-plots for throughfall (TF) depth fraction (TF/P_g), and relative $\triangle(TF\text{-}P_g)$ $\delta^{18}O$ and d-excess for 11 events in the fall and 7 events in the spring sampling periods. The box-plots show the 90% confidence interval of throughfall, with filled circles indicating throughfall samples exceeding this interval. For the fall period, two outlier throughfall collector's values are marked, named Collector1 and Collector2. Stemflow is indicated for events when it was sampled with an open circle. Dates associated with these sampling periods are listed in Table 1.

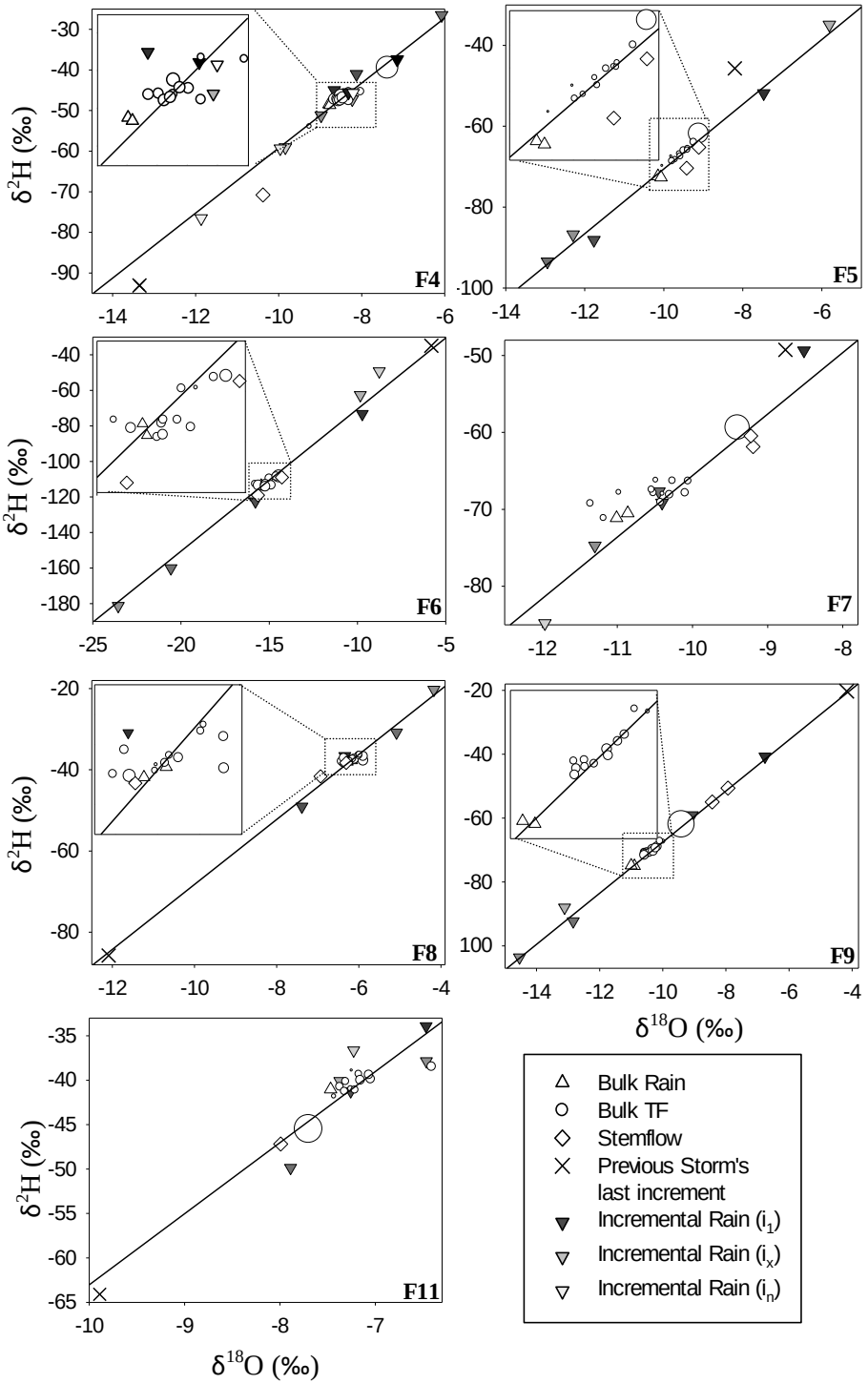

Figure 2.3 Dual isotope plots for select events in the fall collection periods' rain, throughfall, and stemflow. Event MWL is indicated by the line, with a slope of 8 intersecting the origin at the precipitation's mean d-excess. Size of the bulk TF symbols are scaled to relative TF depth. Incremental samples are indicated by downward triangles becoming lighter with successive increment.

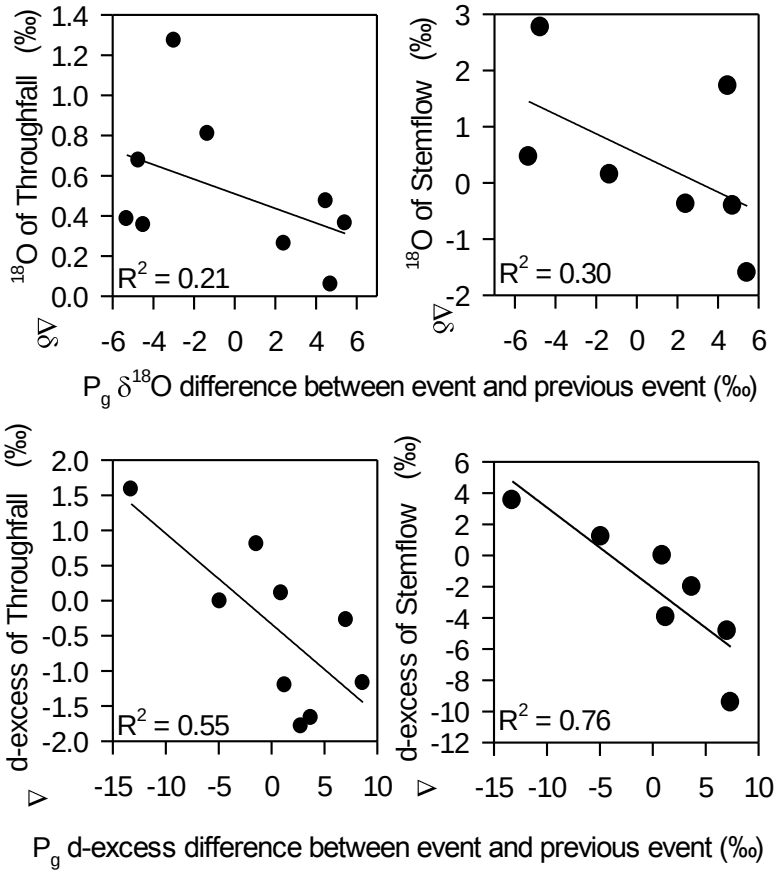

Figure 2.4 Previous event differences versus TF-P_g differences. $\triangle\delta^{18}O$ (top) and $\triangle$d-excess (bottom) of throughfall (left) and stemflow (right) are plotted against, respectively, the difference between each event and the previous event's $\delta^{18}O$ (top) and d-excess (bottom) for the fall dataset.

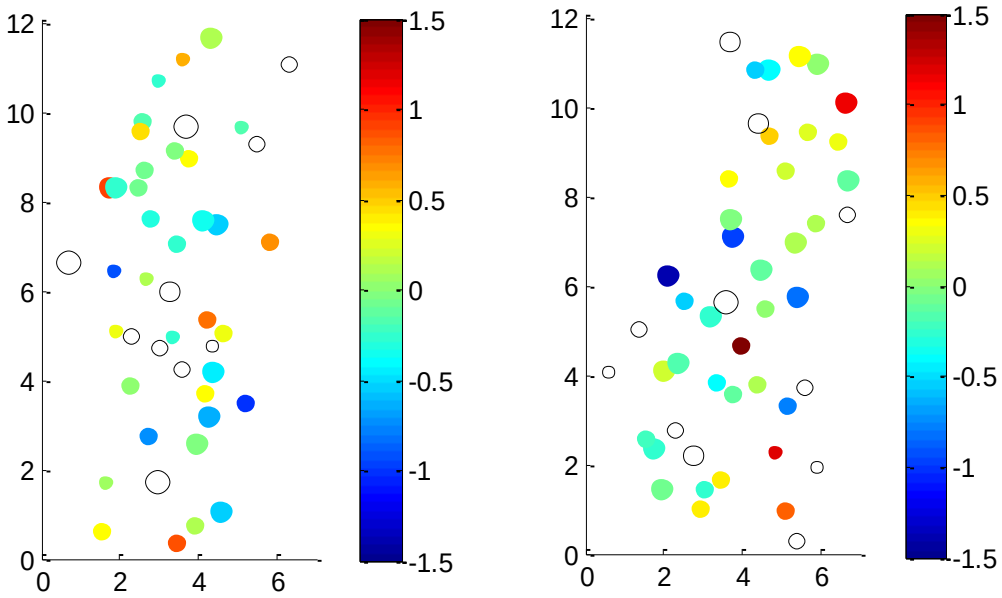

Figure 2.5 Plot layout for the two plots of the spring collection period. The x and y axes indicating distance in meters. Color indicates relative normalized $\delta^{18}O$ value and size indicating relative depth. Open circle are locations of trees, scaled to size.

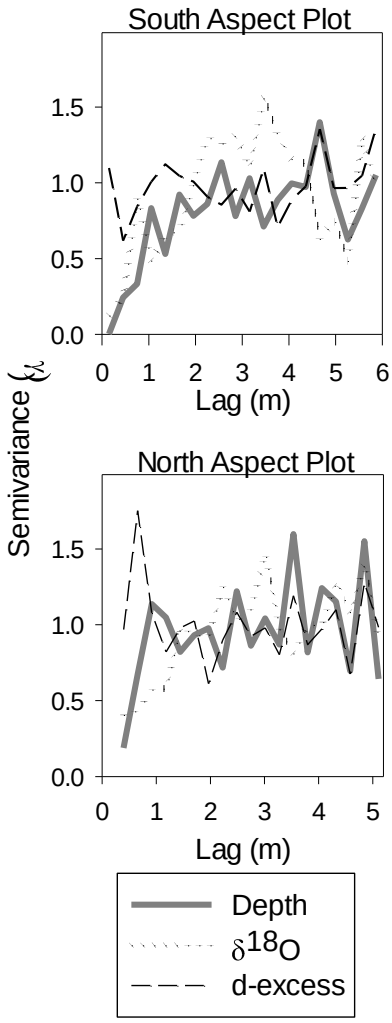

Figure 2.6 Experimental variograms for SAP (top) and NAP (bottom) of the spring collection period.

Table 2.2 Spherical variogram model fitting parameters for the spring collection period. Nugget refers to the value at the origin, sill is the value the variance stabilizes at, and the range is the distance until the variance reaches the sill.

	South-Aspect		North-Aspect	
	Depth	$\delta^{18}O$	Depth	$\delta^{18}O$
Nugget	0	0.1	0	0
Sill	1.1	0.9	1	1.1
Range	2.7	3	1.2	2.4

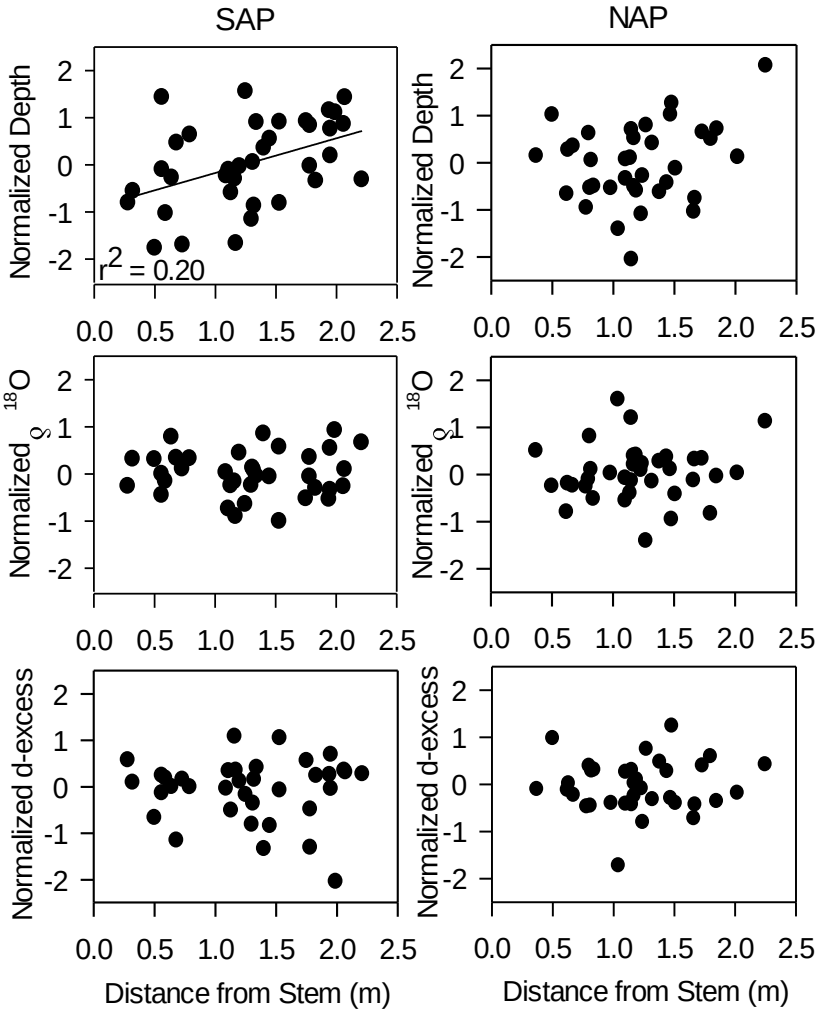

Figure 2.7 Depth and isotopic composition versus distance from stem. Normalized depth, $\delta^{18}O$, and d-excess versus distance from stem for the North Aspect Plot (NAP) and South Aspect Plot (SAP) for the spring collection period. Each marker indicates a single collector's normalized values averaged over time.

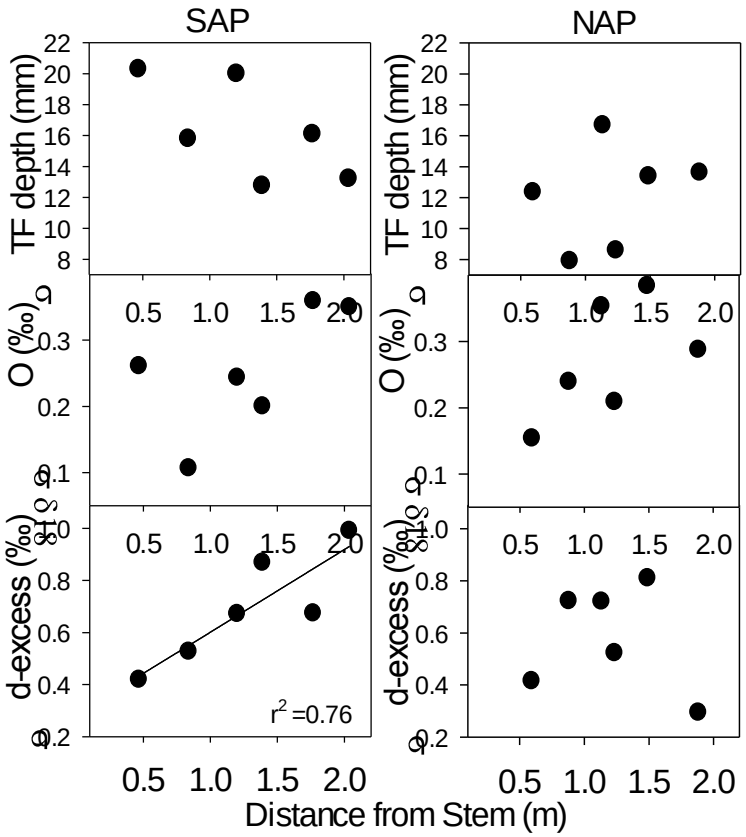

Figure 2.8 Spatial variability versus distance from stem for the North Aspect Plot and South Aspect Plot from the spring collection period. Spatial variability is quantified as the standard deviation (σ) of binned throughfall collector mean values. The 36 collectors at each plot were divided into six bins of six collectors.

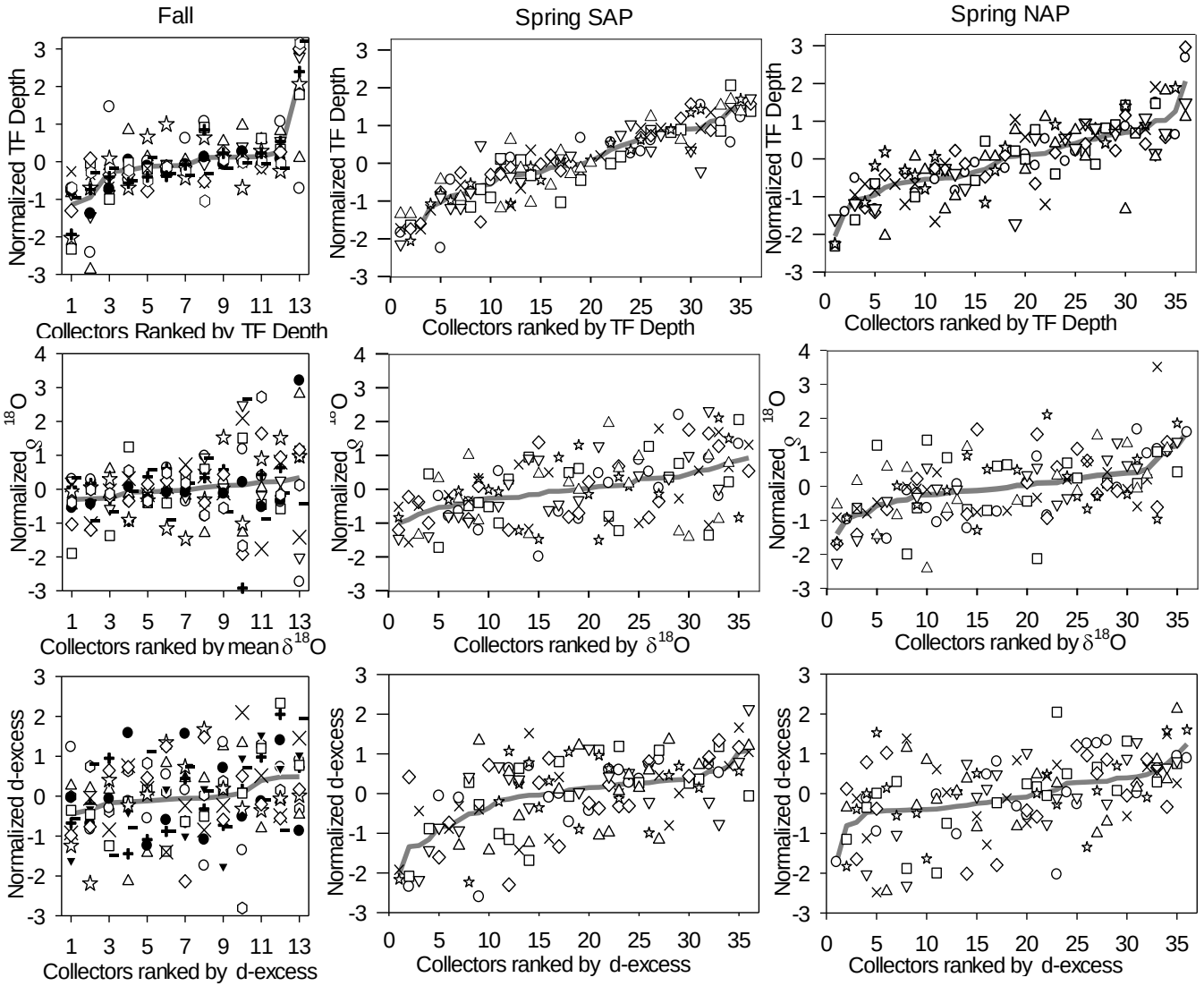
Fall
Spring SAP
Spring NAP
Normalized TF Depth
Collectors Ranked by TF Depth
Collectors ranked by TF Depth
Normalized δ18O
Collectors ranked by mean δ18O
Collectors ranked by δ18O
Normalized d-excess
Collectors ranked by d-excess

Figure 2.9 Time-stability plots. Data plotted are normalized depth, $\delta^{18}O$, and d-excess of throughfall for the fall, spring south-aspect-plot and spring north-aspect-plot. Each point refers to a single measurement of throughfall depth at a single location, with the values normalized $\tilde{x}= \frac{\bar{\bar{x}}-x_i}{\sigma}$. Each symbol refers to a different sampling event: ○: S1, □: S2, ◇: S3, ☆:S4, ▽:S5, ×:S6, △:S7. △:F1, ○: F2, + :F3, ▽:F4, •:F5, □: F6, ×:F7, ☆:F8, - :F9, ◇: F10, ⬢:F11. Collectors are ranked by the mean value of the dependent variable for each collector, shown by the grey line.

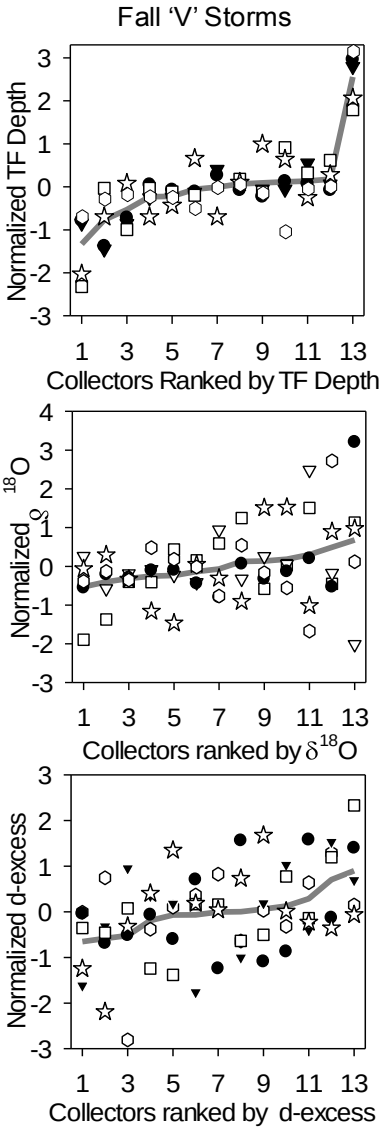

Figure 2.10 Time-stability plot for 'V' storms. V storms are storms ending with the last increment of rain being more enriched than the bulk rainfall. ▽:F4, •:F5, □: F6, ☆:F8, ⬢:F11.

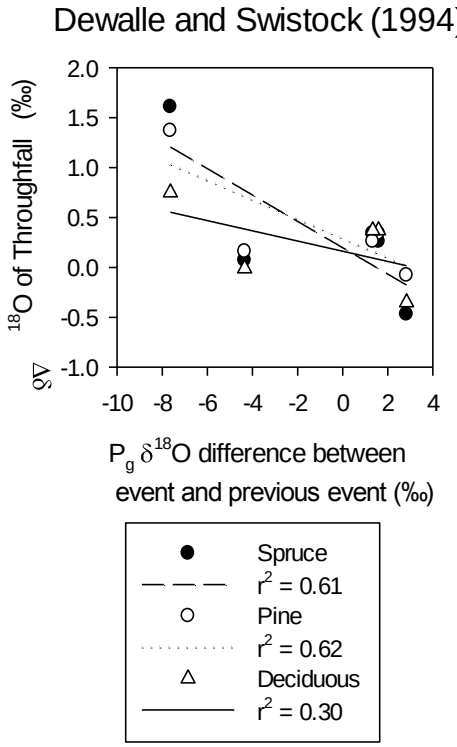

Figure 2.11 Data collected by Dewalle and Swistock (1994) reanalyzed for investigating residual moisture carryover. Data from five events that occurred less than three days after another event were used, following the same analysis as (Fig. 4). $\triangle\delta^{18}O$ of throughfall was plotted against the difference in each event and each event's previous $\delta^{18}O$ of gross precipitation (P_g).

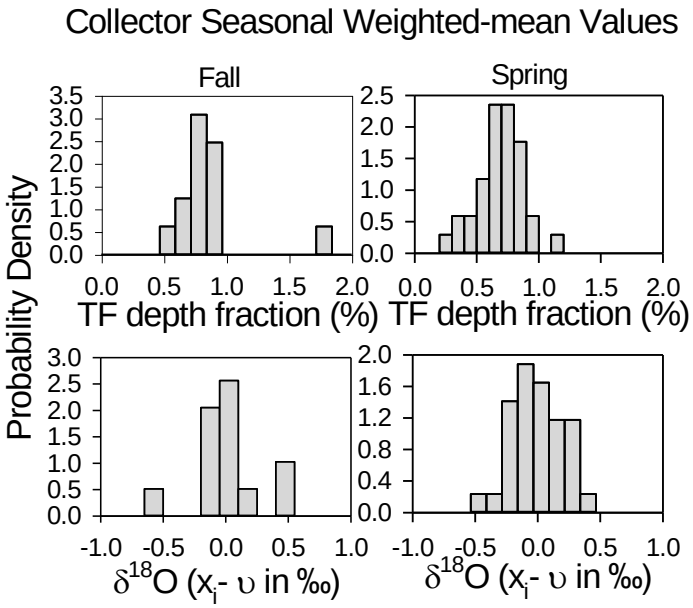

Figure 2.12 Probability-density histograms for depth and $\delta^{18}O$ deviation from the seasonal mean values. The fall data are weighted means over 11 events. Due to the sampling regime, the spring dataset is composed of weighted-means over at least four events.

3 SPATIAL PATTERNS OF CANOPY INTERCEPTION LOSS IN A HEADWATER CATCHMENT: CONTROLS AND INTERACTIONS

Allen, S. T.

McDonnell, J. J.

Bond, B. J.

Journal: *Ecohydrology*

John Wiley & Sons, Ltd. Massachusetts, USA

In Preparation

3.1 INTRODUCTION

Canopy interception loss (IL) is an important component of the hydrologic cycle, reducing the annual water input to the forest floor by 10 – 50 % in headwater catchments (Carlyle-Moses and Gash, 2011). Total evaporative losses accumulate through the repeated filling and drying of water retained in the canopy / trunk storage. During the initial phase of a rain event, nearly all of gross precipitation (P_g) is temporarily intercepted. As surfaces for adhesion and absorption in the canopy and bark become filled, water will either drip from the canopy as throughfall (TF) or run down the trunk of trees as stemflow (SF), comprising the two components of net precipitation (P_n) (Levia *et al*., 2011). Intercepted water continuously evaporates from the canopy, with the rate dependent on meteorological conditions (Carlyle-Moses and Gash, 2011). Once the storm ends, the drip rates decrease and the residual water films on the canopy surface continue to evaporate.

One common finding is that the factors driving IL: precipitation characteristics (Toba and Ohta, 2005), vegetation structure (Pypker *et al.,* 2005), and the energy balance (Teklehaimanot and Jarvis, 1991; Adsak *et al*., 1999), can all be highly variable, even within a small spatial domain (Daly *et al.*, 2007; Gutiérrez-Jurado and Vivoni, 2012) due to topography and other natural sources of heterogeneity. We expect that IL could be highly heterogeneous due to topographic complexity. Despite IL's potential heterogeneity, few (if any) studies have documented the spatial patterns of IL at the catchment scale. The dramatic implications of precipitation variability to

ecological (Hanson *et al.,* 2001) and hydrological systems (Hopp and McDonnell, 2011; Tetzlaff and Uhlenbrook, 2005) is known; therefore, IL heterogeneity is potentially very important because it directly regulates the amount and distribution of P_n.

Variability of P_n at the tree-scale and plot-scale have been well studied (e.g. Navar and Bryan 1990; Raat *et al.,* 2002; Keim *et al.,* 2005), but quantifying P_n and IL variability at the catchment-scale is a measurement grand-challenge. In measuring TF, the number of TF collectors needed to constrain the error of the mean within ± 10% can exceed 60 (Holwerda 2006) along a 160 m transect due to physical redistribution within the canopy. This creates a measurement conundrum of quantifying IL at multiple locations to assess the heterogeneity across a basin and means that the important question of what drives IL variability at the catchment-scale has not yet been tackled.

Here we explored spatial variations in IL at the catchment scale by applying a simple physically-based interception model (Fig. 3.1) to a forested, topographically-complex, 1 km^2 watershed at the H.J. Andrews Experimental Forest in Oregon, USA. We developed vegetation interception parameters by relating LiDAR-derived canopy metrics with modeled LAI values scaled by previously measured storage-per-leaf-area indices (Keim *et al.,* 2006). We then used a digital elevation model (DEM) to calculate potential solar radiation values distributed across our watershed, and then scaled potential solar radiation by real-time measurements of irradiance and

atmospheric transmissivity. We used measurements of temperature, humidity, and wind-speed to calculate potential evaporation with the Penman-Monteith model (Monteith, 1965).

We used this approach to examine how much heterogeneity in IL may result from the spatial variability of solar radiation, vegetation, and precipitation. We tested two hypotheses: (1) the relative influences of the spatial drivers of IL vary from event to event, depending on temporally variable storm characteristics and (2) heterogeneity in both vegetation characteristics and the incident solar radiation patterns are equally responsible for control over the spatial heterogeneity of IL.

We expected that the IL spatial distribution and magnitude of IL variation would vary from event to event, enhanced by lower amounts and intensities of precipitation, and reduced by low evaporation rates. Large storms should have small differences in IL because a large, high-intensity rain event will far exceed the canopy storage, and likely be less affected by evaporation (Toba and Ohta, 2005) regardless of heterogeneities in vegetation structure. Alternatively, small precipitation events might not exceed canopy storage and result in high IL with the spatial distribution reflecting the fraction intercepted. IL during small events is also likely to be more influenced by storage capacity because the storage alone comprises a larger fraction of P_g. Temporal variations in the amount of IL heterogeneity could cause IL heterogeneity to be functionally significant during only certain meteorological conditions, specific to seasons or individual rain events. If the spatial patterns are highly stable in time, it

would mean certain locations receive more net precipitation event after event (and likely year after year), which could enhance the significance of the IL patterns to ecohydrological characteristics that develop over extended periods of time, such as soil moisture deficits (Granier *et al*., 1999), soil flow-paths (Lin, 2010) or vegetation structure and composition (McDonald *et al*., 2008).

For the second hypothesis, we expect that both spatial variability in radiation and vegetation could be important drivers of IL heterogeneity. Vegetation is inherently heterogeneous; thus the precipitation intercepted should also be heterogeneous. Studies have demonstrated that at smaller scales, the amount of TF is highly related to canopy cover and leaf area (Marin *et al.,* 2000; Loescher *et al.,* 2002; Fleischbein *et al.,* 2005; Staelens *et al.,* 2006). At larger scales, the same relationships are assumed true (e.g. Valente *et al.,* 1997; Germer *et al.,* 2005; Carlyle-Moses and Gash, 2011), which could cause large scale heterogeneities in IL to be driven by vegetation variability within a catchment. Solar radiation could potentially also be a major control over IL variability because aspect and slope strongly influence the amount of direct solar radiation received by a surface in complex terrain (Dubayah and Rich, 1995). Solar radiation is a driver of the evaporation rate (Monteith and Unsworth, 2008). Even if radiation differences on the landscape are reduced during a storm due to the high proportion of diffuse radiation (Fu and Rich, 1999), the sky-viewshed differences (Fu and Rich, 1999) in a steep headwater catchment could still result in diffuse radiation heterogeneity. For our study, spatial variation in the

modeled evaporation rate was only due to solar radiation differences, and did not include variations in vapor pressure deficit and aerodynamic conductance; this is discussed further in sections 3.2.2.3 and 3.4.6. While precipitation amount is also highly heterogeneous in complex terrain (e.g. Diodato, 2005; Daly *et al.*, 2007), we do not expect it will have a large effect on IL; spatial variability in P_g depth would undoubtedly affect P_n depth.

The question of what drives IL (and thus P_n) heterogeneity and how this heterogeneity varies spatially requires a discussion of the functional significance of this heterogeneity to the catchment's ecohydrological processes. Beyond testing our hypotheses, an additional objective of this paper is to discuss the potential importance of the ecohydrologic coupling on spatial patterns at the whole-basin scale.

Our study was conducted using watershed 1 (WS1) at the H.J. Andrews experimental forest, in the western Cascades range of Oregon. WS1 was chosen as an ideal system for this project due to vast amount of data available as a Long Term Ecological Research site. Additionally its 80-100 % slope side-slopes (Rothacher, 1965) oriented to be roughly north and south facing could maximize the effects of topography. Within WS1, elevations range from 457 m to 1057 m with an average slope gradient of 59 % (Geren, 2006).

WS1 has a dense, 45-year-old forest cover, unevenly re-established from a clear-cut harvest that took during in 1962 through 1966. Re-establishment of vegetation has been described in depth (Halpern, 1989; Lutz and Halpern, 2006). The

primary species, listed in order of percent of the watershed's total basal area are: *Pseudotsuga Menziesii* (82.1 %), *Tsuga heterophylla* (4.2 %), *Acer macrophyllum* (4.2 %), *Castanopsis chrysophylla* (3.5 %), *Prunus emarginata* (2.1 %), *Arbutus menziesii* (1.2 %), *Alnus rubra* (1.2 %) *Thuja plicata* (1 %), with 0.3 % other. The vegetation is further described in section 3.2.4 regarding vegetation parameterization.

The climate is characteristic of the western Cascades range of the PNW, with an annual precipitation of roughly 2000 mm with 80% falling between October and April (Table 1). Winters are moist and mild while summers are typically hot and dry. The complex terrain causes the relative distribution of radiation and temperature to vary diurnally and seasonally (Smith, 2002). The H.J. Andrews's climate, meteorology and vegetation are described in Daly *et al.* (2007) and the geology and management history of this site is thoroughly described in Rothacher *et al.* (1967) and Lutz and Halpern (2006). Our approach was not to perfectly mimic WS1 IL, but to use WS1 to provide a model representation of a hypothetical watershed that could be used as a virtual testing ground for novel initial investigations into the importance and driving factors IL spatial variability.

3.2 METHODS

3.2.2 Model Inputs:

3.2.2.1 Sensor Meteorological Data

Meteorological data for the 2006-2007 and 2007-2008 water years (Oct. 1-Sept. 30) were used as the input dataset for the model (Daly and McKee, 2011). Precipitation and radiation were measured at the Andrews' Primet meteorological station (Henshaw *et al.,* 1998), which is about 500 m from WS1. Precipitation was measured on 5-minute intervals with a standard tipping bucket rain gage and transformed into 15-minute data for the model. For the modeling "experiments," we assumed that all precipitation fell as rain, although in reality some winter precipitation falls as snow at this site. We made this assumption because it better conformed with our modeling goals of investigating potential IL variability, as opposed to attempting to perfect realism. Solar radiation was also obtained from the Primet station at 15-minute interval.

Relative humidity (RH), temperature, and wind-speed were measured on a 37 m tall tower (Bond, 2010) located near the outlet of WS1 (Fig. 3.2). RH was measured at 14 m height with a HMP45c sensor (Campbell-Scientific Inc.). A shielded thermistor (Model 107 temperature probe, Campbell-Scientific Inc., Logan, UT) mounted to the tower was used to measure temperature within the surrounding canopy at 25 m. Wind speed was measured using sonic anemometers (WS425, Vaisala, Helsinki, Finland) at 31 m height. All measurements on the tower were measured at 1 Hz and averaged over 15 min intervals. In addition to measurements at the towers, there were several measurements locations along a north-south transect in WS1 (Bond, 2011); temperature and RH were measured at four locations at 12 m

height with HMP45c sensors (Campbell-Scientific Inc., Logan UT) measured every 15 s and averaged over 15 min.

Quality assurance and control measures were applied by H. J. Andrews data management staff using the Forest Science Data Bank quality control/assurance plan (Henshaw *et al.*, 1998) for Primet data (Precipitation, solar radiation). Every data point collected from the tower (RH, Temperature, and Wind speed) and transect (RH, Temperature) on WS1 was visually inspected for plausibility using moving time series plots, plotting multiple sensors for inter-comparison. For wind speed, time consistency checks (Zahumenský, 2004) were also conducted to ensure that wind speed variation from one measurement to the next did not exceed six times the standard deviation of the time measurements over previous three hours. Removed data were replaced by linear interpolation.

3.2.2.2 Solar Radiation

This section describes the spatial datasets and algorithms used to develop spatially explicit radiation and precipitation data.

Solar radiation is a complex variable to spatially extrapolate due to its dependence on elevation, aspect, slope, topographic shading, atmospheric transmissivity, and the relative proportions of direct beam radiation and diffuse radiation. The distribution of extra-terrestrial radiation (k_{et}), i.e., the potential solar radiation ignoring atmospheric attenuation, was calculated using a 10 m DEM with the ArcGIS Solar Radiation tool (ESRI Redlands, CA) by setting transmissivity to 100 %

and diffusivity to 0 %. This tool uses an algorithm that accounts for time, aspect, topography, sky conditions, and the locations' viewsheds (Rich *et al.,* 1994; Fu and Rich 2000). The model produced 15-minute k_{et} for the first day of each month; other days of the month were estimated by interpolating between the model output days.

The k_{et} values were used to scale real-time measurements of global radiation (k_g), the solar radiation received at the surface, consisting of a diffuse (k_d) and direct (or beam) component (k_b). Partitioning k_g into k_b and k_d was necessary for calculating the incident solar radiation on heterogeneous terrain. If no radiation data were available, studies can be restricted to temperature-based methods of partitioning radiation components and attenuating k_{et} for atmospheric effects (Bristow and Campbell, 1984), which have been applied to landscape hydrological and ecological models (MT-CLIM: Running *et al.,* 1987; DHSVM: e.g. Wigmosta *et al.,* 1994; RHESSYS: e.g. Tague and Band, 2004). Although these methods are commonly used, they would be less appropriate for an IL study because it would require us to assume uniform transmissivity / diffuse fraction (k_d/k_g) for each day, which is likely to result in significant errors because IL processes vary over much shorter time scales.

Instead, we used measurements of k_g from Primet to calculate k_b and k_d as a function of k_g / k_{et} (Orgill and Hollands, 1977; Bristow *et al.,* 1985) using a method similar to Aguilar *et al.* (2010). Aguilar *et al.* (2010) calculated potential evapotranspiration and solar radiation over a 1300 km^2 watershed using a daily clearness index (k_g / k_{et}) which accounted for both attenuation by clouds and the

atmosphere. In their study, measurements from four meteorological stations were interpolated and the cell-clearness index was used to estimate k_d and k_b at each cell. Then k_d and k_b was downscaled to hourly data following the k_{et} diel trend. Radiation components were topographically adjusted to each cell. The clearness index was not calculated on an hourly scale because of the risk of heterogeneity in clearness across a 1300 km^2 watershed, despite that the approach used by Aguilar *et al*. (2010) was based on the work of Orgill and Holland (1977), which used hourly data. WS1 is a much smaller watershed, allowing us to assume clearness was homogeneous across the watershed and thus extrapolate atmospheric conditions from a single meteorological station; all points on the watershed are within 1.75 km from the meteorological station.

We used a short time-step (1 hour running-averages calculated for every 15 minutes) to capture the rapid increase in k_b and therefore k_g heterogeneity when the sun comes out after a storm, which could have dramatic effects on the spatial variability canopy evaporation rate between storms. We directly applied Orgill and Hollands (1977) equation, which calculated K ($K = k_d/k_g$) as a function of transmissivity ($K_t = k_g/k_{et}$):

$$K(K_t) = \begin{cases} 0.177, & K_t > 0.75 \\ 1.557 - 1.84K_t, & 0.35 \leq K_t \leq 0.75 \\ 1.0 - 0.249K_t, & K_t \leq 0.35 \end{cases} \qquad \text{Eq.1}$$

This equation was originally formulated for Toronto, Canada, but Jacovides *et al.*, (1996) demonstrated that K(Kt) is generally not location dependent. While diffuse radiation is mostly constant across the watershed, it is a function upon the fraction of

visible sky. We assumed the sky to be spatially uniform under fully diffuse conditions. This was acquired indirectly by again running the ArcGIS solar radiation tool with diffusivity greater than zero and extracting just the relative diffuse radiation proportion. A diffuse radiation index (D_j) was calculated by dividing the modeled diffuse radiation at each grid cell by the modeled diffuse radiation at the met station. Diffuse radiation at the met station was scaled by D_j to estimate diffuse radiation at each grid cell (k_{dj}) so that

$$k_{d-j} = K \times D_j \times k_g \qquad \text{Eq.2}$$

Direct solar radiation at each cell ($k_{b\text{-}j}$) was calculated following the general rule from Iqbal (1983):

$$\begin{matrix} \textit{Beam irradiance} \\ \textit{on an inclined} \\ \textit{surface} \end{matrix} = \begin{matrix} \textit{Beam irradiance} \\ \textit{on a horizontal} \\ \textit{surface} \end{matrix} \times \frac{\begin{matrix} \textit{Extraterrestrial irradiance} \\ \textit{on an inclined surface} \end{matrix}}{\begin{matrix} \textit{Extraterrestrial irradiance} \\ \textit{on a horizontal surface} \end{matrix}} \qquad \text{Eq. 3.1}$$

which is equal to:

$$k_{b-i} = \frac{k_{et-i} \times (k_{g-met} - k_{d-met})}{k_{et-met}} \qquad \text{Eq. 3.2}$$

Because $k_g = k_b + k_d$. This allows us to convert this equation to a function K and K_t,

$$k_{b-i} = k_{et-i} \times \left[\frac{k_{g-met}}{k_{et-met}} - \left(\frac{k_{d-met}}{k_{et-met}} \times \frac{k_{g-met}}{k_{g-met}}\right)\right] \qquad \text{Eq. 3.3}$$

$$k_{b-j} = k_{et-j} \times [K_t - (K_t \times K)] \qquad \text{Eq. 3.4}$$

Where $k_{et\text{-}j}$ is the k_{et} at each grid cell and the subscript '-met' indicates measurements at Primet. When $k_{et\text{-}j}$ was positive at some cells but not at the meteorological station, K_t and K were calculated based nearest time when Primet potentially does receive beam radiation, using future values of K_t and K in the early morning, and previous values in the evening. When k_{et} at Primet was zero, k_d at Primet equaled measured k_g.

Our ability to verify this approach was limited because: (1) meteorological stations with radiation sensors are usually placed in openings where there is a large sky view rather than at the bottom of steep valleys or shaded slopes, for which we were often predicting, and (2) pyranometers are placed level so terrain slope and aspect effects are not incorporated. Using our algorithm, we predicted the radiation values for an independent meteorological station 10 km away from Primet, Cenmet, with a coefficient of determination of 0.92 and RMSE of 0.25 MJ/(m^2hr) (Fig. 3.3). Some of the variance could have been due to factors that cannot be predicted, such as a very different K_t value from one station versus another due to differences in cloud elevation or other factors. WS1 is only 500 m to 1700 m from Primet so there should be less unexplained variance. Despite our lack of verification of the Orgill and Holland's method (1977) to our site, this method was still most appropriate for this study because our goal was to explore potential variations in modeled IL rather than to develop a model that perfectly mimics processes on WS1. We found that the range of variation between grid-cells was highly dependent on the amount of diffuse radiation, as expected (Fig. 3.4).

3.2.2.3 Temperature and Relative Humidity

The small scale heterogeneity in temperature at H.J. Andrews has been extensively described (Daly *et al.*, 1994; Smith, 2002; Daly, 2006) and could be represented by temporally downscaling PRISM temperature grids (Smith, 2002) as in Diluzio *et al.* (2008) or Hunter and Meentmeyer (2005). Temperature affects evaporation by modifying the saturation vapor pressure (Monteith and Unsworth, 2008); therefore the vapor pressure deficit is temperature dependent for a fixed relative humidity. However, the differences in vapor pressure deficit for a fixed relative humidity are small when considering the 2-3°C range of variation in WS1 (Smith, 2002). For the frequently used MT-CLIM algorithm, Running *et al.* (1987) reported dew point to be relative constant over large areas, which would result in relative humidity being highly variable with WS1's spatial temperature range. However, for an IL study, we were only interested in RH during and just after storms, where relative humidity approaches saturation. The MT-CLIM algorithm results in unrealistic RH variations during rain events, which resulted in a RSME of 5.9 % RH between 4 sensors on the WS and their predicted RH values. Alternatively, RH was distributed uniformly, equal to the average of the five sensors (four from the transect, and one from the tower). Validated against each of the five sensors, this was effective during both rainy (RMSE = 1.8 % RH) and non-rainy (RMSE = 3.13 % RH) conditions. With a uniform RH, there was little reason to use a spatially explicit temperature measurement. When we ran the model using spatially-varying

temperature fields, adapting the method used by Hunter and Meentmeyer (2005), the varying temperature resulted in only ± 0.1 % in range of IL spatial variability. Because of the lack of sensitivity of IL to spatial variability in temperature, a uniform temperature measurement from the WS1 tower was used for all grid cells in all model runs used.

3.2.2.4 Precipitation

Although precipitation is spatially variable at HJA (Daly *et al.*, 2007), we used a spatially uniform precipitation input for the initial model runs so precipitation amount could be treated purely as a temporal variable and would not confound the spatial variability that was caused by differences in energy and vegetation. As a separate experiment with the model, we introduced a spatially variable precipitation dataset to test the effect of precipitation variability on IL variability. We used PRISM model output precipitation grids (Bredensteiner 1998; Daly 2005) of monthly precipitation ($P_{monthly}$) to extrapolate point measurements of 15-minute data, using the approach of Hunter and Meentmeyer (2005) or Running *et al.* (1987). For every month, the relative precipitation index (R_P) described the precipitation amount relative to the measurement location (the subscript 'j' indicates a spatial variable),

$$R_{P-j} = P_{monthly-j}/P_{Monthly-met-station} \qquad \text{Eq.4}$$

which was then multiplied by 15-minute measurements of precipitation at Primet to obtain the distributed temporal dataset (P_{ij}):

$$P_{ij} = R_{P-j} \times T_{met-i} \qquad \text{Eq. 5}$$

By using this method, we assumed the spatial distribution of precipitation is 100 % stable. While the rainfall pattern on the actual WS1 is not stable, our assumption of stability allows us to use a distribution with a realistic range and pattern as would be expected on WS1.

3.2.2.5 Wind speed and aerodynamic resistance

Wind speed was also distributed uniformly across space as an input variable for the model, following other spatially distributed models (Wigmosta *et al.*, 1994; Tague and Band, 2004) because little is known about spatial variations in wind-speed aerodynamic conductance (Waring and Running, 2007). This is a simplification of the true environmental conditions where both wind speed and aerodynamic resistance may be highly variable.

3.2.2.6 Vegetation

Metrics obtained from a LiDAR survey of the H.J. Andrews in 2008 (Spies, 2011) were used for estimating the canopy interception storage capacity as well as the free throughfall (i.e. the fraction that falls through the canopy without being intercepted). For estimates of free throughfall, we used a canopy cover metric that was calculated at a 5 m resolution using Fusion (United Stated Forest Service Remote Sensing Applications Center, Salt Lake City UT). All LiDAR flight details are viewable at: http://andrewsforest.oregonstate.edu/data/aerial/hj_andrews_report.pdf.

All 5 m cells within our 50 m grid cells were averaged to obtain a 50 m canopy cover corresponding with each grid cell.

Tree height was calculated on a 1 m resolution by measuring the distance of the first return from the LiDAR (Goerndt *et al.,* 2010). Canopy cover was multiplied by height for every 1 m cell and then averaged over the 50 m cells to get the cover times height index (CH) for each grid cell. CH has been demonstrated to be a good indicator of biomass (Lefsky *et al.*, 2002). We used CH to estimate both leaf area index (LAI) and the bark mass index (BMI), which are used for calculating canopy storage and trunk storage capacity respectively.

LAI was estimated by comparing the CH index to LAI estimates at 131 vegetation study plots of 250 m^2 along transects spanning WS1 (Halpern, 1989; Halpern and Dyrness, 2010). At each plot, tree species and diameter at breast height (DBH) were recorded in 2007. LAI was calculated using sapwood area-DBH allometric relationships developed from measurements taken at H.J. Andrews. For coniferous species, we used species specific algorithms (Turner *et al.,* 2000) for calculating leaf area from DBH for *P. menziesii, T. heterophylla,* and *T. plicata*. Hardwood species specific algorithms were used if available. *A. macrophyllum* was calculated using a power-law relationship between basal area and sapwood basal area for WS1 and 2 at HJA (Moore *et al.,* 2004).

$$SBA = 2.6485 \times OBBA^{0.7288} \qquad \text{Eq. 6}$$

where OBBA is the outer bark basal area and SBA is the sapwood basal area. For all other hardwood species, which generally had small DBHs, we assumed that all of the stem-wood is sapwood so SBA was calculated,

$$SBA = \pi[0.5 \times (DBH - BD)]^2 \qquad \text{Eq. 7}$$

where BD is bark depth, which was assumed to be one tenth of the DBH. This assumption has been previous used at H.J. Andrews (Moore, 2004) for small trees (DBH < 6 cm), and we found that it applied to all size hardwood trees in the data collected by Bond and Moore (2007): the coefficient of determination between measured and estimated SBA for *P. emarginata* and *A. rubra* were 0.902 and 0.75 respectively. The number of trees in this category comprised a very small fraction of the leaf area in WS1.

We estimated leaf area from basal sapwood area for *C. chrysophylla* and *A. macrophyllum* using ratios reported by Waring *et al.* (1977). *A. rubra* SBA:LAI ratio was assumed to be the mean of the two values reported by Moore *et al.* (2011), 0.39 m^2/cm^2 at one plot and 0.52 m^2/cm^2 at another. We applied this same conversion factor to all hardwood species for which we could not find literature values. Plot LAI equaled the sum of every tree's leaf area in each plot divided by the plots' projected areas. Plot CH was regressed against plot LAI to give LAI as a linear function of CH, used for estimating LAI at the 50 m grid-cells (Fig. 3.5). Although the coefficient of determination between plot CH and LAI is not high (0.3), it is the strongest

explanatory variable we observed and using this method provided a realistic distribution of values.

Bark biomass was also estimated as a function of CH using the plot data along with equations for estimating bark biomass that were developed at H.J. Andrews (Gholz *et al.*, 1979). For each plot, bark biomass was calculated for every *P. menziesii*, *T. heterophylla*, *T. plicata*, *C. chrysophylla*, and *A. macrophyllum*. These five species are the rough-bark species on the watershed and make up 95 % of basal area in the watershed. Because previous studies have shown that smooth-bark species have negligible bark water absorption (e.g. Liu, 1998; Navar *et al.*, 1998), we used the sum of these five species to calculate bark mass per plot. Bark mass index (BMI) was calculated:

$$BMI(kg/m^2) = \frac{(\sum bark\ mass)}{projected\ Area} \qquad \text{Eq. 8}$$

BMI was regressed against each plot CH to get a linear relationship that then used to estimate BMI for each 50 m grid-cell (Fig. 3.5).

3.2.3 Potential Evaporation Model

The Penman-Monteith model (Monteith and Unsworth, 2008) was adapted for calculating wet canopy evaporation by removing the surface resistance component:

$$\lambda E = [\Delta(Rn - G) + \rho C_p VPD/r_a]/(\triangle + \gamma) \qquad \text{Eq. 9}$$

Where λE is the latent heat flux (W/m^2), R_n is the net radiation (W/m^2), G is the surface heat flux (W/m^2), ρ is the density of water, $\triangle$ is the slope of the saturated

vapor pressure curve at temperature T, γ is the psychrometric constant, C_p is the specific heat of water, and r_a is the aerodynamic resistance. $\triangle$,γ, G, the long-wave radiation components of R_n and the reflection coefficient were calculated as described in Allen (1998).

Methods of calculating r_a have been debated regarding the use of stability corrections (Price, 1987; Monteith and Unsworth, 2008) and whether momentum flux accurately represents vapor flux (Gash *et al.,* 1999; Oke, 1978) versus the additional need of a heat / vapor flux correction term (Gash *et al.,* 1999; Monteith and Unsworth, 2008). Gash *et al.* (1999) found that setting the roughness length (z_0) of heat flux equal to measured z_0 of momentum flux provided a better estimate of IL over scaling r_a using an empirical z_0-heat:z_0-momentum ratio. Link *et al.* (2004) modeled IL in a Douglas-fir forest and found only minor differences between using and not using a z_0 momentum-to-heat scaling coefficient. In any case, Murakami (2006) argued that the Penman-Monteith equation is not based on the physical mechanism of wet-canopy-evaporation and that it only agrees with observations because of how r_a is used as a tuning factor. Therefore it seems reasonable to use an approach for parameterizing r_a that has been successfully used often in IL studies (e.g. Rutter *et al.,* 1975; Schellekens *et al.,* 2000):

$$r_a = \frac{\left(\ln \frac{z-d}{z_0}\right)^2}{k^2 u_{(z)}} \qquad \text{Eq. 10}$$

where z = the height of wind measurement, d = the zero plane displacement height, z_0 = roughness length, u_z = wind speed, and k is the von Karman constant, assumed to be 0.41. We estimated z_0 and d based on measurements by Gay and Stewart (1973, in Jarvis *et al.*, 1976) where $z_0 = 0.14h$ and $d = 0.75h$ for a 35-year-old naturally regenerated Douglas-fir stand in southern Washington with an average height of 28 m, which is very similar to our site (tree height = 29 m at the tower). The wind-profile from this equation corresponded well with the wind profile measured on the tower (Fig. 3.6). Pertaining to the objectives of this study, there was no reasonable way to calibrate our model with IL measurements on WS1. It would not be possible to measure IL at all of our grid-cells. Also, if we "tuned" the model based on one grid cell, we would be assuming that this calibration at one cell would work for all grid cells, violating our assumptions that the processes on the watershed are heterogeneous.

3.2.4 Interception Model

Interception was modeled using a modified version of the "sparse" Rutter model (Valente *et al.*, 1997), which is similar to the original Rutter model (Rutter *et al.*, 1971) but partitions covered and uncovered areas to make it more appropriate for a non-closed canopy forest. While the majority of our watershed was closed-cover with a mean canopy cover of 86 %, there were grid-cells that had a cover as low as 39 %, making the sparse model more appropriate than the original formulation. Another benefit of this model was a simplified drainage term that does not require using empirical drainage coefficients (Rutter *et al.*, 1971; Rutter *et al.*, 1975). We used the

model as previously described (Valente, 1997), except that we directly calculated trunk storage and canopy storage capacity for the whole plot, rather than for only the covered area within the plot. The modeling approach is illustrated in Fig. 3.2.

P_g was partitioned into rainfall to the covered area fraction (c) which was intercepted (P_{gi}) and uncovered faction (1-c) which was free TF (TF_f):

$$P_{gi} = c \times P_g \qquad \text{Eq. 11}$$

$$TF_f = (1 - c) \times P_g \qquad \text{Eq. 12}$$

All of the P_{gi} was intercepted and added to canopy storage reservoir (C). The canopy storage reservoir lost water by canopy evaporation (E_c) as well as by canopy drainage (D_c) when canopy storage capacity (S_c) was exceeded. E_c was scaled by saturation of canopy and by a scaling factor (e) for partitioning the evaporative demand between trunk evaporation (E_t) and Ec.

$$E_c = \begin{cases} (1 - e)E_p \frac{C_c}{S_c}, & C_c < S_c \\ (1 - e)E_p, & C_c > S_c \end{cases} \qquad \text{Eq. 13}$$

$$D_c = \begin{cases} S_c - C_c, C_c > S_c \\ 0, \quad C_c < S_c \end{cases} \qquad \text{Eq. 14}$$

A fraction of D_c directly drained from the canopy as TF, which combined with TF_f, comprised total TF,

$$TF = (1 - p_d)D_c + TFf \qquad \text{Eq. 15}$$

The other fraction of D_c drained to the trunk (D_t), also governed by the D_c partitioning coefficient (p_d),

$$D_t = D_c \times p_d \qquad \text{Eq. 16}$$

The trunk reservoir (C_t), similar to the canopy, lost water by evaporation (E_t) and by drainage via stemflow (SF) when the trunk storage reservoir was exceeded (S_t).

$$E_t = \begin{cases} c * (e)E_p \frac{C_t}{S_t}, & C_t < S_t \\ (e)E_p, & C_t > S_t \end{cases} \qquad \text{Eq. 17}$$

$$SF = \begin{cases} S_t - C_t, C_c > S_c \\ 0, \quad C_c < S_c \end{cases} \qquad \text{Eq. 18}$$

3.2.5 Interception Model Parameterization.

Our interception model was largely parameterized using data from other studies, particularly in similar-aged, Douglas-fir dominated forests. The LiDAR-calculated cover was used for c. Robins (1974) found e to be 0.04 and p_d to be 0.15 for a 44-year-old Douglas-fir stand. Due to the age-similarity of the dominant Douglas-fir trees in our plots, we directly implemented these values of p_d and e as fixed parameters.

S_c was estimated based on calculations from Keim *et al.* (2006) of storage depth per LA for 6 tree species of Pacific Northwest Forests: *P. menziesii* (PM), *T. heterophylla* (TH), *T. plicata* (TP), *A. macrophyllum* (AM), *Acer circinatum* (AC), and *A. rubra* (AR). We used a weighted average of the storage values for the lowest

simulated rain intensity to make a single scaling factor to multiply by our modeled LAI. We used a single broadleaf index, equal to mean (± SE), 0.19 ± 0.01 mm/m^2 of AM, AC, and AR, which were all very similar. Storage values were weighted by basal area fraction (BA_f).

$$\overline{Sc/_{LAI}} = (BA_f \times Sc/LAI)_{PM} + (BA_f \times Sc/LAI)_{TH} + (BA_f \times Sc/LAI)_{TP} + (BA_f \times Sc/LAI)_{broadleaf}$$

so that:

$$\overline{Sc/_{LAI}} = 0.82 \times 0.259\frac{mm}{m^2} + 0.042 \times 0.501\frac{mm}{m^2} + 0.01 \times 0.259\frac{mm}{m^2} + 0.128 \times 0.186\frac{mm}{m^2}$$

$$\overline{Sc/_{LAI}} = 0.260 \pm 0.025\frac{mm}{m^2}$$

$$Sc_j\ (mm) = \overline{Sc/_{LAI}} * LAI_j \qquad \text{Eq. 19}$$

S_c values ranged spatially from 0.2 mm to 4.3 mm with an average of 2.1 which corresponds with the range of values measured for Douglas-firs (Rutter *et al.*, 1975; Klaasen *et al.*, 1998 ;Link *et al.*, 2004; Pypker *et al.*, 2005)

S_t was calculated by scaling BMI using field measurements of bark moisture from WS1. Twelve Douglas-fir bark samples were extracted with an increment borer on 19 days throughout the fall wet-up period of 2010. Bark-water-capacity was calculated by determining difference in the water-weight per bark-weight for the wettest sampling period, 1.54 ± 0.19 mg/mg (measured during a heavy rain event), and

the driest samples, 0.80 ± 0.03 mg/mg (preceded by 12 days of no precipitation) yielding 0.74 mg/mg. To verify that the rough-barked species all had a similar elastic storage, five dry ~1cm^2 samples of bark from five trees of *T. heterophylla*, *A. macrophyllum*, *T. plicata*, *P. menziesii*, and two *C. chrysophylla* were re-saturated in the lab, and then reweighed after a five minute period allowing excess moisture to drip. All species had very similar bark moisture storage capacity except *T. plicata* which appeared to hold more droplets on its exterior within its fibrous structure. Because *T. plicata* comprised a small fraction of bark-biomass on the watershed, we assumed that elastic moisture storage capacity is homogeneous for all rough-bark species, so

$$St\ (mm)\ =\ BMI\ \left(\frac{kg}{m^2}\right) \times 0.739 \frac{mg}{mg} \times 1 \frac{mm \times m^2}{kg_{H_2O}} \qquad \text{Eq. 20}$$

was used to obtain a gridded trunk-storage capacity. Using this method, our grid-cell-averaged bark storage capacities ranged from 3.62 mm in a cell containing mature-Douglas-firs, to 0.2 mm in a plot that is rocky and shrubby, with a cell-mean of 1.7 mm. These values for elastic moisture storage in bark were higher than what Robins (1974) measured at Yeately Wood, UK (0.89 mm), but the plot basal area of our site was over double that of the Yeately Wood site (Hinson and Fourt, 1970).

3.2.6 Data Analysis

In the data analysis, we segregated all rain into discrete events, defined as periods where rain intensity did not decrease below a rate of 0.2 mm / hr for a period

in excess of 12 hours. This threshold was chosen to group repeated showers into single events but to allow separate storms to defined even if very light precipitation occurred during the drying period. However, as a side effect, what we call a single storm may span a week and actually represent multiple events. Reported storms values of temperature, solar radiation, RH and wind-speed refer to the entire storm period excluding the dry out period following the storm.

All statistical analyses and model implementation were run on MATLAB (MathWorks: Natick MA).

3.3 RESULTS

3.3.1 Seasonal Trends in Spatial Variability of IL

Environmental characteristics were similar between the two years with warm, dry summers and moist, moderate winters, characteristic of the region (Table 3.1). The seasonal average pattern of depth-weighted-mean IL was mostly consistent for all four seasons (Fig. 3.6); however, the magnitude of variability changed seasonally: IL varied from 10 % to 43 % in the summer, but only 1.5 % to 6 % in the winter. On a seasonal time-scale, as mean-IL increased, the range of IL variation also increased. This also applied for events partitioned by size class rather than season (Table 3.2).

The spatial pattern of IL followed a patchy distribution roughly similar to the spatial distribution of canopy cover (Fig. 3.7A) and canopy storage (Fig. 3.7B), but unlike the spatial distribution of solar radiation (Fig. 3.8). The cells with low c and S

in the center of the south-facing hillslope distinctly had the lowest IL for all four seasons.

Even though solar radiation was lower for large events (which tended to occur in fall and winter), a higher portion of PE was energy from net radiation. For large, medium and small events respectively, 34 %, 24 % and 15 % of the potential evaporative energy was from solar radiative energy with the remainder from advective heat transfer. As a result, the winter and fall, which had higher depth events, had IL distributions that also reflected the solar radiation differences between the north and south aspect slopes (Fig. 3.8). The drivers of the spatial pattern in IL are discussed further in section 3.3.4.

To investigate how well field measurements may estimate watershed-average IL, we tested the errors that would result from running the model with various inputs that represent potential field-measurement approaches: vegetation parameters at the tower grid cell with meteorological variables from the tower, mean vegetation with meteorological variables from the tower, mean vegetation with solar radiation from Primet and other meteorological variables from the tower, versus the mean vegetation with mean of distributed meteorological variables and the mean of the output with distributed meteorological variables (Table 3.3). Differences were small, especially when the mean vegetation parameters were used. The mean difference between each cell's annual IL and the spatial mean IL is only 1.3 % of P_g. Using a multiple regression, we found that S and c together explained 94 % of the spatial variation of

annual IL. For estimating IL variability in a location like WS1, the location of meteorological measurements is less important than characterizing the vegetation.

3.3.2 Temporal controls over Event Spatial Variability

With variable radiation and vegetation inputs, the range of spatial variability of IL varied dramatically from event to event (Fig. 3.9). Large events tended to have a small range in IL variation associated with the small magnitude of IL. Large events (> 50 mm) during the fall and spring tended to have a bigger range and a higher IL than large events during the winter. Small events (< 10 mm) all had high IL and a large range of IL spatial variability. In small events where the canopy storage was not exceeded, IL variability was determined exclusively by the spatial variability of c (Fig. 3.9). The range of IL spatial variability was maximized when S was exceeded in cells with low S but not in cells with high S. In the highest range event, IL ranged from 14 % to 95 % of P_g for the same event.

To test which temporally variable factors drove IL and the spatial variability in IL, Spearman correlation coefficients were calculated for log-transformed event-mean IL versus log-transformed event-mean PE, P_g, and P_g-intensity for all, large, medium and small events (Table 3.4). Although PE, P_g, and P_g-intensity were not independent of each other, none predicted more than 30 % of the variability in the others. Across all events, P_g depth was the primary drivers of IL magnitude and variability. For medium and large events, PE had the highest correlation with IL magnitude and

variability. For small events, P_g depth was strongly related to IL magnitude, but no variables were highly correlated with IL variability.

As an experiment, we universally scaled the aerodynamic conductance by a factor of two to see what effect this would have on the relative weighting of the temporal controls. Despite the resulting evaporation rate being nearly doubled, the correlation coefficients did not change significantly.

3.3.3 Spatial controls over spatial variability

We used three analyses to determine: (1) which of the spatial variables (k_g, c, and S) most strongly determined the pattern of IL, (2) how stable this pattern was, and (3) what spatial variables determined the range of variation. First, we plotted individual-event Spearman correlation coefficients between IL and the spatially variable factors to assess relative distributions comparing the relative influence of the spatial variables and how they change with varying PE and P_g depth (Fig. 3.10). Secondly, time-stability plots were used to demonstrate whether the spatial distribution of IL was stable from event to event (Fig. 3.11). Lastly, the coefficient of variation (CV) of IL due to each spatial variable was calculated while holding the other variables fixed to see the influence of each spatial variable individually (Table 3.5).

3.3.3.1 Control over distribution and pattern

For most event sizes, c was the most important spatial control over the IL distribution (Fig. 3.10A). S generally had nearly as high r values as c, but it is important to note that S was strongly related to c ($r^2 = 0.59$). For events in the 2-20 mm depth range, S often has higher correlation coefficients, but the r value decreased for both higher and lower depth events. The influence of solar radiation increased with event P_g depth, and was the primary control over the spatial pattern for several larger events. For this same reason, PE rate appeared to have a strong effect on determining the IL correlation with the k_g distribution (Fig. 3.10B): winter events generally had the lowest evaporation rate but also correspond with the biggest spatial variability in k_g, coincident with large storms that are less sensitive to vegetation differences. The flat trend (Fig. 3.10A) at low P_g events occurred because the distribution is entirely determined by cover when the canopy storage capacity is not exceeded. For all size events, the influence of cover decreased at low evaporation, corresponding with an increase in correlation with solar radiation and a decrease in the amount of intercepted water that was evaporated.

3.3.3.2 Temporal Stability

As a result of the varying spatial influence by each of the drivers, which inevitably have different distributions, the relative amount of IL at each grid cell was not constant over time (Fig. 3.11). However, the IL distribution was very stable between events in that cells that had low IL for one event tended to for all events, and vice versa. This stable trend in IL pattern was likely an artifact of our parameterizing

vegetation as unchanging throughout the year. Events with high or low evaporation rates tended to diverge most from the temporal-mean-IL (Fig. 3.11).

3.3.3.3 Individual Parameters' Effects

By running iterations of the model with one parameter spatially varying and holding the rest spatially uniform, we disaggregated effects of individual drivers (Table 3.5). For large events and during the winter and fall seasons, canopy cover, canopy storage capacity, and radiation all caused a roughly equal amount of variation. As event size decreased, the CV due to storage increased and the CV of IL due to k_g variations decreased substantially. The combined effect of varying cover and storage together was nearly the sum of the two components individually; i.e. the similar distributions caused a superimposed additive effect. However, adding variable k_g actually decreased the spatial CV of IL from just S and c, exhibiting the contrast in distributions between k_g, S and c.

3.3.4 IL and P_n heterogeneity with spatially variable P_g

Previous analyses have assumed that the precipitation input was spatially uniform. In this section we assessed the potential effect of a spatially variable precipitation input on IL and P_n. Overall, IL decreased with spatially varying P_g because the spatial mean of the variable P_g input was greater than the uniform P_g value used (Fig. 3.12). However, the IL distribution remained similar under both uniform (Fig. 3.6) and variable P_g (Fig. 3.13). The lower amount of P_g on the north-aspect-

slope (Fig. 3.12) counterbalanced the lower radiation (Fig. 3.8), causing the north-aspect-slope to generally have higher IL than the south (Fig. 3.13), opposite of what we saw without variable P_g. In conjunction with the other spatial variables, adding P_g variability did not have a substantial effect on variability of IL (Table 3.5), showing the counteraction between the P_g and k_g distributions. Alternatively, when just precipitation was variable, the IL CV was large, comparable to the effect of c (Table 3.5).

With variable P_g, the distribution of P_n (Fig. 3.14) was dramatically different from that of IL (Fig. 3.13). It is necessary to describe the effect of spatially variable precipitation on P_n, rather than just the effect of P_g. Under spatially variable precipitation, variations in P_n would not necessarily be reflected by the amount of variability in IL because IL is reported as a ratio. The influence of variable P_g on the P_n CV was much greater than the influence of any of the other spatial controls, except for during small events when storage and cover were more important. In general, values of the spatial CV for P_n were much lower than the spatial CV for IL except for small events because IL can exceed P_n (Table 3.6). For example, large events (with varying C, S, k_g) had a mean IL of 4.5 % ranging from 1.7 % to, 5.5 % so the minimum was 38 % of the mean, and the maximum was 122 % of the mean; this corresponds with a large-event P_n of 95.5 % of P_g, ranging from 94.5 % to 98.3 %, so the minimum was 99 % of the mean, and the maximum is 103 % of the mean. When spatial variability in P_g was considered, the effects of P_g heterogeneity on P_n

heterogeneity far outweighed the effects of IL heterogeneity on P_n heterogeneity for all but small events.

3.3.5 IL variability with higher annual IL

Annual IL for Douglas-fir canopies at other sites have been measured to be as high as ~40 % (Rutter *et al.*, 1975; Tiktak and Bouten 1994). Considering the drivers of IL, to have 40 % IL under a similar canopy would either require a very different precipitation regime or much higher evaporation rates, which would have to be primarily due to more advective exchange. At the previously described Yeatley Wood site, UK used by Rutter *et al.* (1975), P_g averaged 65.3 mm/month over the collection period. We took the spring period for our site, which had a wide variety of events and temperature conditions, and scaled the spring mean of 153 mm/month down to 65.3 mm/month by dividing intensity over the whole period by 2.23. Running the IL model for WS1 with this constructed climate, the mean spring IL was 40%, ranging spatially from 12.8% to 54.5% with a standard deviation of 6.5 % IL. This range of IL means that the cell with the lowest IL would have 92 % greater annual P_n than the cell with the highest IL. This demonstrates two things: the range of variability is highly sensitive to temporal variables (i.e. precipitation) and the IL heterogeneity may be functionally much more important in areas that have higher IL.

3.4 DISCUSSION

While spatial heterogeneity in the environment can be viewed as an impediment to developing simple scalable relationships (Pickett and Cadenasso, 1995), it is also a tantalizing goal to develop an understanding of patterns of heterogeneity and causes for these patterns. More recently, there has been an increased focus on the importance of spatial patterns in driving ecological processes (Turner, 2005) and ecohydrological interactions (Jenerette *et al.*, 2011). In hydrology, dramatic variations within and between watersheds has greatly impeded our understanding of hydrological processes and emergent watershed properties (McDonnell *et al.*, 2007). However, by understanding the mechanisms of spatial patterns, we gain the capability of prediction (Levin, 1992) as we move away from seeing heterogeneity as random, background "noise." In this study we asked if the spatial heterogeneity of interception loss is functionally significant, and what controls its spatio-temporal variability.

3.4.1 On the patterns of IL at the watershed scale

The pattern of IL can determine the pattern of P_n, and therefore the pattern of moisture input to both ecological and hydrological processes. We found that the amount lost and heterogeneity of IL decreased in the winter due to the abundance of large storms. Alternatively, spatial variation during the summer reached a maximum. Rothacher (1963) found net precipitation to have a similar magnitude of difference in TF between plots for summer precipitation in Oregon (May through September); summer TF was 65.7 % of P_g at the lowest TF plot, and 87.8 % at the highest. While

both plots were old-growth Douglas-fir, the plots were structurally different enough to result in fairly dramatic IL differences between the plots.

The IL pattern we observed remained largely stable throughout the year. However, there was a more apparent aspect-effect on the IL distribution during the fall and winter. There are three reasons why the aspect effect is strongest in the winter: low sun angles, solar radiation made up a bigger fraction of PE, and the relative effects of vegetation were less important for large events.

From event to event, the interception loss heterogeneity varied significantly, largely controlled by the P_g depth of the event and the season. This agrees well with field observations by Toba and Ohta (2005) who observed that evaporation rates have a negligible effect on IL during large rain events with high intensity. Larger storms almost always correspond with lower IL (Carlyle-Moses and Gash, 2011). Because we found that IL and IL variability are strongly related, it is not surprising that storm size is a primary control over the amount of IL variability.

Although we hypothesized that solar radiation and the vegetation would be equally important controls over IL variability, we found that vegetation differences had a bigger impact than solar radiation differences. While there have been no previous studies looking at the effects of radiation differences on IL differences, studies have found vegetation differences to be related to IL differences (Aston, 1979; Marin *et al.,* 2000; Loescher *et al.,* 2002; Fleischbein *et al.,* 2005; Staelens *et al.,* 2006), albeit at a smaller spatial scale. Fleischbein *et al.* (2005) found cover was

better than LAI (which we used to estimate canopy storage) for explaining IL variations, consistent with our model results.

Unexpectedly, the hydrological implications of IL were dwarfed by the P_g variability during the wet season, October-May. It is well know that P_g can be highly heterogeneous (Daly *et al.,* 1994) within small areas and affect watershed processes (Chaubey *et al.,* 1999; Tetzlaff and Uhlenbrook, 2005). Our study shows initial insight into the relative importance of IL versus P_g heterogeneity on the distribution of net precipitation. The magnitude of variability will determine the relative importance of each source of variability. For this reason, it is only during the summer that IL variability is a more important driver of the spatial distribution of P_n.

3.4.2 Ecohydrological implications of these findings

With a moist climate and frequent large winter rain storms at our study site, the heterogeneity in P_n due to IL would not likely affect rainfall-runoff responses. The majority (~67%) of the rain falls annually with large storms (> 50 mm), where IL was 4.6 ± 0.7 % (mean ± spatial st. dev.), which corresponds with a mean of large-storm P_n of 106.7 ± 0.8 mm (± spatial st. dev.) over the two-year period. The spatial variability of IL is negligible for large storms, and major differences were only seen at the vegetation maximums and minimums. Although we hypothesized this variability would be hydrological important, it is difficult to estimate whether this degree of P_n heterogeneity could cause a noteworthy effect on the runoff response. Regardless of

hydrological implications, the effect of IL on P_n during large events was negligible compared to the effect of topography-induced precipitation variability, which alone resulted in a P_n spatial st. dev. of ± 10 mm for the depth-weighted-mean of large events.

Although the heterogeneity in P_n due to IL may be insignificant for a single large event, the higher heterogeneity associated with smaller events and summer events could accumulate to result in highly heterogeneous soil moisture content (Granier *et al.*, 1999).

In the PNW's Mediterranean climate, the soil moisture stored at the end of the wet season is used by vegetation for the duration of the dry period, often with minimal replenishment. There is typically minimal rain following June, by which point ET usually exceeds P_g, drying out the soil. IL and IL variability are maximized during the small summer events that mostly do not exceed S, and thus the expected soil moisture recharge would be highly variable. July through September of 2008 had a total of 4.7 cm of rain with P_n ranging spatially from 2.1 to 4.2 cm. At the onset of the fall-winter rainy season, the additional moisture in low IL zones could result in them reaching critical thresholds (Lehmann *et al.*, 2007) for subsurface flow generation, long before reached in zones of higher IL. A catchment's discharge can be a signal that reflects the distribution of antecedent moisture content across the entire basin (Martina and Entekhabi, 2006). In a PNW climate, soil moisture content would cease to be a function of variability in previous moisture inputs after the wet-up period.

IL could be a critical influence over the growth, stress, and survival of vegetation during dry periods (Hanson *et al.,* 2001; Breda *et al.,* 2006) because of IL's effect on the heterogeneity in soil-moisture recharge. IL heterogeneity could be critical to ecological processes in the PNW because the maximum range of IL spatial heterogeneity emerges during the summer when soil moisture is most scarce. A reasonable assumption for the available moisture holding capacity is 11 cm based on Hawk and Dyrness (1972) and Duan (1996). With the additional 4.2 versus 2.1 cm of summer net precipitation, a Douglas-fir forest could potentially transpire at typical summer rates (Moore *et al.,* 2011) for a month longer than at the grid-cell with the higher IL. While this is an extreme simplification of the soil-plant-atmosphere system, differences in the net summer precipitation input could cascade through the system, resulting in differences in moisture availability, and ultimately differences in productivity (Granier *et al.,* 1999). Additionally, this difference in water availability may be a factor controlling the composition and succession of shrub and herbaceous understory communities. Understory growth may even smooth differences in canopy-induced IL heterogeneity because areas with more sparse canopies will have higher radiation transmission, driving greater shrub growth (Van Pelt and Franklin, 2000) and therefore greater shrub interception of TF dripping off the canopy. If regional climate changes result in hotter, drier summers (Mote and Salanthe, 2010), these summer rain events could become critical, and the relative distribution of IL may become more

prominent as a forcing factor on environmental stress and productivity and alter the ecological community trajectory.

Considering the relationship between the spatial patterns of vegetation and of IL, the question arises, "what is the long-term trajectory of this ecohydrologic coupling due to the coincidence of the two patterns?" The highest biomass areas are consistently receiving less P_n compared to nearby areas with lower biomass. In general, greater leaf area corresponds with greater interception (Aston 1979), and greater transpiration until a maximum leaf area is reached (Bond *et al.,* 2007). It has been observed that leaf area is positively correlated with a regions average annual precipitation (Grier and Running, 1977; Hinckley *et al.,* 1978); although these studies were at larger spatial scales, the same principles should apply to eco-physiological differences on a small scale, due to the increased transpiration cost of increasing leaf area. In a water-limited system, such as Douglas-fir forest in the west during the summer (Littell *et al.,* 2008), these interactions could result in a negative feedback cycle between IL and productivity. We speculate that a negative feedback cycle between interception and forest growth could act to regulate growth in a dynamic process that could enhance ecosystem resilience to a changing local climate (Daly *et al.,* 2009). This proposed feedback cycle invites questions on the potential for this system's ecohydrologic self-organization, especially if water-stress becomes increasingly important (Jenerette *et al.,* 2011).

It also must be noted that we focused only on interception loss from the canopy, although evaporation from understory vegetation (Zhang *et al.,* 2006), the forest floor (Gerrits *et al.,* 2010), and woody debris (Sexton and Harmon, 2009) can all significantly contribute to total losses and counter variations in canopy IL.

3.4.3 On the causes and implications of interception's spatial patterns

The distribution of IL is primarily driven by the variations in vegetation and, to a lesser degree, solar radiation. However, the underlying cause of these distributions may be critical to the net effect of the IL pattern on a watershed's ecohydrological function. A concurrent study to this one is finding evidence that WS1's vegetation distribution is largely controlled by soil rockiness (Peterson, unpublished data), resulting in the patchy pattern of vegetation on WS1. Therefore it is the underlying geology and geomorphology that may be controlling aspects of both carbon and water cycling on WS1.

However, alternative patterns of IL could dramatically enhance the hydrologic effects of IL heterogeneity. Management of a forest may result in older forests in the protected riparian area versus the rest of the watershed that is younger because it is harvested on an interval. Mackay and Band (1997) observed that the dense vegetation in regions with greater connectivity to the stream channel (i.e. riparian areas), resulted in lower stream-flow than would be expected if they had just assumed IL was uniform across the watershed. This could especially have an impact on the runoff due to rainfall during summer low-flow periods when rainfall on hillslopes has minimal

streamflow response (Rothacher, 1965). However, rain falling directly in the riparian area can contribute to streamflow regardless of surrounding soil conditions. In addition to the greater age of riparian areas, they may also have significantly higher interception loss due to the presence of epiphytes (Pypker *et al.,* 2006), which are associated with both older forests and riparian areas (Peck and Muir, 2001).

We also consider what potential impacts could result if solar radiation (and thus topography) were driving the biomass distribution. In arid and semi-arid regions, north-aspect slopes often have greater net productivity (e.g. Gutiérrez and Vivoni, 2012), and therefore we assume they have greater interception. This could result in a sharp distinction between zones within a watershed: a north-aspect slope of high interception and a south-aspect slope of low interception loss. While Hopp and McDonnell (2011) found that throughfall redistribution occurred on too small of a scale to affect subsurface flow generation, two large regions with a persistently different P_n amount could result in a very different hydrologic response. Other research has recently shown the importance of aspect as a primary controlling factor over hydrologic transit time, not only due to differences in hillslope structure, but also due to development eco-geo-hydrological effects caused by energy differences (Broxton *et al.,* 2009).

3.4.4 Broader implications

The watershed we investigated has extremely high variability of P_g, very steep north and south facing slopes that maximized radiation differences, and highly

heterogeneous leaf area and biomass, which all inevitably affected our findings regarding the influence of each of these drivers on IL variability. Topography drove the P_g distribution as well as the radiation distribution. Therefore in a less steep landscape, vegetation may be the only driver of IL heterogeneity where both energy and P_g variation are irrelevant. The topographic effects may also be further enhanced or diminished under different climates, demonstrated by our seasonal variations.

By representing IL with the physical model we used, it was inevitable that large storms would have small IL variations, because large storms not only suppress the vegetation effect, they also inevitably result in conditions with a small vapor pressure deficit and low net radiation. However, in a climate where the precipitation regime was not dominated by large, long-duration events, annual IL heterogeneity could be much greater; this was evidenced by the manipulated P_g-rate results. As IL increases, the relative importance of IL variability over P_g variability increases with respect to the distribution of P_n. The importance of IL heterogeneity and the controls over that heterogeneity are site-dependent, creating one additional element of complexity to be incorporated into our perception of watershed processes and their sit-specific nature.

Regardless of the watershed's characteristics, a fundamental requirement of understanding the hydrological response to a precipitation input is to know what that input is. Even if able to accurately estimate the mean value of IL for a watershed, the mean may not be sufficient for representing the sum of the processes occurring at

every location. Therefore, the potential heterogeneity of IL should be considered. It seems reasonable that this could be done in most watersheds by an assessment of the vegetation's heterogeneity over the entire spatial domain, which could be accomplished through direct measurement of throughfall or a survey measuring more easily acquired canopy metrics (e.g. LAI or cover).

3.4.5 Model considerations and the value of this approach

3.4.4.1 Energy heterogeneity and lateral energy transfer

The only spatially variable energy component used in our analyses was solar radiation, despite there being numerous other potential causes of energy heterogeneities: e.g. wind-speed, aerodynamic conductance, lateral energy transfer between cells, and vapor pressure deficit. Therefore our model does not predict the true heterogeneity of IL, but is a prediction of the IL heterogeneity due to spatial variations in kg, c, S and P_g.

The surface radiation energy balance for estimating PE was calculated for each individual cell assuming no energy transfer between cells. Although lateral energy transfer can influence energy transfer in heterogeneous terrain (Raupach and Finnigan, 1995), we assumed advective heat exchange was uniform. Lateral transfer of sensible heat due to k_g spatial heterogeneity could have decreased the effects of k_g heterogeneity, but radiative energy variations were mostly unimportant. Alternatively, because advective heat transfer is the primary control over PE for IL processes

(Teklehaimanot and Jarvis, 1991), by using a uniform RH we may have under-represented the heterogeneity of PE.

Further variability in convective heat exchange could have emerged from heterogeneities in canopy aerodynamic properties and wind patterns. Spatially distributed models typically use uniform wind (Dolman, 1992; Dunn and Mackay, 1995; Aguilar *et al.,* 2010) or a constant above-canopy wind-speed with r_a varying spatially with vegetation height (Tague and Band, 2004) or vegetation type (Mo *et al.,* 2004). Wind varies significantly within single tree crowns (Daudet *et al.,* 1999), but we would have had to predict wind speed at a greater scale where the driving factors are not known. Spatial heterogeneity in wind-speed and r_a could have resulted in considerably more PE heterogeneity than caused by k_g heterogeneity if PE had a comparable magnitude of spatial variability. Regardless, PE heterogeneity especially had minimal effects on summer IL variability, which we argue is when the IL distribution was most important.

3.4.4.2 Model calibration

Calibrating the P-M model for its use in this interception model typically involves adjusting the value of r_a to fit the observed evaporation rate. This calibration has no physical basis, and arguably, the P-M method does not have a physical basis for representing wet-canopy evaporation (Murakami, 2006). Most distributed hydrological models calibrate and validate their model on stream flow because it is a spatially integrated signal. However, with our model, select cells would have to be

selected for calibration and validation. By calibrating the whole model to individual cells, we would be manually adjusting certain coefficients, which would invalidate the assumption that the interception / evaporation drivers vary spatially due to the high intra-plot variability.

Using an un-calibrated Rutter-style model is not uncommon (Muzylo *et al.*, 2009) because it is a physically-based model using the ubiquitous Penman-Monteith model to quantify potential evaporation.

Without calibrating we had strong agreement with other measurements of TF from Douglas-fir in the PNW. In the data collection for chapter 2, we measured 87% TF /P_g in the fall and 69% in the spring. Our model output was 83% and 69% on average for the studied two year period. Our modeled throughfall (79 % of P_g) is in agreement with throughfall measured for select events in Pypker *et al.*, (2005) for a young Douglas-fir forest in the PNW (also 79 % of P_g), although our calculated SF (10% of P_g) was greater than their estimated 5 %. Our modeled value of SF corresponds well with Hamdan and Schmidt's (2012) measurements of SF under a closed-canopy Douglas-fir stand in the PNW.

3.4.4.3 Precipitation distributions:

The dramatic precipitation distribution was the primary control over the amount of P_n heterogeneity for storms over 10 mm. Because we used monthly-mean precipitation grids, these are an average of many rain events. The individual rain event heterogeneity must often be even greater that mean heterogeneity. With

temporally varying P_g distributions, we would expect the stability signal of IL and P_n to reduce dramatically for all but the small showers, which would likely still be controlled by the vegetation.

3.4.4.4 LiDAR metrics versus canopy cover and storage

The importance of cover and storage to IL heterogeneity was demonstrated. While the relationship between CH and S captured the general range of variability, it would not necessarily be sufficient for attempting to accurately estimate storage. The ability to directly relate remotely sensed metrics to interception parameters is necessary for future work in scaling IL at the landscape scale.

3.5 CONCLUSIONS

Interception losses from seasonal, annual, and individual events were considerably heterogeneous when modeled with spatially varying inputs of canopy cover, solar radiation, and storage capacity. Solar radiation on the north-aspect-slope was often only a fraction of that on the south-aspect-slope, but this was mostly insignificant to IL because solar radiation variations only impacted IL during periods when both solar radiation and IL were low. Spatial variation in the structure of the canopy caused significant IL variations that further increased as P_g depth and rate became smaller, or evaporation rates increased. Despite the high IL variability, in a landscape like WS1 with a steep precipitation gradient driven by topography, the variability of P_n is much more affected by the variability in P_g than by the variability

of IL. This was especially true for larger rain events. But for small storms, particularly those occurring during the summer when moisture is critical to potentially water-stressed plants, there was the spatial variability in moisture input was highly variable due to IL.

3.6 ACKNOWLEDGEMENTS

Data and financial support were provided by the HJ Andrews Experimental Forest research program, funded by the National Science Foundation's Long-Term Ecological Research Program (DEB 08-23380), US Forest Service Pacific Northwest Research Station, and Oregon State University. This project was possible with previous research at HJ Andrews by C. Daly, G. Moore, J. Moreau, T. Spies, K. Olsen, and others. K. S. Peterson contributed to the initial development of this project.

3.7 REFERENCES

Aguilar C, Herrero J, Polo MJ. 2010. Topographic effects on solar radiation distribution in mountainous watersheds and their influence on reference evapotranspiration estimates at watershed scale. *Hydrology and Earth System Sciences* **14**: 2479-2494.

Allen RG, Pereira LS, Raes D, Smith M. 1998. Crop evapotranspiration: Guidelines for computer crop water requirements. *FAO Irrigation and drainage paper 56*. Rome, Italy: Food and Agriculture Organization of the United Nations,.

Asdak C, Jarvis PG, van Gardingen P, Fraser A. 1998. Rainfall interception loss in unlogged and logged forest areas of Central Kalimantan, Indonesia. *Journal of Hydrology* **206** (3): 237-244.

Aston AR. 1979. Rainfall interception by eight small trees. *Journal of Hydrology* **42** (3-4): 383-396.

Bond BJ. 2010. Airshed tower data in watershed 1 in the Andrews Experimental Forest. Long-Term Ecological Research. Forest Science Data Bank, Corvallis, OR. [Database]. Available: http://andrewsforest.oregonstate.edu/data/abstract.cfm?dbcode=MV001 (27 May 2012).

Bond B. 2011. Ecohydrology and Ecophysiology in Watershed 1 at the Andrews Experimental Forest. Long-Term Ecological Research. Forest Science Data Bank, Corvallis, OR. [Database]. Available: http://andrewsforest.oregonstate.edu/data/abstract.cfm?dbcode=TW006 (27 May 2012).

Bond BJ, Meinzer FC, Brooks JR. 2007. How trees influence the hydrological Cycle. In *Hydroecology and Ecohydrology: Past, Present and Future.* (eds.) Wood PJ, Hannah DM, Sadler JP. John Wiley and Sons: West Sussex, UK.

Bond B, Moore G. 2007. Sap flow measurements to estimate overstory water use in small watersheds at the Andrews Experimental Forest. Long-Term Ecological Research. Forest Science Data Bank, Corvallis, OR. [Database]. Available: http://andrewsforest.oregonstate.edu/data/abstract.cfm?dbcode=TW003 (27 May 2012).

Bouten W, Heimovaara TJ, Tiktak A. 1992. Spatial patterns of throughfall and soil water dynamics in a Douglas fir stand. *Water Resources Research* **28** (12): 3227-3233.

Breda N, Huc R, Granier A, Dreyer E. 2006. Temperate forest trees and stands under severe drought: a review of ecophysiological responses, adaptation processes, and long-term consequences. *Annals of Forest Science* **63**: 625-644.

Bredensteiner KC. 1998. An investigation of vegetation: hydrology interactions in watershed 1 at the H.J. Andrews Experimental Forest. Thesis, Oregon State University, Corvallis Oregon.

Bristow KL, Campbell GS. 1984. On the relationship between incoming solar radiation and daily maximum and minimum temperature. *Agricultural and Forest Meteorology* **31** (2): 159-166.

Bristow KL, Campbell GS, Saxton K. 1985. An equation for separating daily solar radiation into direct and diffuse components. *Agricultural and Forest Meteorology* **35**: 123-131.

Broxton PD, Troch PA, Lyon SW. 2009. On the role of aspect to quantify water transit times in small mountainous catchments. *Water Resources Research* **45**: W08427, doi:10.1029/2008WR007438.

Carlyle-Moses DE, Gash JHC. 2011. Rainfall interception loss by forest canopies. In *Forest hydrology and biogeochemistry: synthesis of past research and future directions*. Levia DF, Carlyle-Moses D, Tanaka T (eds). Ecological Studies. Vol. **216**. Springer: New York.

Chaubey I, Haan CT, Grunwald S, Salisbury JM. 1999. Uncertainty in the model parameters due to spatial variability of rainfall. *Journal of Hydrology* **220**: 48-61.

Daly C. 2005. Average monthly and annual precipitation spatial grids (1980-1989), Andrews Experimental Forest. Long-Term Ecological Research. Forest Science Data Bank, Corvallis, OR. [Database]. Available: http://andrewsforest.oregonstate.edu/data/abstract.cfm?dbcode=MS027 (26 March 2012).

Daly C. 2006. Guidelines for assessing the suitability of spatial climate data sets. *International Journal of Climatology* **26**: 707-721.

Daly C, Conklin DR, Unsworth MH. 2009. Local atmospheric decouplings in complex topography alters climate change impacts. *International Journal of Climatology*, DOI: 10.1002/joc.2007.

Daly, C.; McKee, W. 2011. Meteorological data from benchmark stations at the Andrews Experimental Forest. Long-Term Ecological Research. Forest Science Data Bank, Corvallis, OR. [Database]. Available: http://andrewsforest.oregonstate.edu/data/abstract.cfm?dbcode=MS001 (27 May 2012).

Daly C, Neilson RP, Phillips DL. 1994: A statistical-topographic model for mapping climatological precipitation over mountainous terrain. *Journal of Applied Meteorology* **33**: 140-158.

Daly C, Smith JW, Smith JI, McKane RB. 2007. High-resolution spatial modeling of daily weather elements for a catchment in the Oregon Cascade Mountains, United States. *Journal of Applied Meteorology and Climatology* **46**: 1565-1586.

Daudet FA, Roux XL, Sinoquet H, Adam B. 1999. Wind speed and leaf boundary layer conductance variation with tree crown consequences on leaf-to-

atmosphere coupling and tree functions. *Agricultural and Forest Meteorology* **97**: 171-185.

Jong SMd, Jetten VG. (2007): Estimating spatial patterns of rainfall interception from remotely sensed vegetation indices and spectral mixture analysis, *International Journal of Geographical Information Science* **21**(5): 529-545.

Diodato N. 2005. The influence of topographic co-variables on the spatial variability of precipitation over small regions of complex terrain. *International Journal of Climatology* **25** (3): 351-363. DOI: 10.1002/joc.1131.

DiLuzio M, Johnson GL, Daly C, Eischeid JK, Arnold JG. 2008. Constructing retrospective gridded daily precipitation and temperature datasets for the conterminous United States. *Journal of Applied Meteorology and Climatology* **47**: 475-497

Dolman AJ. 1992. A note on areally-averaged evaporation and the value of effective surface conductance. *Journal of Hydrology* **138**: 583-589.

Duan J. 1996. A coupled hydrologic-geomorphic model for evaluation effects of vegetation change on watersheds. Dissertation, Oregon State University: Corvallis, Oregon.

Dubayah R, Rich PM. 1995. Topographic solar radiation models for GIS. *International Journal of geographical information systems* **9** (4): 405-419.

Dunn SM, Mackay R. 1995. Spatial variation in evapotranspiration and the influence of land use on catchment hydrology. *Journal of Hydrology* **171**: 49-73.

Faures J, Goodrich DC, Woolhiser DA, Sorooshian S. 1995. Impact of small-scale spatial rainfall variability on runoff modeling. *Journal of Hydrology* **173**: 309-326.

Fleischbein K, Wilcke W, Goller R, Boy J, Valarezo C, Zech W, Knoblich K. 2005. Rainfall interception in a lower montane forest in Ecuador: effects of canopy properties. *Hydrological Processes* **19**: 1355-1371.

Fu P, Rich PM. 1999. Design and implementation of the Solar Analyst: an ArcView extension for modeling solar radiation at landscape scales. *Proceedings of the Nineteenth Annual ESRI User Conference*.

Fu P, Rich PM. 2000. *The Solar Analyst 1.0 Manual*. Helios Environmental Modeling Institute (HEMI), USA.

Gash JHC, Valente F, David JS. 1999. Estimate and measurements of evaporation from wet, sparse pine forest in Portugal. *Agricultural and Forest Meteorology* **94**: 149-158.

Gay LW, Stewart JB. 1973. Presented to Swecon Seminar.

Geren BA. 2006. Predicting sediment delivery from small catchments in the western Cascades of Oregon using the U.S.F.S. disturbed Water Erosion Prediction Project (WEPP) model. Corvallis, OR: Oregon State University. 79 p. M.S. thesis.

Germer S, Elsenbeer H, Moraes JH. 2006. Throughfall and temporal trends of rainfall redistribution in an open tropical rainforest, south-western Amazonia (Rondonia, Brazil). *Hydrology and Earth System Science* **10**: 383-393.

Gerrits AMJ, Pfister L, Savenije HHG. 2010. Spatial and temporal variability of canopy and forest floor interception in a beech forest. *Hydrological Processes* **24**: 3011- 3025. DOI: 10.1002/hyp.7712

Gholz HL, Grier CC, Campbell AG, Brown AT. 1979. Equations for estimating biomass and leaf area of plants in the pacific northwest. *Forest Research Lab research paper 41*.

Goerndt ME, Monleon VJ, Temesgen H. 2010.Relating forest attributes with area-and tree-based light detection and ranging metric for western Oregon. *Western Journal of Applied Forestry* **25** (3): 105-111.

Granier A, Breda N, Biron P, Villette S. 1999. A lumped water balance model to evaluate duration and intensity of drought constraints in forest stands. *Ecological Modelling* **116**: 269-283.

Grier CC, Running SW. 1977. Leaf area of mature Northwestern coniferous forests: relation to site water balance. *Ecology* **58**: 893-899.

Gutierrez-Jurado HA, Vivoni ER. 2012. Ecogeomorphic expressions of an aspect-controlled semiarid basin: II. Topographic and vegetation controls on solar irradiance. *Ecohydrology*: DOI: 10.1002/eco.1263.

Halpern CB. 1989. Early successional patterns of forest species: Interaction of life history traits and disturbance. *Ecology* **70** (3): 704-720.

Halpern C, Dyrness C. 2010. Plant succession and biomass dynamics following logging and burning in the Andrews Experimental Forest Watersheds 1 and 3,

1962-Present. Long-Term Ecological Research. Forest Science Data Bank, Corvallis, OR. [Database]. Available: http://andrewsforest.oregonstate.edu/data/abstract.cfm?dbcode=TP073 (27 May 2012).

Hamdan K, Schmidt M. 2012. The influence of bigleaf maple on chemical properties of throughfall, stemflow, and forest floor in coniferous forest in the Pacific Northwest *Canadian Journal of Forest Research*, 10.1139/x2012-042.

Hanson PJ, Todd Jr DE, Amthor JS. 2001. A six-year study of sapling and large-tree growth and mortality response to natural and induced variability in precipitation and throughfall. *Tree Physiology* **21**: 345-358.

Sexton JM, Harmon ME. 2009. Water dynamics in conifer logs in early stages of decay in the Pacific Northwest, U.S.A. *Northwest Science* **83** (2): 131-139.

Hawk GM, Dyrness CT. 1972. Vegetation and soils of watersheds 2 and 3, H.J. Andrews Experimental Forest. *USDA Forest Service Internal Report 49*.

Henshaw DL, Bierlmaier FA, Hammond HE. (1998). The H.J. Andrews climatological field measurement program. In *Data and information management in the ecological sciences: a resource guide*. Michener WK, Porter JH, Stafford SG (eds). LTER Network Office, University of New Mexico, 117–122

Hinckley TM, Lassoie JP, Running SW. 1978. Temporal and spatial variations in the water status of forest trees: *Forest Science Monograph* 20. Society of American Foresters, Washington, D.C.

Hinson WH, Fourt DF. 1970. Water relations of tree crops: A comparison between Corsican pine and Douglas Fir in South-East England. *Journal of Applied Ecology* **7** (2): 295-309.

Holwerda F, Scatena FN, Bruijnzeel LA. 2006. Throughfall in a Puerto Rican lower montane rain forest: A comparison of sampling strategies. *Journal of Hydrology* **327** (3-4): 592-602.

Hopp L, McDonnell JJ. 2011. Examining the role of throughfall patterns on subsurface stormflow generation. *Journal of Hydrology* **409**: 460-471.

Hunter RD, Meentemeyer RK. 2005: Climatologically aided mapping of daily precipitation and temperature. *Journal of Applied Meteorology* **44**: 1501–1510.

Jacovides CP, Hadjioannou L, Pasiardis S, Stefanou L. 1996. On the diffuse fraction of daily and monthly global radiation for the Island of Cyprus. *Solar Radiation* **56** (6): 565-572.

Jarvis PG, James GB, Landsberg JJ. 1976. Coniferous Forest. In *Vegetation and the Atmosphere*, Volume 2. Monteith JL (ed). Academic Press Inc.: New York, New York.

Jenerette GD, Barron-Gafford GA, Guswa AJ, McDonnell JJ, Villegas JC. 2011. Organization of complexity in water limited ecohydrology. *Ecohydrology*: DOI: 10.1002/eco.217.

Keim RF, Skaugset AE, Weiler M. 2006. Storage of water on vegetation under simulated rainfall of varying intensity. *Advances in Water Resources* **29**: 974-986.

Keim RF, Skaugset AE, Weiler M. 2005. Temporal persistence of spatial patterns in throughfall. *Journal of Hydrology* **314** (1-4): 263-274.

Klaassen W, Bosveld F, Water ED. 1998. Water storage and evaporation as constituents of rainfall interception. *Journal of Hydrology* **212-213**: 36-50.

Lefsky MA, Cohen WB, Harding DJ, Parker GG, Acker SA, Gower ST. 2002. LiDAR remote sensing of above-ground biomass in three biomes. *Global Ecology & Biogeography* **11**: 393-399.

Lehmann P, Hinz C, McGrath G, Tromp-van Meerveld HJ, McDonnell JJ. 2007. Rainfall threshold for hillslope outflow: an emergent property of flow pathway connectivity. *Hydrology and Earth System Sciences* **22**: 2047-1063.

Levin SA. 1992. The problem of pattern and scale in ecology: The Robert H. MacArthur Award Lecture. *Ecology* **73** (6): 1943-1967.

Lin H. 2010. Linking principles of soil formation and flow regimes. *Journal of Hydrology* **393**: 3-19.

Link TE, Unsworth M, Marks D. 2004. The dynamics of rainfall interception by a seasonal temperate rainforest. *Agricultural and Forest Meteorology* **124**: 171-191.

Liu S. 1998. Estimation of rainfall storage capacity in the canopies of cypress wetlands and slash pine uplands in North-Central Florida. *Journal of Hydrology* **207** (1-2): 32-41.

Littell JS, Peterson DL, Tjoelker M. 2008. Douglas-fir growth in mountain ecosystems: water limits tree growth from stand to region. *Ecological Monographs* **78** (3): 349 – 368.

Loescher HW, Powers JS, Oberbauer SF. 2002. Spatial variation of throughfall volume in an old-growth tropical wet forest, Costa Rica. *Journal of Tropical Ecology* **18** (3): 397-407.

Lutz JA, Halpern CB. 2006. Tree mortality during early forest development: A long-term study of rates, causes and consequences. *Ecological Monographs* **76** (2): 257-275.

Mackay DS, Band LE. 1997. Forest ecosystem processes at the watershed scale: dynamics coupling of distributed hydrology and canopy growth. *Hydrological Processes* **11**: 1197-1217.

Marin CT, Bouten W, Sevink J. 2000. Gross rainfall and its partitioning into throughfall, stemflow, and evaporation of intercepted water in four forest ecosystems in western Amazonia. *Journal of Hydrology* **237**: 40-57.

Martina MLV, Entekhabi D. 2006. Identification of runoff generation spatial distribution using conventional hydrologic gauge time series. *Water Resources Research* 42, W08431, DOI: 10.1.1029/2005WR004783.

McDonald AL, Kinucan RJ, Loomis LE. 2008. Ecohydrological interactions within banded vegetation in the northeastern Chihuahuan Desert, USA. *Ecohydrology* 2(1): 66-71. DOI: 10.1002/eco.40.

McDonnell JJ, Sivapalan M, Vache K, Dunn S, Grant G, Haggerty R, Hinz C, Hooper R, Kirchner J, Roderick ML, Selker J, Weiler M. 2007. Moving beyond heterogeneity and process complexity A new vision for watershed hydrology. *Water Resources Research* **43**: W07301.

Mo X, Liu S, Lin Z, Zhao W. 2004. Simulating temporal and spatial variation of evapotranspiration over the Lushi basin. *Journal of Hydrology* **285**: 125-142.

Monteith JL. 1965. Evaporation and environment. In *Symposium of the Society for Experimental Biology, the State and Movement of Water in Living Organisms.* Fogg GE (ed). ***19***: 205-234.

Monteith JL, Unsworth M. 2007. *Principles of Environmental Physics*, Third Edition. Academic Press, Elsevier: New York.

Moore GW, Bond BJ, Jones JA. 2011. A comparison of annual transpiration and productivity in monoculture and mixed species Douglas-fir and red alder stands. *Forest Ecology and Management* **262**: 2263-2270.

Moore GW, Bond BJ, Jones JA, Phillips N, Meinzer FC. Structural and composition controls on transpiration in 40-and 450-year-old riparian forests in western Oregon USA. *Tree Physiology* **24**: 481-491.

Mote PW, Salanthe EP. 2010. Future Climate in the Pacific Northwest. *Climatic Change*, DOI 10.1007/s10584-010-9848-z.

Murakami S. 2006. A proposal for a new forest canopy interception mechanism: Splash droplet evaporation. *Journal of Hydrology* **319**: 72-82.

Muzylo A, Llorens P, Valente F, Keizer JJ, Domingo F, Gash JHC. 2009. A review of rainfall interception modeling. *Journal of Hydrology* **370** (1-4): 191-206.

Navar J, Charles F, Jurado E. 1999. Spatial variations of interception loss components by Tamaulipan thornscrub in northeastern Mexico. *Forest Ecology and Management* **124**: 231-239.

Navar J, Bryan R. 1990. Interception loss and rainfall redistribution by three semi-arid growing shrubs in Northeastern Mexico. *Journal of Hydrology* **115**: 51-63.

Oke TR. 1978 *Boundary Layer Climates*. Routledge: London, UK.

Orgill JF, Hollands KGT. 1977. Correlation equation for hourly diffuse radiation on a horizontal surface. *Solar Energy* **19** (4): 357-359.

Peck JE, Muir PS. 2001. Estimating the biomass of harvestable epiphytic moss in central western Oregon. *Northwest Science* **75** (2): 99-106.

Pickett STA, Cadenasso ML. 1995. Landscape ecology: Spatial heterogeneity in ecological systems. *Science*, New Series **268** (5222): 331-334.

Price DT. 1987. Some effects of variation in weather and soil water on canopy evapotranspiration and net photosynthesis of a Douglas-fir stand. Dissertation: University of British Columbia, Vancouver, BC Canada.

Pypker TG, Bond BJ, Link TE, Marks D, Unsworth MH. 2005. The importance of canopy structure in controlling the interception loss of rainfall: Examples from a young and an old-growth Douglas-fir forest. *Agricultural and Forest Meteorology* **130** (1-2): 113-129.

Pypker TG, Unsworth MH, Bond BJ. 2006. The role of epiphytes in rainfall interception by forests in the Pacific Northwest. II, Field measurements at the branch and canopy scale. *Canadian Journal of Forest Research* **36**: 819-832.

Raat KJ, Draaijers GPJ, Schaap MG, Tietema A, Verstraten JM. 2002. Spatial variability of throughfall water and chemistry and forest floor water content in a Douglas fir forest stand. *Hydrology and Earth System Sciences* **6**: 363-374.

Raupach MR, Finnigan JJ. 1995. Scale issues in boundary-layer meteorology: surface energy balances in heterogeneous terrain. *Hydrological Processes* **9**: 589-612.

Rich PM, Dubayah R, Hetrick WA, Saving SC. 1994. Using viewshed models to calculate intercepted solar radiation: applications in ecology. *American Society for Photogrammetry and Remote Sensing Technical Papers*: 524-529.

Robins PC. 1974. A method of measuring the aerodynamic resistance of the transport of water vapour from forest canopies. *Journal of Applied Ecology* **11** (1): 315-235.

Rothacher J. 1963. Net precipitation under a Douglas-fir forest. *Forest Science* **9**(4): 423-429.

Rothacher J. 1965. Streamflow from small watersheds on the western slope of the Cascades Range of Oregon. *Water Resources Research* **1**(1): 125-134.

Rothacher J, Dyrness CT, Fredriksen RL. 1967. Hydrologic and related characteristics of three small watersheds in the Oregon Cascades. USDA forest Service Pacific Northwest Forest and Range Experiment Station, Corvallis OR.

Running SW, Nemani RR, Hungerford RD. 1987. Extrapolation of synoptic meteorological data in mountainous terrain and its use for simulation forest evapotranspiration and photosynthesis. *Canadian Journal of Forest Research* **17**: 472-483.

Rutter AJ, Kenshaw KA, Robins PC, Morton AJ. 1971. A predictive model of rainfall interception in forests. I. Derivation of the demo from observation in a plantation of Corsican pine. *Agricultural and Forest Meteorology* **9**: 367-384.

Rutter AJ, Kenshaw KA, Robins PC. 1975. A predictive model of rainfall interception in forests. II. Generalizations of the model and comparison with observations in some coniferous and hardwood stands. *Journal of Applied Ecology* **12**: 367-380.

Schellekens J, Bruijnzeel LA, Scatena FN, Bink NJ, Holwerda F. 2000. Evaporation from a tropical rain forest, Luquillo Experimental Forest, eastern Puerto Rico. *Water Resources Research* **26** (8): 2183-2196.

Schellekens J. 2000. The interception and runoff generating processes in the Bisley Catchment, Luquillo Experimental Forest, Puerto Rico. *Physics and Chemistry of the Earth, Part B: Hydrology, Oceans and Atmosphere* **25** (7-8): 659-664.

Smith JW. 2002. Mapping the thermal climate of the H.J. Andrews Experimental Forest, Oregon. Thesis, Oregon State University, Corvallis Oregon. 239p.

Spies T. 2011. LiDAR data (August 2008) for the Andrews Experimental Forest and Willamette National Forest study areas. H. J. Andrews Experimental Forest. Forest Science Data Bank, Corvallis, OR. [Database]. Available: http://andrewsforest.oregonstate.edu/data/abstract.cfm?dbcode=GI010 (27 May 2012).

Staelens J, Schrijver AD, Verheyen K, Verhoest NEC. 2006. Spatial variability and temporal stability of throughfall water under a dominant beech (Fagus sylvatica L.) tree in relationship to canopy cover. *Journal of Hydrology* 330: 651-662.

Tague CL, Band LE. 2004. RHESSys: Regional hydro-ecologic simulation system-an object-oriented approach to spatially distributed modeling of carbon, water, and nutrient cycling. *Earth Interactions* **8**: 1-42.

Teklehaimanot Z, Jarvis PG. 1991. Direct measurement of evaporation of intercepted water from forest canopies. *Journal of Applied Ecology* **28**: 603-618.

Tetzlaff D, Uhlenbrook S. 2005. Significance of spatial variability in precipitation for process-oriented modeling: results from two nested catchments using radar and ground station data. *Hydrology and Earth System Science* **9**: 29-41.

Tiktak A, Bouten W. 1994. Soil water dynamics and the long-term water balances of a Douglas-fir stand in the Netherlands. *Journal of Hydrology* **156**: 265-283. DOI: 10.1002/hyp.3360060407.

Toba T, Ohta T. 2005. An observational study of the factors that influence interception loss in boreal and temperate forests. *Journal of Hydrology* **313**: 208–220.

Turner DP, Acker SA, Means JE, Garman SL. 2000. Assessing alternative allometric algorithms for estimating leaf are of Douglas-fir trees and stands. *Forest Ecology and Management* **126**: 61-76.

Turner MG. 2005. Landscape ecology: What is the state of the science. *Annual Review of Ecology, Evolution, and Systematics* **36**: 319-344.

Valente F, David JS, Gash JHC. 1997. Modeling interception loss for two sparse eucalypt and pine forest in central Portugal using reformulated Rutter and Gash analytical models. *Journal of Hydrology* **190**: 141-162.

Van Pelt R, Franklin JF. 2000. Influence of canopy structure on the understory environment in tall, old-growth, conifer forests. *Canadian Journal of Forest Research* **30**: 1231-1245.

Waring RH, Gholz HL, Grier CC, Plummer ML. 1977.Evaluating stem conducting tissue as an estimator of leaf area in four woody angiosperms. *Canadian Journal of Botany* **55:**1474-1477.

Waring RH, Running SW. 2007. *Forest Ecosystems: Analysis at Multiple Scales*. Academic Press: Amsterdam.

Wigmosta MS, Vail LW, Lettenmaier DP. 1994. A distributed hydrology-vegetation model for complex terrain. *Water Resources Research* **30**(6): 1665-1679.

Zahumensky I. 2004. Guidelines on quality control procedures for data from automatic weather stations. World Meteorological Organization: Geneva, Switzerland.

Zhang G, Zeng GM, Jiang YM, Huang GH, Li JB, Yao JM, Tan W, Xiang R, Zhang XL. 2006. Modeling and measurement of two-layer-canopy interception loss in a subtropical evergreen forest of central-south China. *Hydrology and Earth System Sciences* **10** (1): 65-77.

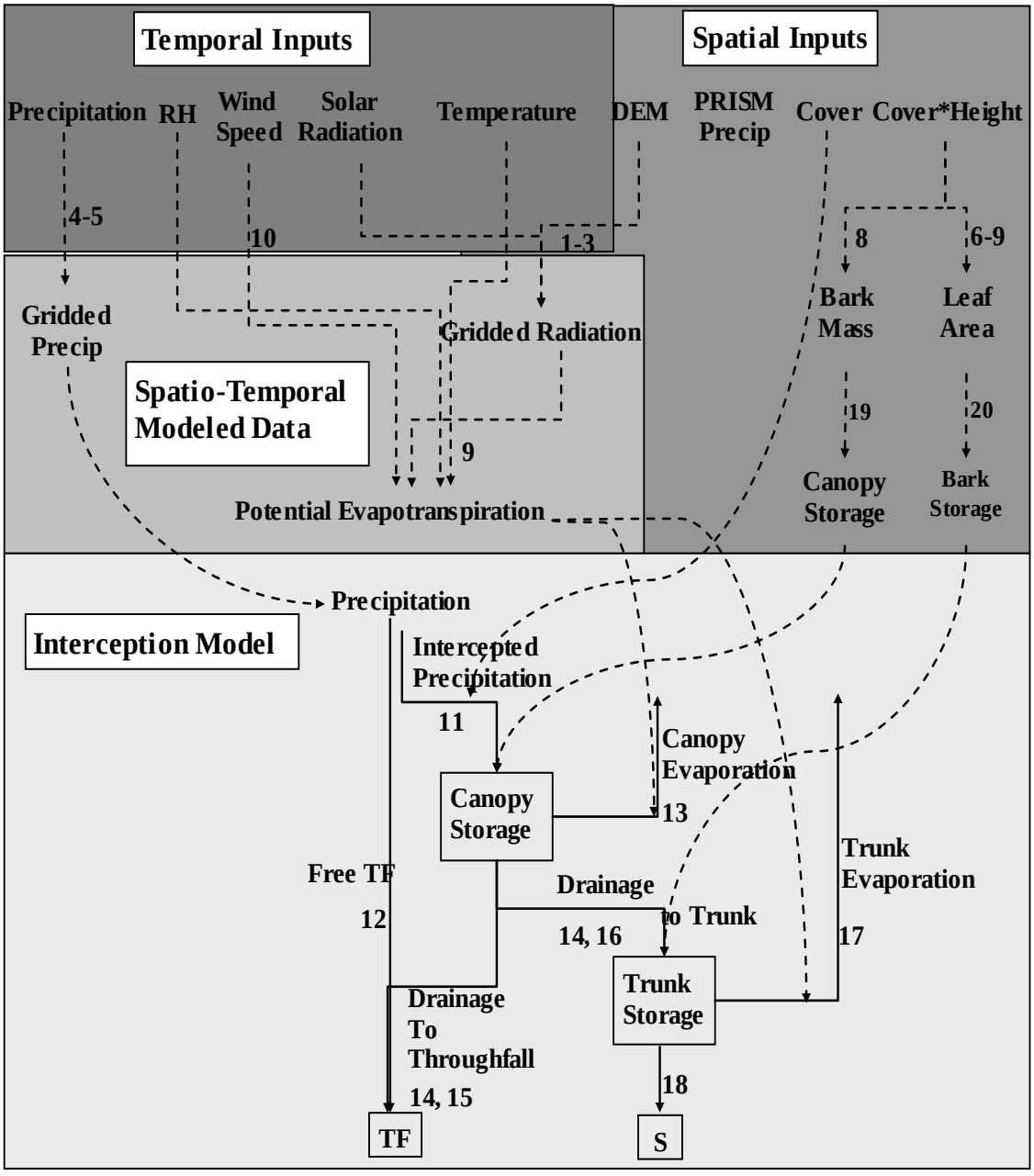

Figure 3.1 Model diagram for input data-sets and interception modeling. Numbers refer to equation number describing the flow. Solid lines indicate processes and dashed lines indicate influences.

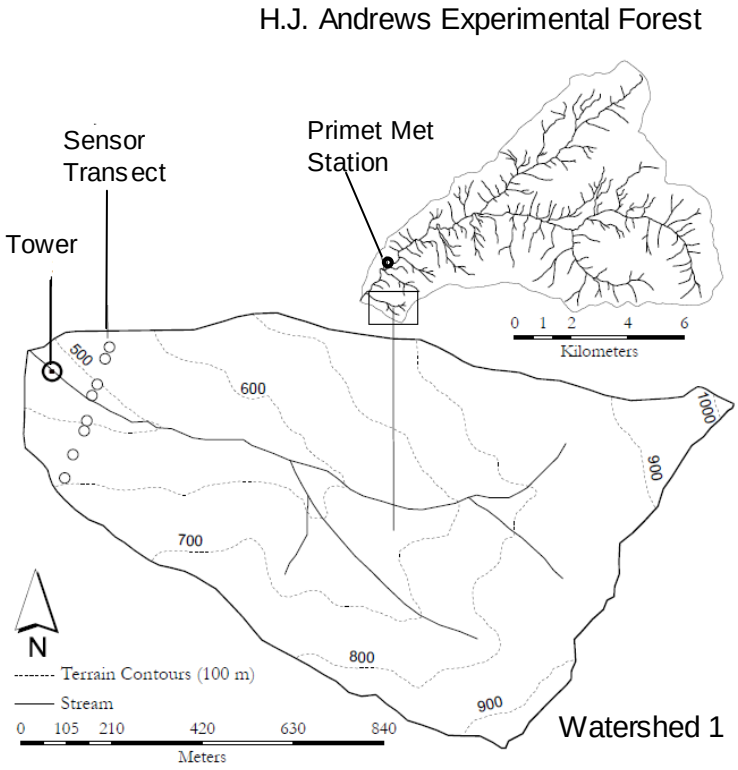

Figure 3.2 Map of WS1 in relation to H.J. Andrews Experimental Forest

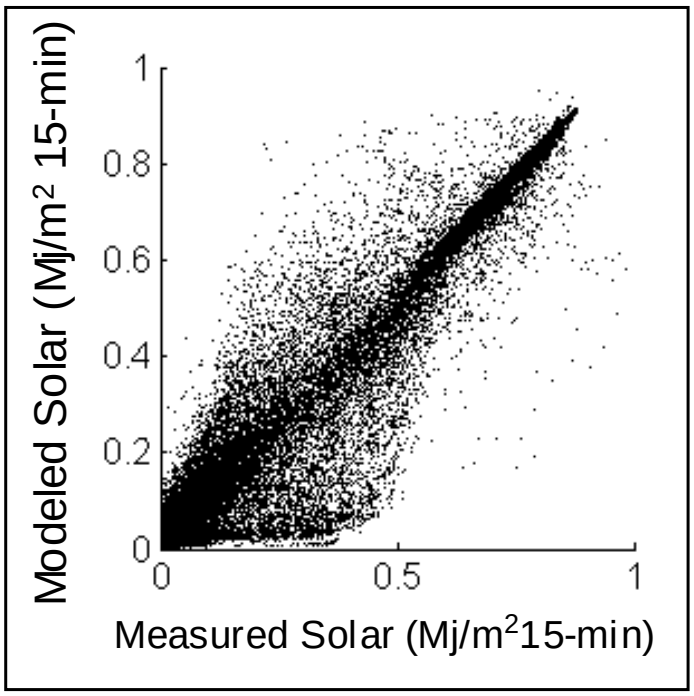

Figure 3.3 Modeled versus measured solar radiation at Cenmet meteorological station, H.J. Andrews Experimental Forest. Coefficient of determination, r^2 = 0.92.

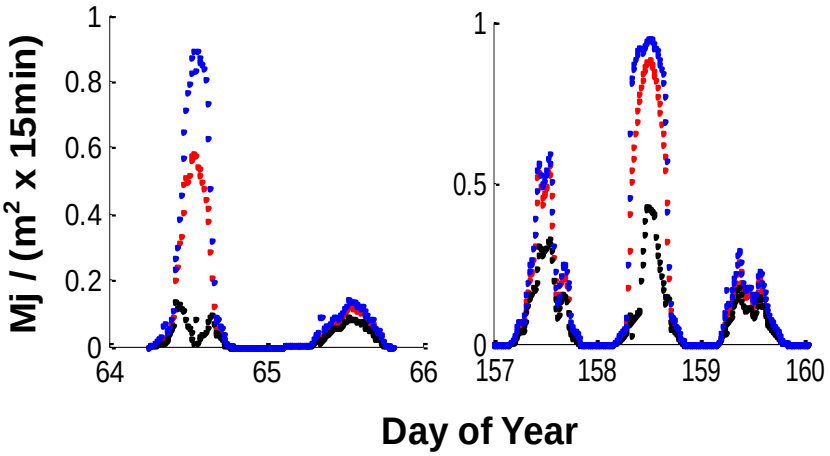

Figure 3.4 Solar radiation diel patterns over a winter and spring period showing radiation patterns during clear and cloudy conditions. The instantaneous maximum, average, and minimum cell on the watershed are indicated by the blue, red, and black.

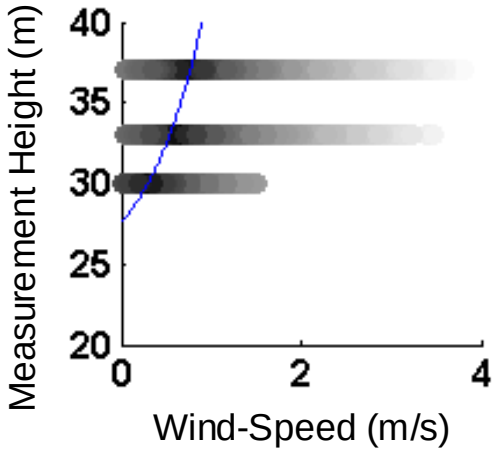

Figure 3.5 Wind speed at 30 m, 33 m and 37 m. The horizontal bars indicate the range of variation over the two year period. The shade of grey indicates the frequency of measurements. The line is the wind profile parameterized so that z_0 =0.14h and d = 0.75h.

Table 3.1 Monthly-mean weather measured at H.J. Andrews over the two years study period.

	2006 - 2007 Water Year												2007 - 2008 Water Year											
	O	N	D	J	F	M	A	M	J	J	A	S	O	N	D	J	F	M	A	M	J	J	A	S
Max. Temperature (°C)	15	7	4	3	7	13	16	22	24	30	28	23	12	7	3	2	6	8	12	19	22	29	27	25
Min. Temperature (°C)	4	3	0	-2	1	2	3	5	8	13	10	7	4	1	0	-2	-1	0	0	6	6	11	11	7
Precipitation (cm)	6.9	68	37	25	33	17	14	7.1	5.7	2.1	2.6	6.6	29	32	45	44	18	33	19	7.6	8	0.2	4.1	0.7
Relative Humidity (%)	81	96	97	92	93	89	82	72	70	69	67	69	91	94	98	95	92	92	86	77	71	60	69	66
# of Days with Rain	9	26	15	13	21	20	15	7	8	4	3	5	20	15	25	19	16	26	19	14	11	1	7	4

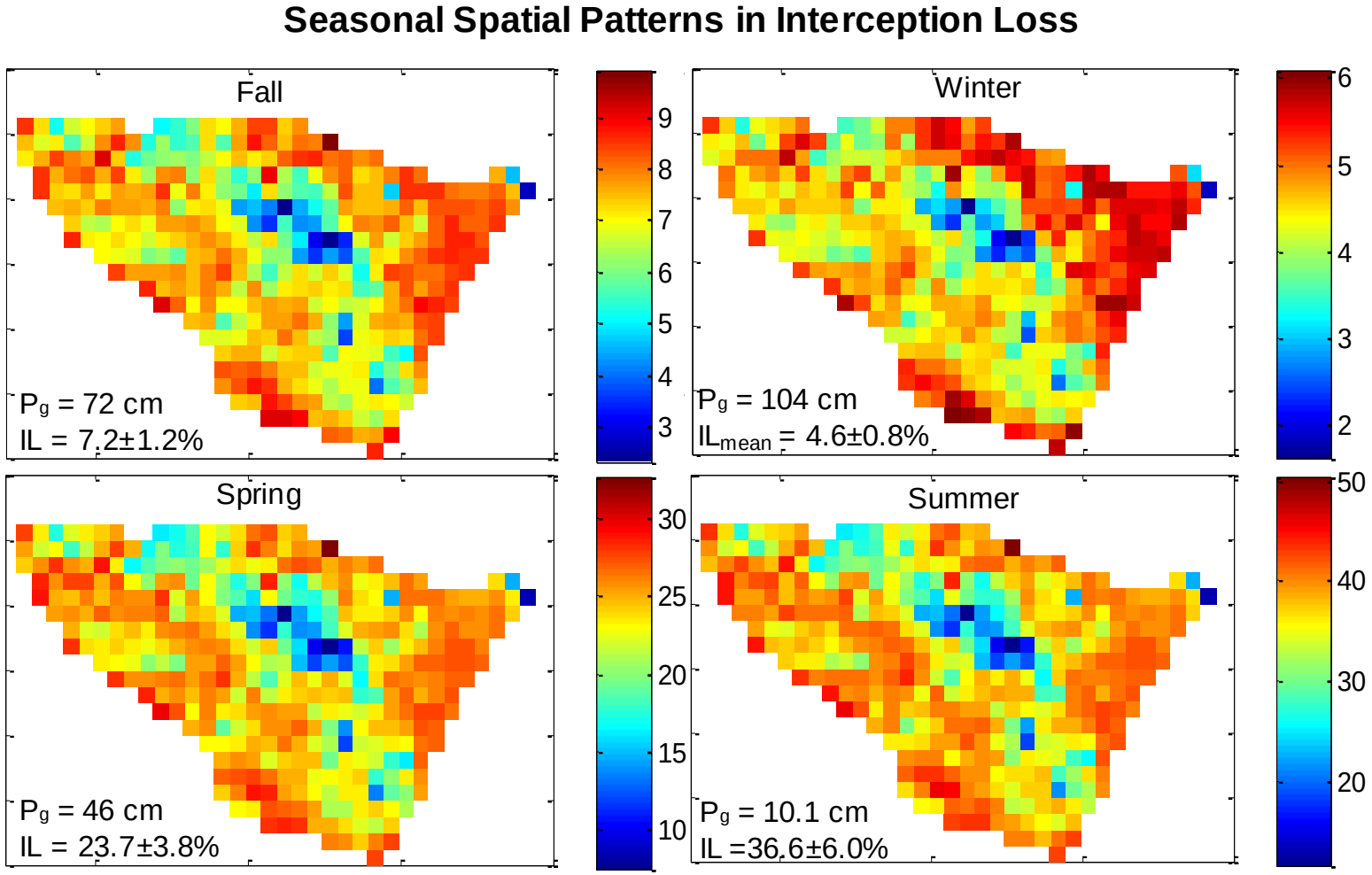

Figure 3.6 Total interception loss of the 2006-2008 water years. Gross precipitation (P_g) depth and IL (%) are the averages of the two year period with mean ± standard deviation.

Table 3.2 Interception loss descriptive statistics and meteorological data. Data are listed for all storms and separated by size class with large being above 50 mm, med is 10-50 mm, and small is less than 10 mm. Interception loss and P_g data are depth-weighted means, and other parameters are time-weighted means, calculated for the duration of rain events. The standard deviation is the standard deviation of all grid cells' weighted mean values.

		Interception Loss mean (%)	max	min	P-M PET (mm/hr)	k_g (MJ/m^2hr)	T (°C)	RH (%)	P_g (mm)	P_g-rate (mm/h	Wind (m/s)
ALL	**μ ± σ**	11 ± 1.7	15	3.5	0.1 ± 0.005	0.1 ± 0.02	5.22	97	30	0.246	0.544
large	**μ ± σ**	4.6 ± 0.7	5.8	1.7	0.05 ± 0.005	0.1 ± 0.01	4.42	98	111	0.3015	0.53
med	**μ ± σ**	19 ± 3.3	27	5.8	0.15 ± 0.006	0.2 ± 0.03	5.98	96	23.9	0.206	0.564
small	**μ ± σ**	53 ± 8.6	72	16	0.16 ± 0.005	0.1 ± 0.02	6.87	95	2.53	0.085	0.573

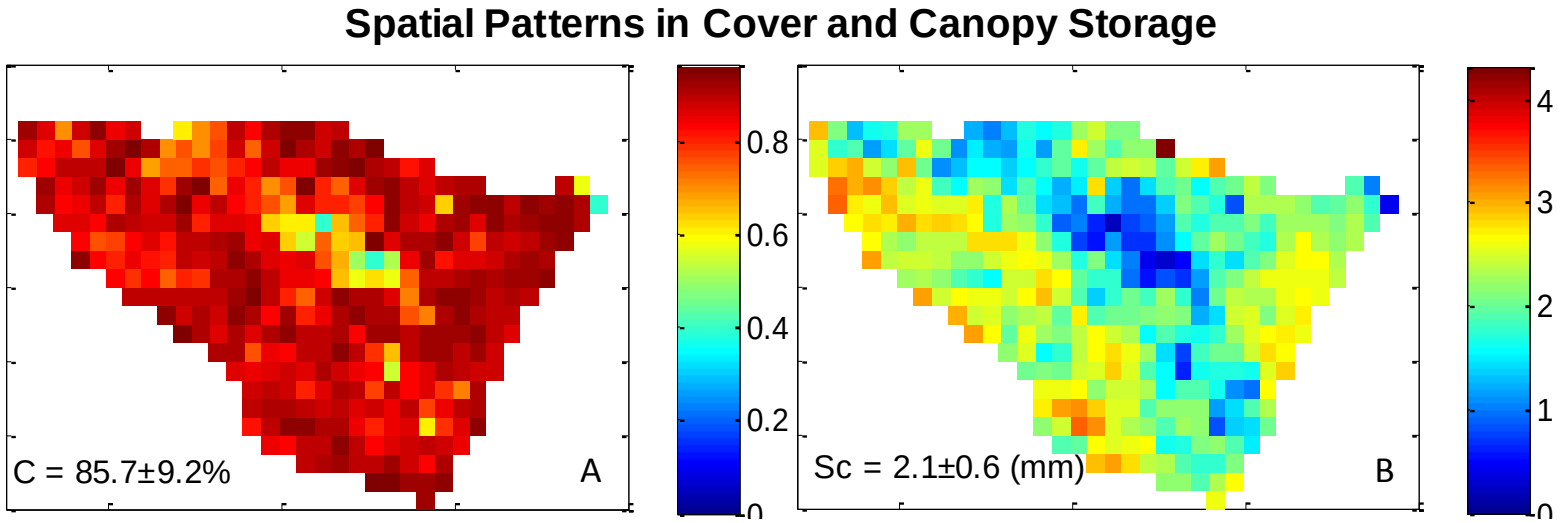

Figure 3.7 Canopy cover distribution (A; unitless) and canopy storage capacity distribution (B; mm) on WS1.

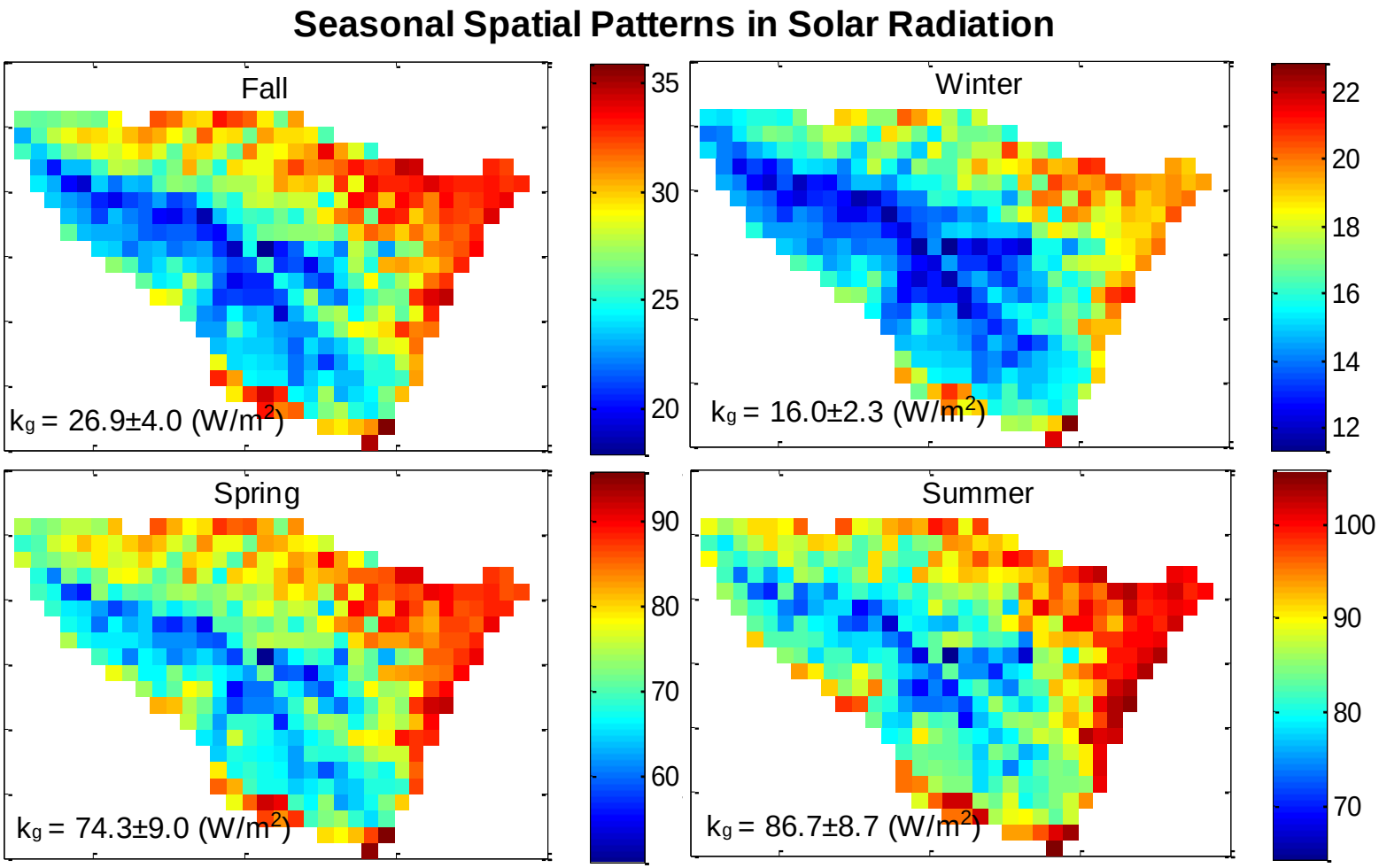

Figure 3.8 Time-weighted average of global solar radiation (k_g) during rain events of the 2006-2008 water years. Units of the color-bars are in W/m^2.

Table 3.3 Calculations of annual interception loss using alternate inputs. Primet and Tower refers to meteorological, solar radiation, or vegetation measurements / calculations specific to the Primet meteorological station or the tower on WS1. Mean is the mean of all locations on WS1.

			Interception Loss (%)			
Met	**Sol**	**Veg**	**F**	**W**	**Sp.**	**Su.**
Tower	Primet	Tower	9	5.5	28.8	43.8
Tower	Primet	Mean	7.7	4.8	24.5	31.9
Tower	Tower	Mean	7.5	4.5	24.4	37.2
Mean	Mean	Mean	7.7	4.9	24.3	37.6
Mean of Output			7.6	4.8	24.4	37.1

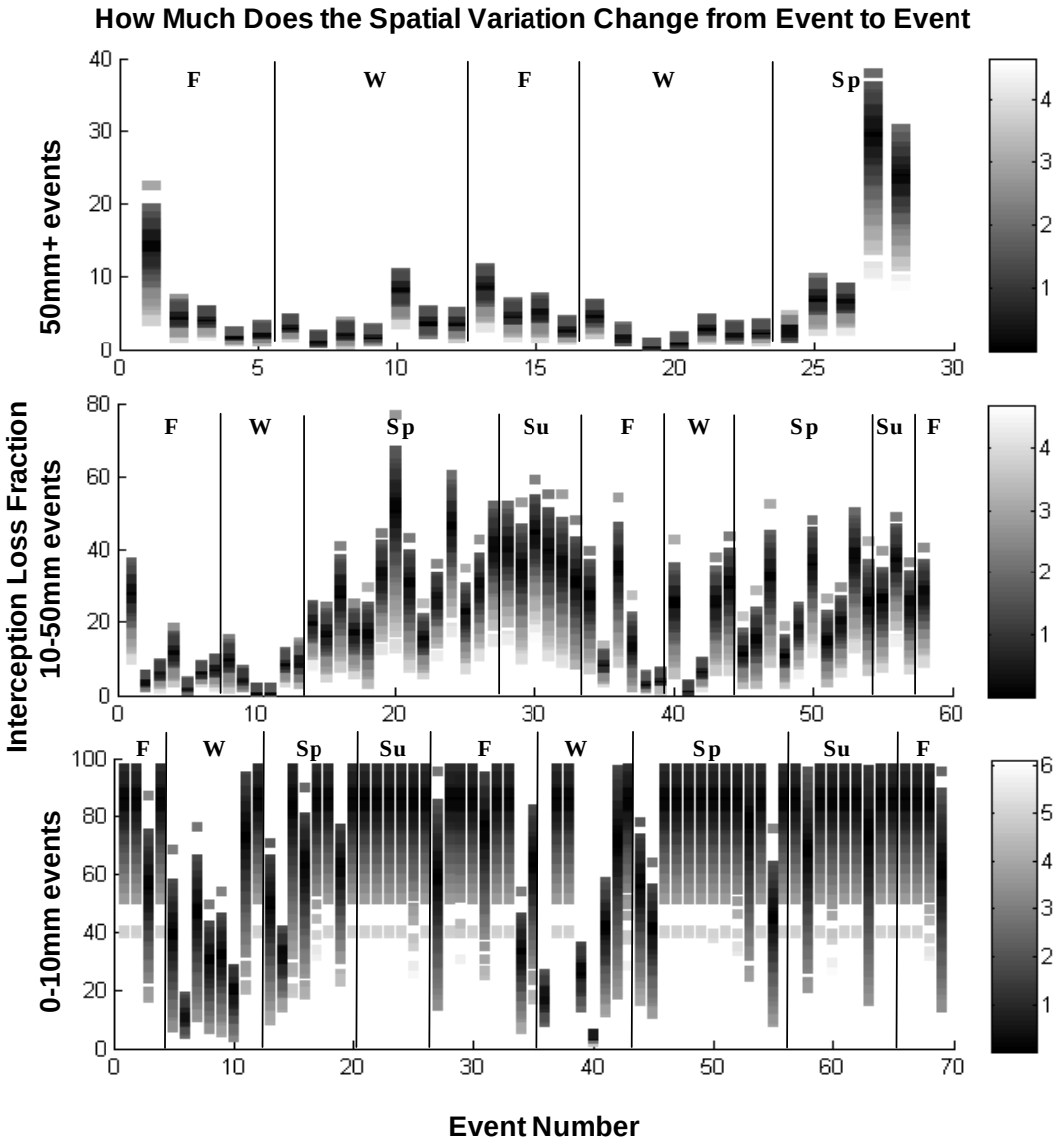

Figure 3.9 Individual event range of spatial variation in interception loss. F, W, Sp. Su. indicate the season of the events. The shade of grey indicates increasing number of standard deviations from the mean as the shade becomes lighter.

Table 3.4 Temporal controls over amount of IL and IL variability. Spearman correlation coefficient of event-mean interception loss, and event-standard deviation of interception loss versus: event-mean Penman-Monteith Potential evaporation (PM PE), gross precipitation (P_g), and P_g-rate.

Mean of IL versus:		PM PE	P_g	P_g-rate
ALL	**r**	0.58	-0.88	-0.59
Large	**r**	0.86	-0.47	-0.41
Med	**r**	0.80	-0.43	-0.66
Small	**r**	0.36	-0.75	0.15

Std. Dev. of IL versus:		PM PE	P_g	P_g-rate
ALL	**r**	0.53	-0.80	-0.65
Large	**r**	0.76	-0.54	-0.50
Med	**r**	0.70	-0.51	-0.55
Small	**r**	0.18	0.24	-0.26

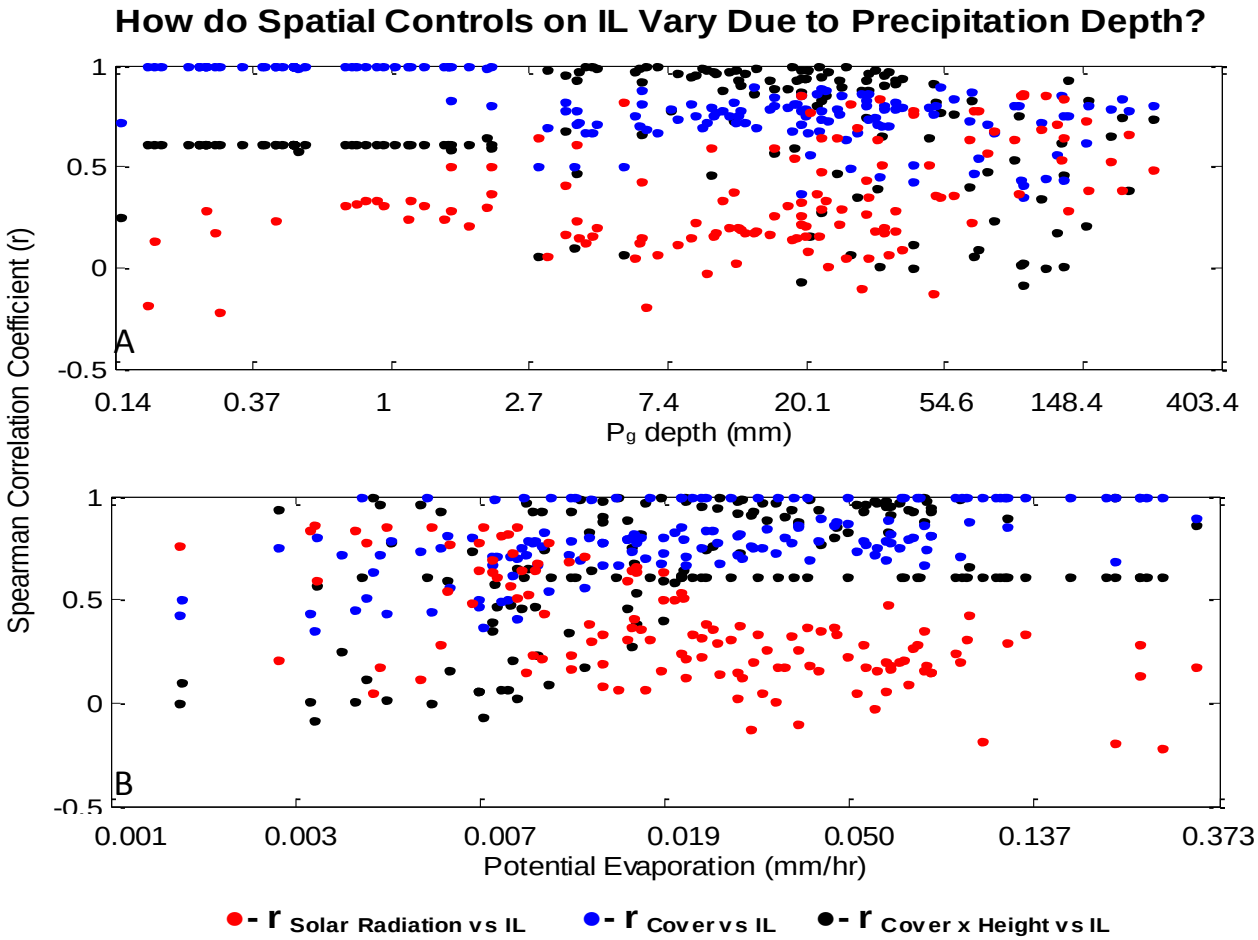

Figure 3.10 Controls over the IL spatial distribution. Spearman correlation coefficients of the spatial distribution of interception loss versus the spatial distribution of solar radiation, canopy cover, and cover x height (which is used to estimate canopy storage capacity). The r values are plotted against storm depth (A) and potential evaporation rate (B) on a log scale. Each point represents a single event. Events that occur at entirely night are not plotted for solar radiation.

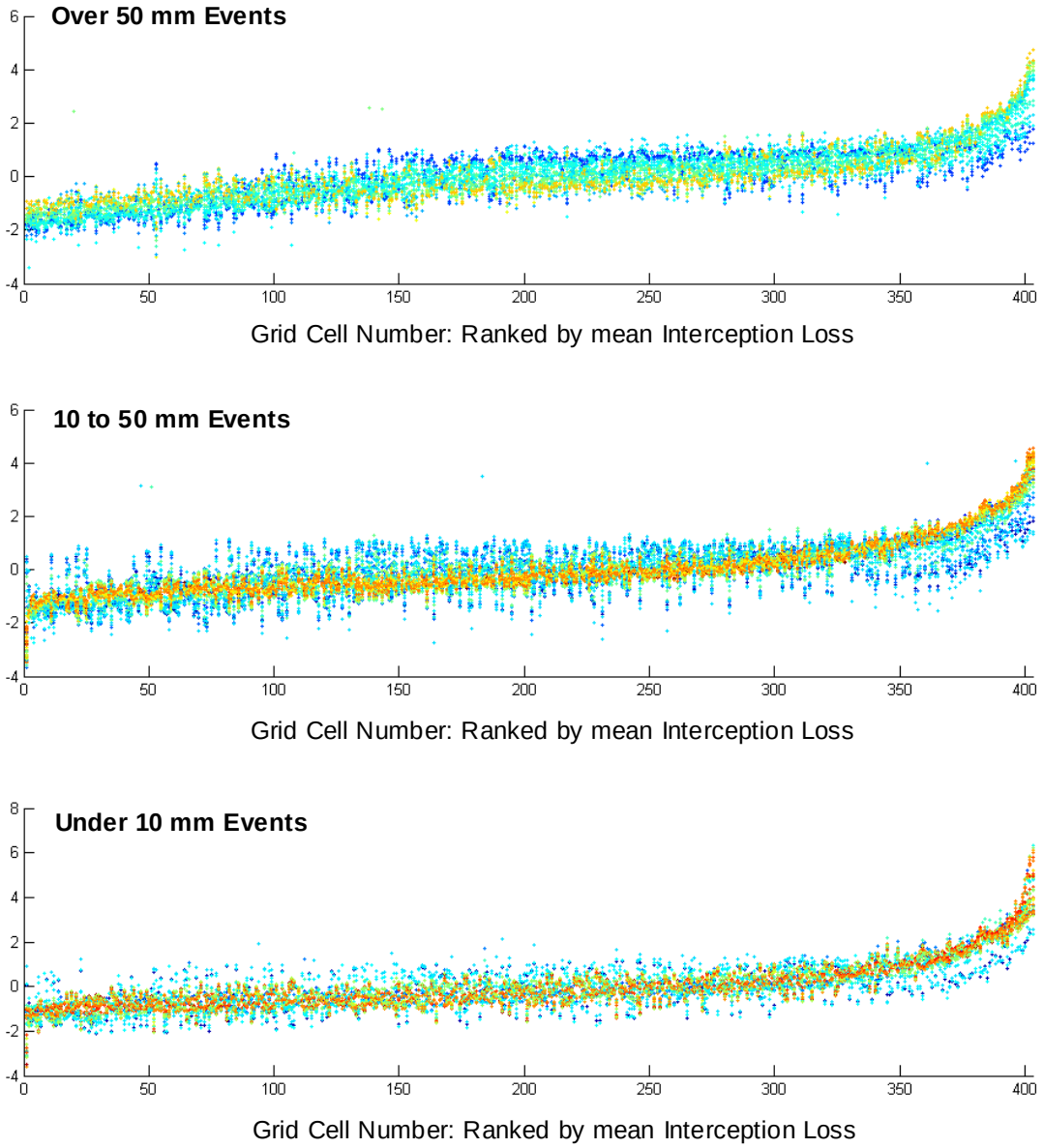

Figure 3.11 Time-stability plots. Plots indicate the persistence of spatial patterns by showing the range of normalized $\frac{(x-\mu)}{\sigma}$ values of interception loss for each grid cell. Color-scale indicates evaporation rate with warmer colors indicating higher evaporation.

Table 3.5 Individual variables' effects on IL variability. The coefficient of variation of IL with certain parameters spatially uniform and while others are variable to indicate the relative contribution of each variable to the interception loss variability. Large, medium, and small events refer to events greater than 50 mm, 10 – 50 mm, and below 10 mm respectively.

Interception Loss Variability with Disaggregated Varying Parameters

Varying Parameters	Coefficient of Variation of Interception Loss (%)						
	Fall	Winter	Spring	Summer	Large	Medium	Small
k_g	5.1	8.7	2.3	1.1	7.3	2.7	1.8
c	7.0	7.8	7.2	7.5	8.3	6.7	7.5
S	11.6	9.9	11.2	10.5	8.0	12.5	11.2
c / S	16.9	15.8	16.6	16.2	14.7	17.4	16.5
k_g / c / S	16.5	16.7	16.4	16.3	15.3	17.2	16.2
P_g	6.4	7.3	6.3	5.0	14.4	13.7	4.4
k_g / c / S / P_g	16.7	15.9	17.2	17.0	18.0	21.8	16.6

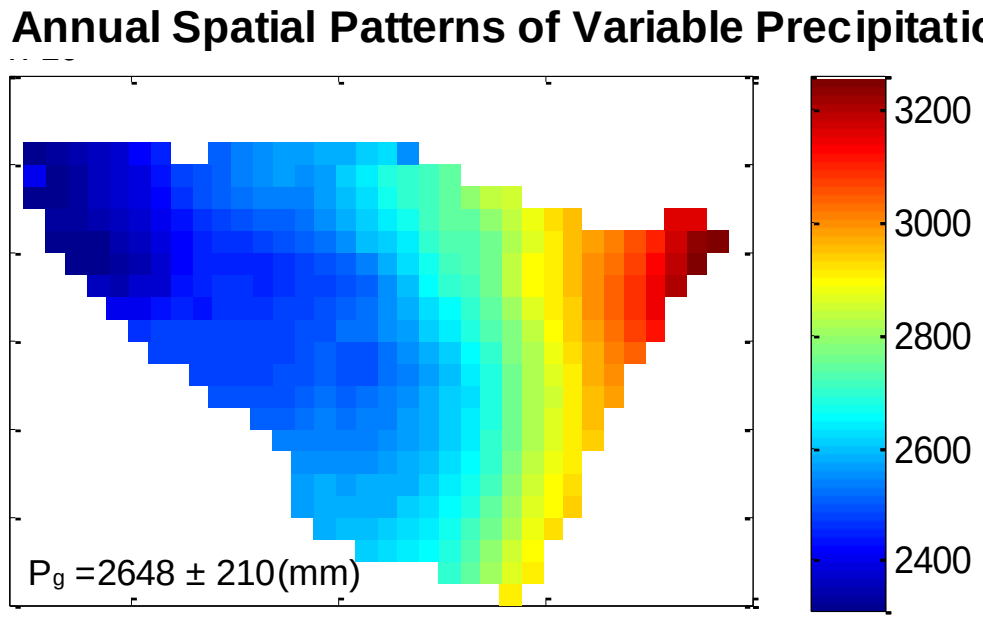

Figure 3.12 Precipitation distribution. Distribution of average annual precipitation from PRISM variable precipitation grid (Daly, 2005). Monthly distributions mostly followed a similar pattern.

Seasonal Spatial Patterns in Interception Loss (with Variable Precipitation)

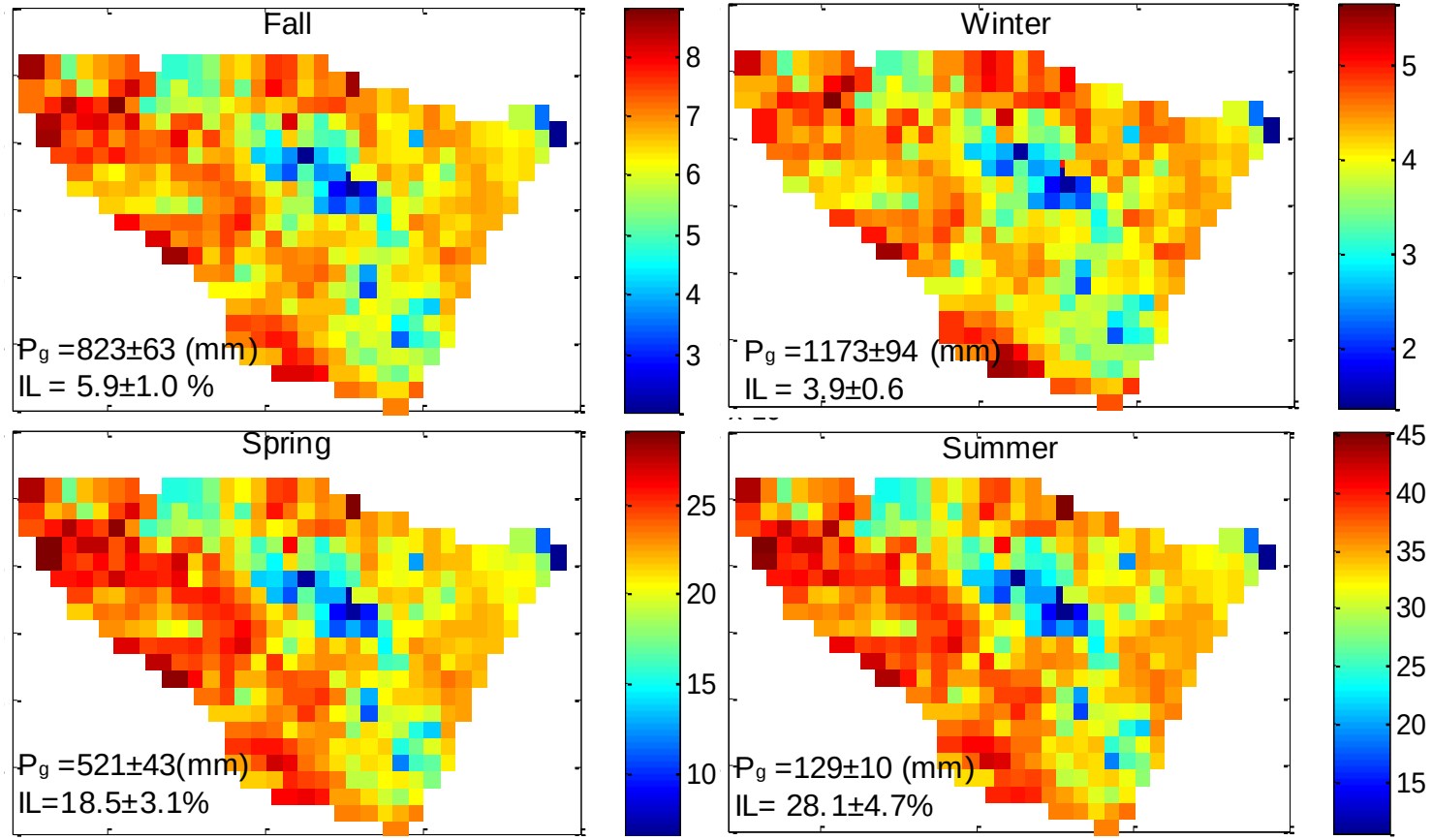

Figure 3.13 Total interception loss for the 2006-2008 water years with spatially variable precipitation. Gross precipitation (P_g) depth and IL (%) are the averages of the two year period with mean ± standard deviation.

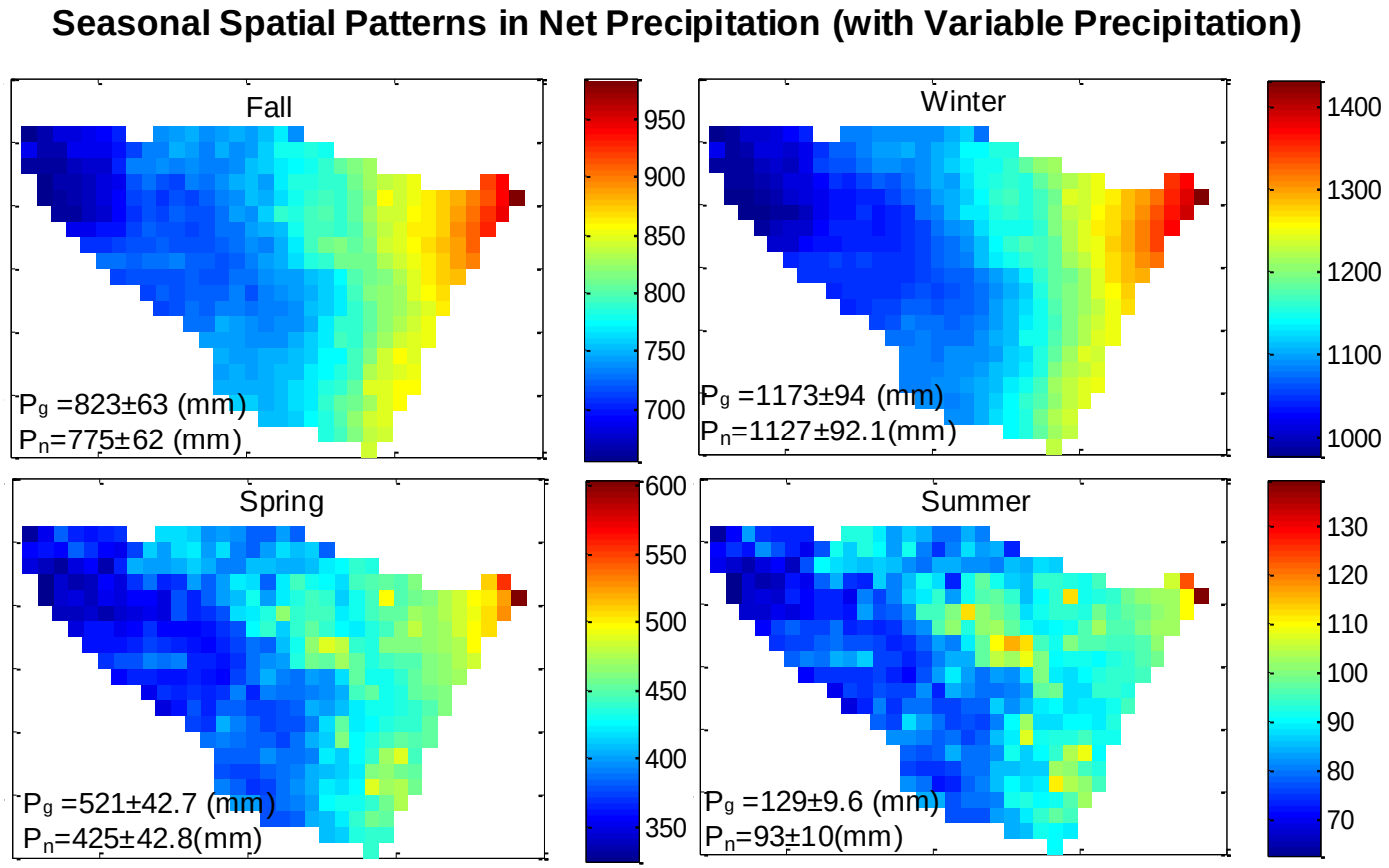

Figure 3.14 Net precipitation (P_n) with spatially variable gross precipitation (P_g) and interception loss.

144

Table 3.6 Individual variables' effects on the P_n distribution. The coefficient of variation while certain parameters are spatially uniform and others variable to indicate the relative contribution of each variable to the interception loss variability. Large, medium, and small events refers to events greater than 50 mm, 10 – 50 mm, and below 10 mm respectively.

Net Precipitation Variability with Disaggregated Varying Parameters

Varying Parameters	Coefficient of Variation of Net Precipitation (%)						
	Fall	Winter	Spring	Summer	Large	Medium	Small
k_g	0.4	0.4	0.7	0.6	0.4	0.6	2.0
c	0.6	0.4	2.2	4.4	0.4	1.6	8.8
S	0.9	0.5	3.5	6.1	0.4	3.0	12.7
c / S	1.3	0.8	5.2	9.4	0.7	4.2	19.0
k_g / c / S	1.3	0.8	5.0	9.4	0.7	4.1	18.4
P_g	8.2	8.4	10.0	10.1	8.3	9.3	12.5
k_g / c / S / P_g	8.0	8.2	10.6	12.6	8.1	9.7	19.5

4 CONCLUSIONS

4.1 CHAPTER 2

4.1.1 Summary

The goal of this study was to understand the effects of (1) pre-event canopy water, (2) selective storage, and (3) evaporative fractionation on the isotopic composition of throughfall and stemflow. We found that pre-event residual water caused isotopic differences between rainfall, throughfall, and stemflow. We did not observe any indicators of selective storage or evaporation affecting TF and SF isotopic composition; however, that does not negate their potential impacts. There were few apparent explanations for the spatial patterns in isotopic composition. The lack of stable spatial patterns of throughfall isotopes further supported the residual moisture hypothesis. However, we did observe strong, persistent patterns in throughfall depth, which indicated the stability of drip points from the canopy (as in Keim *et al*., 2005).

I concluded that there was no direct evidence of evaporation or selective canopy storage in the isotopic composition of throughfall, although it is almost certain that these processes both occurred, based on our current understanding of how water moves through the canopy (Levia *et al*., 2011). With finding residual moisture carryover as a primary cause of isotopic variation, we should have a means for better predicting throughfall-rainfall isotopic differences. However, there were clearly other processes confounding a direct relationship between residual moisture and throughfall / rainfall differences.

Some throughfall samples had a very strong pre-event canopy water signal, and other samples had hardly any. We discussed that this could indicate partitioning within throughfall flow paths: some with significant exchange with the canopy-water and others with much less. Others have discussed the effects of the differences in interception flow paths on evaporation (Murakami, 2006), and biogeochemistry (Puckett, 1991). The ecohydrological importance of this partitioning is still unknown, but our results certainly suggest the need to consider the ecohydrological implications of co-variations in throughfall depth and chemistry (Raat *et al*., 2002)

4.1.2 Future work

Stable isotopes have an enormous potential value, but in order to make use of them, we still must more carefully disentangle the effects of various sources and processes. In particular, the mixing that occurs with rain falling on the canopy. My study indicated the tremendous potential for residual water on the canopy to affect the isotopic composition of throughfall. However, identifying evidence of a process occurring does not equate to an understanding of the details of how that process works. We need a better understanding of the mechanisms of retention and mixing of residual moisture in order to use the isotopic composition of net precipitation to learn of how water moves through the canopy. Up until now, our basic understanding of these processes are largely based on lab experiments (e.g. Herwitz, 1987), and not in situ measurements. Stable isotopes provide a means to go beyond these previous restrictions.

First, further studies need to better confirm the role of residual canopy water. This could simply involve sampling canopy residual moisture throughout the inter-storm period in addition to throughfall and rainfall measurements. Residual moisture could be "wiped" from branches and leaf surfaces with an absorbent material from which water could later be cryogenically extracted. Bark could be sampled as well and the water in the bark matrix could be similarly extracted. That would allow us to determine what part of the previous storm is stored in the canopy (e.g. the last ~2 mm of an event's precipitation?) and how much that residual moisture changes in amount and isotopic composition between events. In addition to providing for a better understanding of the flow-paths and redistribution processes, a better understanding of the role of residual moisture may allow us to accurately predict rainfall-throughfall differences. The isotopic composition of residual moisture could be implemented into a model to predict rainfall-throughfall differences as a potential step forward, following Saxena's approach (1986).

I think our most interesting finding is that the high-depth, persistent, drip-point we observed consistently had the most-apparent effect from residual moisture. The implications of this partitioning among throughfall collectors demands further study. If the throughfall received at Collector1 represented a drip-point, and because this throughfall was isotopically dissimilar from the other throughfall collectors, does this indicate that other throughfall collectors are not receiving water from drip-points? Instead, perhaps splash-droplets (Murakami, 2006) make up the majority of

throughfall by area, and in actuality, water flowing from drips-points is spatially rare. The relative contribution of drip-points versus other sources of throughfall is not known, but a spatial abundance of splash-droplets would justify why the majority of our throughfall collection points did not have a strong residual moisture signal. Further, the apparent interaction of our highest throughfall depth location's with the residual moisture brings up the question "are the high-yield throughfall drip-points chemically different from the lower-depth areas of throughfall?" If ions are sourced from interaction with the canopy, the long residence time of the residual bark moisture could drive throughfall chemistry (Levia and Herwitz, 2005). There could be important ecological implications of residual moisture mixing if the areas of highest depth were chemically distinct from the rest of throughfall. The coincidence of depth and chemistry would also have implications for how the ions associated with throughfall (Raat *et al*., 2002) travel through the subsurface. However, there is currently not a very strong understanding over the spatial variation in throughfall chemistry (Zimmerman *et al.*, 2007). The implications of throughfall depth and chemical heterogeneity on ecological processes (discussed further in section 4.3.1) has not been sufficiently investigated.

4.2 CHAPTER 3

4.2.1 Overview

In the second chapter, we used a spatially-explicit model of interception loss for a small catchment to investigate the potential heterogeneity of interception loss and to investigate the relative importance of the spatio-temporal controls over interception loss heterogeneity. I demonstrated that interception loss can be highly variable, primarily due to variations in vegetation. However, the variability decreased with increasing precipitation-depth; this resulted in the distribution of net precipitation being controlled more-so by variations in gross precipitation, rather than by variations in interception loss. Alternatively, during the summer, interception loss was highly variable and its distribution across the watershed was almost entirely determined by the distribution of vegetation.

The spatial heterogeneity of water loss due to interception may not be very significant during large events that drive most of watershed 1's discharge. This is because the background precipitation is extremely spatially variable, due to the complex terrain. However, this project was a "case study," and therefore the results are somewhat specific to WS1. However the underlying processes must should apply to other environments with different topography or climates. In another setting, interception loss could be more heterogeneous for all storms and be the primary contributor to variations in net precipitation. In watershed 1, the interception loss heterogeneity is most significant during the summer when there is minimal precipitation. Summer interception loss could cause variations in soil moisture availability, and thus cause differences in ecohydrological processes that are a

function of soil moisture availability. Climate forecasts for the Pacific Northwest predict conditions that will enhance interception loss heterogeneity and therefore enhance the heterogeneity of moisture available during the summer dry period (Mote and Salanthe, 2010).

4.2.2 Future work

While our approach was mainly designed as a virtual experiment to explore potential heterogeneity in interception loss, a major step forward in improving our approach would be to develop a robust scaling relationship to allow us to use more commonly measured vegetation metrics (e.g. LAI) to accurately predict interception-model parameters (storage capacity and the fraction intercepted). This would make it possible to quickly gage the potential interception heterogeneity across a larger area.

Additionally, to use this as a predictive model, I would need to determine if variations in the convective heat exchange components of the evaporation rate are minimal, as we assumed. Using our method, I was only able to test the effects of energy heterogeneity due to solar radiation differences. It would extremely useful to measure how convective heat exchange varies between grid-cells at a similar resolution (50 m). This could be accomplished with large, spatially-integrated field measurements of plot-throughfall, perhaps using the plastic sheet method (Calder and Rosier, 1976). An interception loss model could be parameterized with those measurements using standard methods (e.g. Link *et al.*, 2004). Then, based on observations of throughfall amounts, the Gash (1979) model could be used to solve for

the evaporation rates. These measurements could be made throughout a watershed, to quantify spatial variability in wet-canopy evaporation rates.

Future work could also involve virtually testing how various patterns of net precipitation inputs could affect runoff response (*sensu* Hopp and McDonnell, 2011). It would be particularly interesting to test how pattern of vegetation alone affects the hydrology of a watershed. This could be tested in a distributed ecohydrological model (e.g. RHESSYS; Tague and Band, 2004) by maintaining a certain amount of vegetation on a watershed but artificially rearranging it into different distributions with different patterns. I expect that the spatial distribution of vegetation in a catchment is critical to determining that vegetation's net effects on the hydrological functioning of that catchment (e.g. Mackay and Band, 1997).

4.3 BROADER IMPLICATIONS

4.3.1 Ecohydrologic feedback cycles

The present two studies illustrated the magnitude of interception heterogeneity. But in both papers, the true story emerges from putting the results in perspective of the whole environmental system. When we consider the long-term trajectory of integrated ecohydrologic systems, it may be undesirable to disaggregate the ecological and hydrological components. At both of the scales that we investigated interception, the canopy's manipulation of precipitation has the potential to cause ecologic feedbacks that could drive variations in vegetation architecture, growth, and community

structure. Since interception is dependent on the structural characteristics of vegetation, there is also a likely hydrologic feedback, coupling the ecological and hydrological components; this calls for interception to be conceptualized as a component of an integrated ecohydrologic system.

Chapter 2 illustrates a canopy's ability to induce complexity on the precipitation input, not just by spatially redistributing moisture, but also partitioning water to be transmitted by the canopy through various processes that contribute to the total net precipitation. The combination of all of these potential interception and redistribution processes (i.e. flow along branches and stems, storage on surfaces and within the bark matrix, dripping from leaves and needles, and droplets splashing from the canopy) results in a highly heterogeneous input to the forest floor. Isotopic heterogeneities indicated process-heterogeneity related to differences in mixing with a residual pool. We hypothesized that the interaction with the residual pool may be one of the causes of the chemically heterogeneous input to the forest floor (Raat *et al.*, 2002; Zimmerman *et al.*, 2007), which provides critical ions to vegetation (Levia *et al.*, 2011).

Our study is not the first to discuss the potential ecological importance of the stable pattern of throughfall depth that results from interception (Navar and Bryan, 1990; Raat *et al.*, 2002; Keim *et al.*, 2005). However, none of these previous studies have taken measurements to directly relate ecological processes (e.g. soil respiration, root allocation) to the throughfall pattern. Several studies have attempted to link net

precipitation patterns to soil water distributions (Navar and Bryan, 1990; Bouten *et al.*, 1992; Brodersen *et al.*, 2000; Raat *et al.*, 2002; Liang *et al.*, 2009; Gerrits *et al.*, 2010), with largely inconclusive results. A next step could be to directly relate the throughfall distribution to rooting distribution, especially considering recent findings of plants using soil-water distinct from that which is transmitted to streams (Brooks *et al.*, 2009). Navar and Bryan (1990) hypothesized that water used by plants is largely funneled to the roots via stemflow. Eco-physiologists have sought an explanation for lateral root distributions (e.g. Metcalfe *et al.*, 2008; Ceccon *et al.*, 2011) and have found that allocation and clustering can be a function of better local water availability (Kazda and Schmid, 2009). Therefore it is a particularly tantalizing question whether rooting distributions cohere with net precipitation distributions, as has been speculated by Kazda and Schmid (2009) and others. Thus, root distribution could be a consequence of the features of canopy architecture that introduce heterogeneity through channeling and redirecting throughfall.

If the spatial distribution of throughfall and roots co-vary in water-limited systems, this would be evidence of the self-organization of plants to optimize water conditions while minimizing energy put towards root-growth. A canopy's ability to funnel water to points could result in deeper infiltration, decreasing the fraction of water lost to evaporation from the forest floor (Gerrits *et al.*, 2010). Stemflow creates flow routes that bypass the forest floor, leading directly to roots (Navar and Bryan, 1990). Preferential root allocation to stable drip points or stemflow flow-paths could

maximize the effective water availability, increasing resistance and resilience to water stress. This potential coupled above-ground / below-ground organizational feature and co-dependence of ecology and hydrology extends beyond most conceptualizations of forest ecosystem processes, but seems to be in line with the discipline's current trajectory (Jenerette et al., 2011).

Chapter 3 discussed how catchment-scale heterogeneity in interception loss could also lead to vegetation-interception feedbacks. This discussion in chapter 3 identifies the ecohydrological implications of patterns of interception loss for both soil moisture recharge / flow generation as well as ecological processes. Put simply, our theory is that plant growth requires water but also limits available water because more growth means more interception capacity. From the hydrological point of view, I could also speculate that the stable variations in precipitation could result in variations in flow-path development (Sidle *et al.,* 2001; Lorente and Bejan, 2006; Troch *et al.,* 2008; Lin, 2010; Nieber and Sidle, 2010).

4.3.2 Take-away messages

Both of the present studies open up new questions regarding how we view interception loss as an ecohydrologic process. As expressed in Kirchner (2003), asking unanswered questions can be extremely valuable to guiding a scientific field as a whole. The results of both projects tended to lead towards the grand question, "How can we account for interception-induced ecohydrologic complexity and feedbacks in our perception of watershed processes?" The answer may be to seek fundamental

functional traits (McDonnell *et al*., 2007) that result in the pattern and co-dependence of vegetation, soil, and geomorphic properties, that lead to emergent hydrologic traits as opposed to seeking out and explaining every idiosyncratic heterogeneity.

In my opinion, the most important potential impact of this work is that it demonstrates that interception is a critical control over the spatial distribution of water at multiple scales. Consistent with other studies (Raat *et al*., 2002; Keim *et al*., 2005), we observed stable patterns of throughfall depth at the plot scale. Our study went further by using stable isotopes to also demonstrate chemical-distinction and process-distinction between different locations under a canopy. This complexity of the net precipitation input to the forest floor needs to be regarded when considering plot-scale ecological and hydrological processes. Stand-mean values of interception may be sufficient for landscape-scale studies, but within a plot, interception is a primary cause of the spatial variations in the moisture input. Variations in moisture input could result in soil moisture variations, and result in known and unknown variations in ecological, hydrological and biogeochemical processes. Thus, variations in moisture input due to interception must be considered when studying small-scale ecological and hydrological processes.

At the catchment / landscape scale, intra-plot variations may have higher order influences on complexity, but larger-scale variations in IL can also be highly significant (demonstrated in chapter 3). In the hydrological community, this spatial variation is often ignored despite that it could impact the hydrological function of a

whole catchment (e.g. Mackay and Band, 1997). In the ecological community, interception loss is often not even considered, yet water availability is generally considered one of the most important controls over vegetation productivity (Field *et al*., 1995) and diversity (Hawkins *et al*., 2003).

Regardless of scale, the redistribution of moisture due to interception and interception loss induces spatio-temporal heterogeneity on the precipitation input. Complexity of this essential input will trickle down through ecohydrologic systems, likely causing countless interactions and affect the function of the entire system.

4.4 REFERENCES

Bouten W, Heimovaara TJ, Tiktak A. 1992. Spatial patterns of throughfall and soil water dynamics in a Douglas fir stand. *Water Resources Research* **28** (12): 3227-3233.

Brodersen C, Pohl S, Lindenlaub M, Leibundgut C, von Wilpert K. 2000. Influence of vegetation structure on isotope content of throughfall and soil water. *Hydrological Processes* **14**: 1439-1448.

Brooks JR, Barnard HR, Coulombe R, McDonnell JJ. 2010. Ecohydrologic separation of water between trees and streams in a Mediterranean climate. *Nature: Geoscience* **3**: 100-104.

Calder IR, Rosier PTW. 1976. The design of large plastic-sheet net-rainfall gauges. *Journal of Hydrology* **30**(4): 403-405.

Ceccon C, Panzacchi P, Scandellari F, Prandi L, Ventura M, Russo B, Millard P, Tagiliavini M. 2011. Spatial and temporal effects of soil temperature and moisture and the relation to fine root density on root and soil respiration in a mature apple orchard. *Plant and Soil* **342**: 195-206.

Field CB, Randerson JT, Malmstrom CM. 1995. Global net primary production Combining ecology and remote sensing. *Remote Sensing of the Environment* **51**: 74-88.

Gash JHC. 1979. An analytical model of rainfall interception by forests. Quarterly *Journal of the Royal Meteorological Society* **105**: 43-55.

Gerrits AMJ, Pfister L, Savenije HHG. 2010. Spatial and temporal variability of canopy and forest floor interception in a beech forest. *Hydrological Processes* **24**: 3011- 3025. DOI: 10.1002/hyp.7712

Hawkins BA, Field R, Cornell HV, Currie DJ, Guégan J, Kaufman DM, Kerr JT, Mittelbach GG, Oberdorff T, O'Brien EM, Porter EE, Turner JRG. 2003. Energy, water, and broad-scale geographic patterns of species richness. *Ecology* **84**:3105–3117

Herwitz SR. 1987. Raindrop impact and water flow on the vegetative surfaces of trees and the effects on stemflow and throughfall generation. *Earth Surface Processes and Landforms* **12**: 425-432.

Hopp L, McDonnell JJ. 2011. Examining the role of throughfall patterns on subsurface stormflow generation. *Journal of Hydrology* **409**: 460-471.

Jenerette GD, Barron-Gafford GA, Guswa AJ, McDonnell JJ, Villegas JC. 2011. Organization of complexity in water limited ecohydrology. *Ecohydrology*: DOI: 10.1002/eco.217.

Kazda M, Schmid I. 2009. Clustered distribution of tree roots and soil water exploitation. *Progress in Botany* **70** (4): 223-239.

Keim RF, Skaugset AE, Weiler M. 2005. Temporal persistence of spatial patterns in throughfall. *Journal of Hydrology* **314** (1-4): 263-274.

Kirchner JW. 2003. A double paradox in catchment hydrology and geochemistry. *Hydrological Processes* **17**(4): 871-874.

Levia DF, Herwitz SR. 2005. Interspecific variation of bark water storage capacity of three deciduous tree species in relation to stemflow yield and solute flux to forest soils. *Catena* **64** (1): 117-137.

Levia DF, Keim RF, Carlyle-Moses DE, Forest EE. 2011. Throughfall and stemflow in wooded ecosystems. In *Forest Hydrology and Biogeochemistry: Synthesis of Past Research and Future Directions.* Levia DF, Carlyle-Moses DE, Tanaka T (eds). Springer-Verlag: Heidelberg, Germany.

Liang W, Kosugi K, Mizuyama T. 2009. A three-dimensional model of the effect of stemflow on soil water dynamics around a tree on a hillslope. *Journal of Hydrology* **266**: 62-75.

Link TE, Unsworth M, Marks D. 2004. The dynamics of rainfall interception by a seasonal temperate rainforest. *Agricultural and Forest Meteorology* **124**: 171-191.

Lorente S, Bejan A. 2006. Heterogeneous porous media as multiscale structures for maximum flow access. *Journal of Applied Physics* **100**: 114909, DOI: 10.1063/1.2396842.

Mackay DS, Band LE. 1997. Forest ecosystem processes at the watershed scale: dynamics coupling of distributed hydrology and canopy growth. *Hydrological Processes* **11**: 1197-1217.

McDonnell JJ, Sivapalan M, Vache K, Dunn S, Grant G, Haggerty R, Hinz C, Hooper R, Kirchner J, Roderick ML, Selker J, Weiler M. 2007. Moving beyond heterogeneity and process complexity A new vision for watershed hydrology. *Water Resources Research* **43**: W07301.

Metcalfe DB, Meir P, Aragão LEOC, da Costa ACL, Braga AP, Gonçalves PHL, Silva JDA, de Almeida SS, Dawson LA, Malhi Y, Williams M. 2008. The effects of water availability on root growth and morphology in an Amazon rainforest. *Plant and Soil* **311**: 189-199.

Mote PW, Salanthe EP. 2010. Future Climate in the Pacific Northwest. *Climatic Change*, DOI 10.1007/s10584-010-9848-z.

Murakami S. 2006. A proposal for a new forest canopy interception mechanism: Splash droplet evaporation. *Journal of Hydrology* **319**: 72-82.

Navar J, Bryan R. 1990. Interception loss and rainfall redistribution by three semi-arid growing shrubs in Northeastern Mexico. *Journal of Hydrology* **115**: 51-63.

Nieber JL, Sidle RC. 2010. How do disconnected macropores in sloping soils facilitate preferential flow. *Hydrological Processes* **24**: 1582 – 1594.

Puckett LJ. 1991. Spatial variability and collector requirements for sampling throughfall volume and chemistry under a mixed-hardwood canopy. *Canadian Journal of Forest Research* **21**: 1581-1588.

Raat KJ, Draaijers GPJ, Schaap MG, Tietema A, Verstraten JM. 2002. Spatial variability of throughfall water and chemistry and forest floor water content in a Douglas fir forest stand. *Hydrology and Earth System Sciences* **6**: 363-374.

Saxena RK. 1986. Estimation of canopy reservoir capacity and Oxygen-18 fractionation in throughfall in a pine forest. *Nordic Hydrology* **17**: 251-260.

Sidle RC, Noguchi S, Tsuboyama Y, Laursen K. 2001. A conceptual model of preferential flow systems in forested hillslopes: evidence of self-organization. *Hydrological Processes* **15**: 1675-1692, DOI: 10.1002/hyp.233.

Tague CL, Band LE. 2004. RHESSys: Regional hydro-ecologic simulation system-an object-oriented approach to spatially distributed modeling of carbon, water, and nutrient cycling. *Earth Interactions* **8**: 1-42.

Troch PA, Carillo GA, Heidbüchel I, Rajagopal S, Switanek M, Volkmann THM, Yaeger M. 2008. Dealing with landscape heterogeneity in watershed hydrology: A review of recent progress toward new hydrological theory. *Geography Compass* **2**: DOI 1749-8198.2008.00186.x.

Zimmerman A, Wilcke W, Elsenbeer H. 2007. Spatial and temporal patterns of throughfall quantity and quality in a tropical montane forest in Ecuador. *Journal of Hydrology* **343** (1-2): 80-96.